IMPROVEMENT OF ANODIC Pt-BASED ELECTROCATALYSTS FOR DIRECT ETHANOL FUEL CELLS

MS. JARUPUK THEPKAEW

A THESIS SUBMITTED IN PARTIAL FULFILLMENT
OF THE REQUIREMENTS FOR
THE DEGREE OF DOCTOR OF ENGINEERING (CHEMICAL ENGINEERING)
FACULTY OF ENGINEERING
KING MONGKUT'S UNIVERSITY OF TECHNOLOGY THONBURI
2011

Improvement of Anodic Pt-based Electrocatalysts for Direct Ethanol Fuel Cells

Ms. Jarupuk Thepkaew M.Eng. (Chemical Engineering)

A Thesis Submitted in Partial Fulfillment of the Requirements for
the Degree of Doctor of Engineering (Chemical Engineering)
Faculty of Engineering
King Mongkut's University of Technology Thonburi
2011

Thesis Committee

……. Chairman of Thesis Committee
(Lect. Waret Veerasai, Dr.rer.nat.)

……. Member and Thesis Advisor
(Assoc. Prof. Supaporn Therdthianwong, Ph.D.)

……..…… Member and Thesis Co-Advisor
(Assoc. Prof. Apichai Therdthianwong, Ph.D.)

…….……..... Member
(Assoc. Prof. Somnuk Jarudilokkul, Ph.D.)

…….……..... Member
(Asst. Prof. Panchan Sricharoon, Ph.D.)

Thesis Title	Improvement of Anodic Pt-based Electrocatalysts for Direct Ethanol Fuel Cells
Thesis Credits	36
Candidate	Ms. Jarupuk Thepkaew
Thesis Advisors	Assoc. Prof. Dr.Supaporn Therdthianwong Assoc. Prof. Dr.Apichai Therdthianwong
Program	Doctor of Engineering
Field of Study	Chemical Engineering
Department	Chemical Engineering
Faculty	Engineering
B.E.	2554

Abstract

This research aims at enhancing catalytic activity of anodic Pt-based catalysts towards ethanol oxidation reaction and also direct ethanol fuel cells. Three parts of the study, including treatment of carbon support, activity of carbon-supported catalysts and activity of unsupported catalysts, were carried out. Firstly, Vulcan XC-72R carbon was pretreated using acid and thermal activation approaches, and the carbons obtained were then used as supports for PtSn/C catalysts synthesized by a successive reduction method. The results showed that pretreatment by HNO_3 produced various oxygenated functional groups on the support surface and increased its acidic property. The strong acidity of the acid-treated support led to an unfavorable condition for the Pt reduction reaction and resulted in low Pt content but high Sn:Pt ratio in the PtSn/C catalyst. On the other hand, thermal activation increased the base functional groups on the support surface, which enhanced reduction of Pt precursor, and consequently provided an average metal particle size of 2.2 nm which is smaller than that of acid treatment. The results from cyclic voltammetry, chronoamperometry and cell performance testing confirmed that the catalytic activity for ethanol oxidation and the performance in the direct ethanol fuel cell fabricated from the heat-treated carbon-supported PtSn catalyst were superior to those of the fresh PtSn/C catalyst and the acid-treated carbon-supported PtSn catalyst. Even comparing to commercial Pt/C and Pt_3Sn_1/C electrodes, the heat-treated carbon-supported PtSn electrode yielded better fuel cell performance. Moreover, the oxidation of ethanol was enhanced by the consecutive deposition of Pt precursor on the heat-treated carbon-supported tin oxides, due to the combination effects between high metal content and well dispersion of metal on the supports.

For unsupported catalyst study, mesoporous Pt and PtSn nanoparticles were prepared through liquid crystalline templating technique. The result disclosed that the average crystallite size of the prepared Pt and PtSn samples was around 4.3 nm with high electrochemical active surface area of 41 $m^2.g^{-1}$ and 51 $m^2.g^{-1}$, respectively. From cyclic voltammetry data, it was found that addition of 9 at.% Sn in the PtSn sample promoted ethanol oxidation at low potential of 0.2 V *vs.* RHE and yielded higher electrical current than the pure Pt. Moreover, introducing Ru and Os as a third metal into the PtSn sample led to a decrease in their particle sizes, but not increase in their active surface areas because more tin oxides contained in those ternary catalysts acted as a separator and partially covered the active sites. Investigation on ethanol oxidation activity of the

catalysts showed that both ternary catalysts gave the lower onset potentials and the larger currents than PtSn did. However, the higher activity for ethanol oxidation was found in PtSnOs since more oxophilic Os catalyzed the oxidation of CO. Furthermore, the role of Ru and Sn on activity of mesoporous PtRu and PtRuSn for ethanol oxidation was investigated. From x-ray diffraction analysis, the degree of Ru alloyed in PtRu and PtRuSn samples was 31% and 22%, respectively, implying that the unalloyed Ru oxide was favorably formed as Sn was incorporated into the PtRu. The results from chronoamperometry revealed that the long-term poisoning rate of PtRu catalyst was higher than that of PtRuSn catalyst at low potentials ($\leq$ 0.4 V *vs.* RHE) but not at high potentials ($\geq$ 0.5 V *vs.* RHE). As a result, Ru and Sn showed different promotion effects for ethanol oxidation. Sn would promote dissociative adsorption of ethanol molecules while the role of Ru was to activate water molecules. The combination of the promoting roles of Ru and Sn was, therefore, contributed to the improvement of the overall ethanol oxidation in PtRuSn catalyst.

Keywords : Direct Ethanol Fuel Cells / PtSn/C / Ethanol Oxidation Reaction / Mesoporous Catalyst / Liquid Crystalline Templating Technique

หัวข้อวิทยานิพนธ์	การปรับปรุงตัวเร่งปฏิกิริยาที่มีแพลทินัมเป็นตัวเร่งปฏิกิริยาพื้นฐานทางฝั่งแอโนดสำหรับเซลล์เชื้อเพลิงแบบป้อนเอทานอลโดยตรง
หน่วยกิต	36
ผู้เขียน	นางสาวจารุพักตร์ เทพแก้ว
อาจารย์ที่ปรึกษา	รศ.ดร. สุภาภรณ์ เทอดเทียนวงษ์
	รศ.ดร. อภิชัย เทอดเทียนวงษ์
หลักสูตร	วิศวกรรมศาสตรดุษฎีบัณฑิต
สาขาวิชา	วิศวกรรมเคมี
ภาควิชา	วิศวกรรมเคมี
คณะ	วิศวกรรมศาสตร์
พ.ศ.	2554

บทคัดย่อ

งานวิจัยนี้มีความมุ่งหมายที่จะปรับปรุงความว่องไวของตัวเร่งปฏิกิริยาที่มีแพลทินัมเป็นตัวเร่ง-ปฏิกิริยาพื้นฐานทางฝั่งแอโนดสำหรับปฏิกิริยาออกซิเดชันของเอทานอลและเซลล์เชื้อเพลิงแบบป้อนเอทานอลโดยตรง ซึ่งแบ่งการศึกษาออกเป็น 3 ส่วน คือ การปรับสภาพคาร์บอน ความว่องไวของตัวเร่งปฏิกิริยาที่มีตัวรองรับและไม่มีตัวรองรับ โดยงานวิจัยเริ่มต้นจากการศึกษาการปรับสภาพคาร์บอน (Vulcan XC-72R) ด้วยวิธีการกระตุ้นด้วยกรดและวิธีใช้ความร้อน คาร์บอนที่ปรับสภาพแล้วถูกนำไปใช้เป็นตัวรองรับของตัวเร่งปฏิกิริยาแพลทินัม-ดีบุก ซึ่งสังเคราะห์โดยวิธีรีดักชันแบบต่อเนื่อง จากผลการทดลองพบว่าการปรับสภาพคาร์บอนโดยกรดไนตริกได้สร้างหมู่ฟังก์ชันที่มีออกซิเจนเป็นองค์ประกอบหลายชนิดและเพิ่มความเป็นกรดบนพื้นผิวของตัวรองรับคาร์บอน ความเป็นกรดที่แรงของตัวรองรับนี้ไม่เหมาะสมสำหรับการเกิดรีดักชันของแพลทินัม ทำให้ปริมาณของแพลทินัมในตัวเร่งปฏิกิริยานั้นน้อย แต่อัตราส่วนของดีบุกต่อแพลทินัมมีค่าสูง ในทางตรงกันข้ามการกระตุ้นโดยความร้อนได้เพิ่มหมู่ฟังก์ชันที่เป็นเบสบนพื้นผิวของตัวรองรับซึ่งช่วยเพิ่มการเกิดรีดักชันของแพลทินัม และส่งผลให้อนุภาคเฉลี่ยของโลหะมีขนาดเท่ากับ 2.2 นาโนเมตร ซึ่งเล็กกว่าในกรณีของตัวเร่งปฏิกิริยาที่เตรียมจากการปรับสภาพคาร์บอนโดยใช้กรด และผลการทดลองจากไซคลิก-โวลแทมเมทรี โครโนแอมเพอโรเมทรี และการทดสอบสมรรถนะของเซลล์เชื้อเพลิงยืนยันว่าตัวเร่ง-ปฏิกิริยาแพลทินัม-ดีบุกบนตัวรองรับที่ปรับสภาพโดยความร้อนมีความว่องไวต่อปฏิกิริยาออกซิเดชัน

ของเอทานอลและให้สมรรถนะของเซลล์เชื้อเพลิงแบบป้อนเอทานอลโดยตรงที่สูงกว่าตัวรองรับที่ไม่ปรับสภาพและที่ปรับสภาพโดยใช้กรด ทั้งยังให้สมรรถนะของเซลล์เชื้อเพลิงที่สูงกว่าขั้วอิเล็กโทรดที่เตรียมจากตัวเร่งปฏิกิริยาทางการค้า คือแพลทินัมบนคาร์บอนและแพลทินัม-ดีบุกบนคาร์บอน นอกจากนี้ยังพบอีกว่าตัวเร่งปฏิกิริยาแพลทินัม-ดีบุก ที่เตรียมโดยการสังเคราะห์ดีบุกออกไซด์บนตัวรองรับที่ปรับสภาพโดยความร้อนก่อนที่จะเกิดการพอกพูนของแพลทินัมต่อเนื่องตามลำดับนั้น ช่วยเร่งการเกิดปฏิกิริยาออกซิเดชันของเอทานอล ซึ่งเป็นผลจากการมีปริมาณโลหะที่สูงและการกระจายตัวของโลหะบนตัวรองรับที่ดี

สำหรับการศึกษาตัวเร่งปฏิกิริยาที่ไม่มีตัวรองรับนั้น ได้ทำการสังเคราะห์ตัวเร่งปฏิกิริยาที่มีความพรุนตัวระดับกลางขึ้นโดยใช้เทคนิค liquid crystalline templating โดยเริ่มต้นจากการเตรียมตัวเร่งปฏิกิริยาแพลทินัมบริสุทธิ์และแพลทินัม-ดีบุก ซึ่งพบว่าขนาดผลึกเฉลี่ยของตัวเร่งปฏิกิริยาเหล่านั้นมีค่าเท่ากับ 4.3 นาโนเมตร และมีพื้นที่ผิวทางปฏิกิริยาเคมีไฟฟ้าที่สูง คือ 41 ตารางเมตรต่อกรัม และ 51 ตารางเมตรต่อกรัม ตามลำดับ ผลจากไซคลิกโวลแทมเมทรีแสดงให้เห็นว่าการเติมดีบุก 9 เปอร์เซ็นต์โดยอะตอมในตัวเร่งปฏิกิริยาแพลทินัม-ดีบุก ทำให้เกิดการออกซิเดชันของเอทานอลที่ความต่างศักย์ต่ำ คือ 0.2 โวลต์เทียบกับขั้วไฟฟ้าไฮโดรเจนผันกลับได้ และให้กระแสไฟฟ้าสูงกว่าตัวเร่งปฏิกิริยาแพลทินัมบริสุทธิ์ นอกจากนี้จากการศึกษาการเติมโลหะตัวที่สามในตัวเร่งปฏิกิริยาแพลทินัม-ดีบุกพบว่าการใส่รูทีเนียมและออสเมียมทำให้ขนาดอนุภาคของตัวเร่งปฏิกิริยาแพลทินัม-ดีบุก-รูทีเนียมและแพลทินัม-ดีบุก-ออสเมียมลดลง แต่ไม่เพิ่มพื้นที่ผิวการเกิดปฏิกิริยา เนื่องจากดีบุกออกไซด์ทำหน้าที่เป็นตัวกั้นในตัวเร่งปฏิกิริยาเหล่านั้น และอาจปกคลุมจุดว่องไวบางส่วน จากการทดสอบความว่องไวของตัวเร่งปฏิกิริยาต่อการเกิดออกซิเดชันของเอทานอลพบว่าตัวเร่งปฏิกิริยาที่มีโลหะสามชนิดให้ค่าความต่างศักย์เริ่มต้นของการเกิดออกซิเดชันของเอทานอลที่ต่ำกว่า และค่ากระแสไฟฟ้าที่สูงกว่าตัวเร่งปฏิกิริยาที่มีโลหะสองชนิด และแพลทินัม-ดีบุก-ออสเมียมมีความว่องไวต่อการเกิดออกซิเดชันของเอทานอลสูงกว่าแพลทินัม-ดีบุก-รูทีเนียม เนื่องจากออสเมียมสามารถเปลี่ยนไปอยู่ในรูปของออกไซด์ได้ง่ายกว่ารูทีเนียม ซึ่งจะส่งเสริมการเกิดออกซิเดชันของคาร์บอนมอนนอกไซด์ และจากการศึกษาหน้าที่ของรูทีเนียมและดีบุกต่อความว่องไวของตัวเร่งปฏิกิริยาแพลทินัม-รูทีเนียมและแพลทินัม-ดีบุก-รูทีเนียมสำหรับการเกิดออกซิเดชันของเอทานอลพบว่าแพลทินัม-รูทีเนียมและแพลทินัม-ดีบุก-รูทีเนียมมีดีกรีการเกิดรูทีเนียมผสมเท่ากับ 31 เปอร์เซ็นต์ และ 22 เปอร์เซ็นต์ ตามลำดับ ซึ่งแสดงให้เห็นว่าการเกิดเป็นรูทีเนียมที่อยู่ในรูปออกไซด์และไม่ได้เกิดเป็นโลหะผสมนี้จะเพิ่มมากขึ้นในกรณีที่มีการเติมดีบุกเข้าไปในตัวเร่งปฏิกิริยาแพลทินัม-รูทีเนียม และผลจากโครโนแอมเพอโรเมทรีพบว่าแพลทินัม-รูทีเนียมมีอัตราความเป็นพิษระยะยาวสูงกว่าแพลทินัม-ดีบุก-รูทีเนียม ที่ความต่างศักย์น้อยกว่าหรือเท่ากับ 0.4 โวลต์เทียบกับขั้วไฟฟ้าไฮโดรเจนผันกลับได้ แต่ที่ความต่างศักย์มากกว่าหรือเท่ากับ 0.5 โวลต์เทียบกับขั้วไฟฟ้าไฮโดรเจนผันกลับได้ แพลทินัม-

รูทีเนียมกลับมีอัตราความเป็นพิษระยะยาวต่ำกว่าแพลทินัม-ดีบุก-รูทีเนียม ซึ่งแสดงว่ารูทีเนียมและดีบุกทำหน้าที่ในการเกิดออกซิเดชันของเอทานอลที่แตกต่างกัน โดยดีบุกจะส่งเสริมการดูดซับแบบแตกตัวของโมเลกุลเอทานอล ขณะที่หน้าที่ของรูทีเนียมคือการกระตุ้นโมเลกุลน้ำ ดังนั้นจึงสรุปได้ว่าการผสานกันของหน้าที่ที่เสริมกันของรูทีเนียมและดีบุกนำไปสู่การปรับปรุงการเกิดออกซิเดชันของเอทานอลในตัวเร่งปฏิกิริยาแพลทินัม-ดีบุก-รูทีเนียม

คำสำคัญ : เซลล์เชื้อเพลิงแบบป้อนเอทานอลโดยตรง / แพลทินัม-ดีบุกบนคาร์บอน / ปฏิกิริยาออกซิเดชันของเอทานอล / ตัวเร่งปฏิกิริยาที่มีความพรุนตัวระดับกลาง / เทคนิค Liquid Crystalline Templating

ACKNOWLEDGEMENTS

This research would not have been achieved without any helps and suggestions from many people. First of all, I would like to thank my advisor, Assoc. Prof. Dr.Supaporn Therdthianwong, and my co-advisor, Assoc. Prof. Dr.Apichai Therdthianwong, for their valuable advices and their encouragement throughout this research. I would like to extend my appreciation to Assoc. Prof. Dr.Somnuk Jarudilokkul and Asst. Prof. Dr.Panchan, who are my committees, for their comments and recommendations. All laboratory staffs of Chemical Engineering Department and the research group of Fuel Cell and Hydrogen Research and Engineering Center at King Mongkut's University of Technology Thonburi would be gratefully acknowledged. I also would like to give special thanks to Prof. Anthony Kucernak, who supervises me during doing the experiment at Imperial College London, United Kingdom. I truly appreciate his valuable suggestions as well as his numerous supports. Finally, I would like to express my sincere gratitude to the Thailand Research Fund (TRF) through the Royal Golden Jubilee Ph.D. Program (Grant No. PHD/0198/2548) and also the National Research University (NRU) Project of Thailand's Office of the Higher Education Commission for the financial support in this research.

CONTENTS

PAGE

LIST OF TABLES

TABLE **PAGE**

LIST OF FIGURES

FIGURE **PAGE**

LIST OF SYMBOLS

SYMBOLS		UNITS
a_{fcc}	Lattice constant of Pt	nm
E^{o}_{eq}	Equilibrium standard electromotive force	V
G	Gibbs free energy	$kJ.mol^{-1}$
H	Enthalpy	$kJ.mol^{-1}$
L_{Pt}	Pt loading	$mg.cm^{-2}$
M	Molar concentration	$mol.L^{-1}$
Q_{ads}	Charge of hydrogen adsorption	$mC.cm^{-2}$
Q_{CO}	Charge of CO adsorption	$\mu C.cm^{-2}$
Q_{ref}	Hydrogen desorption charge of the Pt single crystallite	$mC.cm^{-2}$
W_e	Theoretical energy density	$kWh.kg^{-1}$

Greek Symbols

β	Width at the peak at the half height	rad
δ	Long-term poisoning rate	$\%.s^{-1}$
ε	Overall efficiency at any working potential	Dimensionless
ε_{rev}	Theoretical efficiency	Dimensionless
θ	Angular position	^{o}
λ	X-ray wavelength	Å
μ	Population mean	nm
σ	Standard deviation	nm

Superscript

0	Denotes standard condition at 25^{o}C, 1 atm

Subscripts

ads	Adsorption
cat	Catalyst
cell	Fuel cell
fcc	Face-centered cubic
max	Maximum
Pt	Platinum
PZC	Point of zero charge
ref	Denotes reference state

LIST OF TECHNICAL ABBREVIATIONS

DAFC	=	Direct alcohol fuel cell
DEFC	=	Direct ethanol fuel cell
DMFC	=	Direct methanol fuel cell
EOR	=	Ethanol oxidation reaction
ESA	=	Electrochemical surface area
GDE	=	Gas diffusion electrode
MEA	=	Membrane electrode assembly
MPD	=	Maximum power density
NHE	=	Normal hydrogen electrode
OCV	=	Open circuit voltage
PEMFC	=	Proton exchange membrane fuel cell
RHE	=	Reversible hydrogen electrode
SCE	=	Saturated calomel electrode
SPEFC	=	Solid polymer electrolyte fuel cell

CHAPTER 1 INTRODUCTION

1.1 Rationale

In the last decade, direct alcohol fuel cells (DAFCs) have become particularly attractive power source for mobile applications. This kind of fuel cell uses alcohol solutions, containing methanol or ethanol, which is fed directly into the cells. In contrast to hydrogen feed fuel cell, such as the proton exchange membrane fuel cells (PEMFC), DAFCs exhibit no problems with handling, fuel storage, transportation, or distribution [1,2]. Due to no requirement of an external reformer, this fuel cell system is also simpler and cheaper. Methanol is considered to be one of the most promising fuels for DAFCs, as it can be effectively oxidized to produce CO_2 and water as the waste products. However, concerns about fuel crossover problems as well as methanol's toxicity to the optical nerves of humans have made ethanol a strong candidate for an alternative liquid fuel [3]. As well as being safer, ethanol has numerous benefits, such as high energy density (8.01 $kWh.kg^{-1}$ in contrast to 6.09 $kWh.kg^{-1}$ of methanol), renewability, and natural availability from the fermentation of biomass resources, which does not release greenhouse gases into the atmosphere [1]. Due to the C-C bonds in an ethanol molecule, the pathway of ethanol's oxidation reaction (EOR) is more complicated than that of methanol [1,4]. Breaking C-C bonds is very difficult at low operating temperature. Consequently, the final products of oxidation consist mainly of acetaldehyde and acetic acid, which lead to a decrease in the fuel cell's efficiency [4,5,6]. Lately, Wang et al. [7] found that the performance of fuel cell operating with ethanol was not significantly interior to that of methanol at 170^{o}C. However, with the limitation of the popular membrane Nafion® type (Dupont) at the working temperature of 120^{o}C, efforts have focused on searching a highly active catalyst for EOR.

Up to now, platinum, Pt, is still the most promising catalyst for oxidation of several small molecules since it has high activity as well as good stability, in particular under acidic circumstance [8]. The expensive Pt can be well dispersed on a high surface area substrate to attain high utilization of noble metals. Vulcan XC-72R carbon is widely used as a support for Pt catalysts in low-temperature fuel cells, due to its low cost and high availability [9]. It also has both a high surface area and adequate electrical conductivity to act as a path for electron flow. The activities of catalysts could be strongly affected by the dispersion effect as well as the interaction effect between the metal precursors and the support materials [10]. Thus, the supports are generally activated before their use to increase metal dispersion and catalytic activity.

Since Pt itself can be easily poisoned by a very low content (10 ppm) of CO which is one of the intermediate species of EOR, one way to enhance the EOR is modification of well-known Pt catalysts by introducing a second metal, such as Ru [8,11,12], Sn [4,8,13,14,15], W [8], Mo [8,16], and Rh [17,18] as an alloying metal. The second metal can promote the dissociation of water to form the OH-species for oxidative CO removal at a lower potential than unalloyed Pt can [4]. As reported in the previous studies [8,19,20,21], PtSn/C catalysts have higher activity towards EOR than the other binary catalysts. Recently, Jiang and co-workers [22] have discovered that the PtSn/C catalyst prepared by a successive reduction procedure could considerably increase catalytic activity for EOR and fuel cell performance rather than the conventionally modified polyol synthesis could. This is due to the catalyst having sufficient surface

OH-species to oxidize the poisoning CO-adsorbed species and free Pt active sites for further ethanol adsorption.

For efficient operation of fuel cell, a thin catalyst layer with high catalyst dispersion on the support has been designed. It was found by Prasanna et al. [23] that Pt content of 20 wt.% in the catalyst yielded the highest performance of fuel cell, due to compromising effects of Pt surface area and thickness of the catalyst layer. To produce high loading and highly dispersed catalysts, unsupported catalysts are of interest especially for solid polymer electrolyte fuel cells (SPEFCs). The preparation of highly ordered, porous metal nanoparticles has been received much attention because they give high surface area with the uniform pore diameter. Initially, Attard and his co-workers have successfully prepared mesoporous Pt [24,25], Sn [26] and Ni [27] by electrodeposition and chemical reduction of metal salts onto a building block through liquid crystalline templating technique with a well-ordered pore network in the size of 2-15 nm. Furthermore, Jiang and Kucernak have applied this approach to produce nanostructured Pt [28], PtRu [29,30] and PtPdRuOs [31] with highly electrochemical surface area; and they found that those are promising catalysts for electro-oxidation of formic acid as well as methanol.

Even in the binary catalyst, the activity for EOR is still low; thus it needs to develop a novel catalyst for EOR by introducing a third element to the binary PtSn catalyst. It was recognized that the popular Ru atom is an oxygen-containing species for the CO oxidative removal by dissociation of water with Ru-$(OH)_{ads}$ species at the potential lower than 0.2 V *vs.* NHE [32]. In comparison to Ru, Os is more oxophilic [33] and consequently it could adsorb water in acidic solutions at potentials slightly more negative than for Ru [34]. It also is evident that metallic Os is able to promote dehydrogenate of both methanol and water [35]. Thus, addition of either Ru or Os to the binary PtSn catalyst may promote electrocatalytic ethanol oxidation. From all these observations, this work aims, therefore, at enhancing catalytic activity of anodic Pt-based catalysts for ethanol oxidation as well as direct ethanol fuel cells.

1.2 Objectives

The objectives of this work are divided into 2 parts as follows.

Part 1: Supported Electrocatalysts (done at KMUTT)

1. To study the effect of pre-treatment approach of a carbon support on activity of PtSn/C electrocatalysts for ethanol oxidation.
2. To evaluate the performance in a direct ethanol fuel cell of the prepared PtSn/C electrodes in comparison to commercial Pt/C and Pt_3Sn_1/C electrodes.
3. To study the effect of metal loading order and solution pH in PtSn/C preparation on ethanol oxidation.

Part 2: Unsupported Electrocatalysts (done at Imperial College London)

1. To examine the activity of Pt and PtSn electrocatalysts prepared by liquid crystalline templating technique for ethanol oxidation.
2. To investigate the effect of a third metal (Ru, Os) added in mesoporous PtSn-based electrocatalysts on their activities towards ethanol oxidation.

1.3 Scope of Work

For supported electrocatalysts, Vulcan XC-72R carbon was firstly pretreated using acid and thermal activation methods, and the carbons obtained were then used as supports for a PtSn/C catalyst synthesized by a successive reduction process according to Jiang et al. [22]. Thereafter, their activities for ethanol oxidation were carried out by using popular electrochemical measurements such as cyclic voltammetry and chronoamperometry techniques. In addition, the prepared PtSn/C catalysts were employed as the anode catalyst and then were tested their performances in the direct ethanol fuel cell using 1 M C_2H_5OH as the fuel. The fuel cell performance of the prepared PtSn/C electrodes was also compared to those of commercial Pt/C and Pt_3Sn_1/C electrodes. Moreover, the effect of metal loading order in PtSn/C preparation on ethanol oxidation was investigated. The platinum precursor was either co-deposited with tin oxides on the heat-treated carbon or consecutively deposited on the heat-treated carbon-supported tin oxides. The final solution pH in PtSn/C preparation was further adjusted by hydrochloric acid, and subsequently its behavior under ethanol oxidation was studied.

For unsupported electrocatalysts, mesoporous Pt, PtRu and PtSn nanoparticles were prepared via co-reduction of metal salts in a lyotropic liquid crystal of a nonionic surfactant [36]. Moreover, both Ru and Os as a third metal were introduced to the binary PtSn sample. Their activities towards ethanol oxidation were also examined by using cyclic voltammetry and chronoamperometry techniques at the reaction temperatures of 20^{o}C and 60^{o}C.

1.4 Expected Results

For supported electrocatalysts,

1. The surface characteristics of the supports pre-treated by acid and thermal activation methods were realized and the pre-treated supports for the highly active PtSn/C electrocatalysts were produced.
2. The performance in a direct ethanol fuel cell of the prepared PtSn/C electrodes compared to those of commercial Pt/C and Pt_3Sn_1/C electrodes was obtained.
3. The metal loading order and solution pH in PtSn/C preparation with high metal loading and well dispersion of metal on the supports were obtained.

For unsupported electrocatalysts,

1. The catalytic behavior of Pt and PtSn electrocatalysts prepared by liquid crystalline templating technique for ethanol oxidation was known.
2. The effect of a third metal (Ru, Os) added in mesoporous PtSn-based electrocatalysts on their activities towards ethanol oxidation was realized.

CHAPTER 2 THEORY AND LITERATURE REVIEW

2.1 Principle of a Direct Ethanol Fuel Cell (DEFC)

A direct ethanol fuel cell (DEFC) is basically derived from a proton exchange membrane fuel cell (PEMFC), which consists of three main components such as anode, cathode and membrane electrolyte. However, instead of feeding hydrogen to a cell at the anode side, ethanol solution is used for the DEFC. The schematic principle of a direct ethanol fuel cell and its components are clearly shown in Figure 2.1.

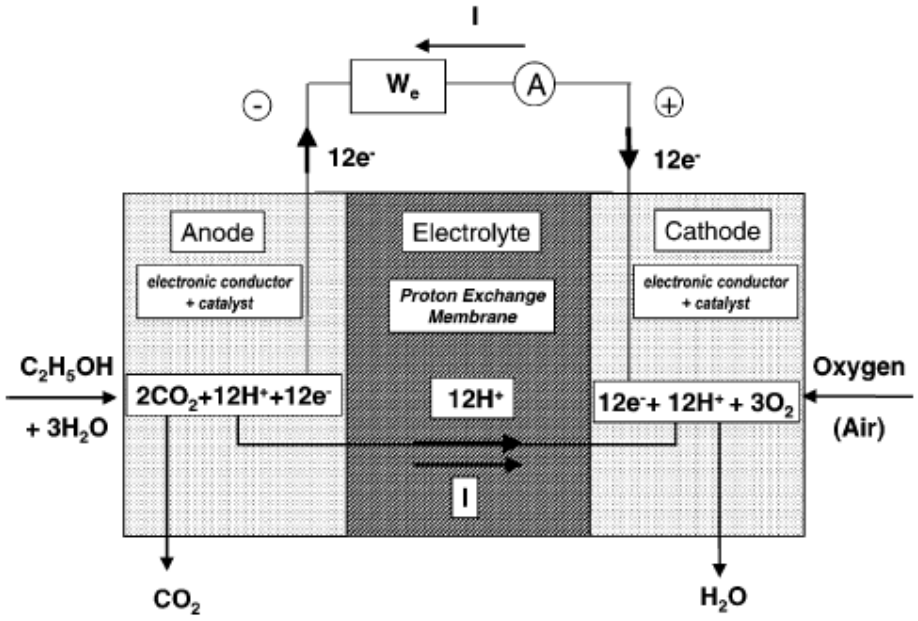

Figure 2.1 Schematic principle of a direct ethanol fuel cell [1]

It can be seen from Figure 2.1 that the ethanol solution used as a fuel is oxidized to carbon dioxide, protons, and electrons at the anode compartment. Only protons can pass through the membrane electrolyte to the cathode whereas electrons flow through an external circuit, and then arrive at the cathode. Either pure oxygen or air is fed to the cathode, where the oxidant is reduced to produce water. Thus, this type of fuel cell gives carbon dioxide and water as the waste products. The redox reactions of PEMFC, DMFC, and DEFC are displayed in the following equations:

H_2 as a fuel:

$$\text{Anode: } H_2 \rightarrow 2H^+ + 2e^- \tag{2.1}$$

$$\text{Cathode: } \frac{1}{2}O_2 + 2H^+ + 2e^- \rightarrow H_2O \tag{2.2}$$

$$\text{Overall: } H_2(g) + \frac{1}{2}O_2(g) \rightarrow H_2O(l) \tag{2.3}$$

CH_3OH as a fuel:

$$\text{Anode: } CH_3OH + H_2O \rightarrow 6H^+ + 6e^- + CO_2 \quad (2.4)$$

$$\text{Cathode: } \frac{3}{2}O_2 + 6H^+ + 6e^- \rightarrow 3H_2O \quad (2.5)$$

$$\text{Overall: } CH_3OH(l) + \frac{3}{2}O_2(g) \rightarrow 2H_2O(l) + CO_2(g) \quad (2.6)$$

C_2H_5OH as a fuel:

$$\text{Anode: } C_2H_5OH + 3H_2O \rightarrow 12H^+ + 12e^- + 2CO_2 \quad (2.7)$$

$$\text{Cathode: } 3O_2 + 12H^+ + 12e^- \rightarrow 6H_2O \quad (2.8)$$

$$\text{Overall: } C_2H_5OH(l) + 3O_2(g) \rightarrow 3H_2O(l) + 2CO_2(g) \quad (2.9)$$

According to those overall reactions, water is the final product in all the fuel cell types. Carbon dioxide, recognized as greenhouse gas, is also produced when operating with alcohol feed. However, ethanol can be easily received from the fermentation of biomass materials, resulting in zero greenhouse gas contribution to the atmosphere.

2.1.1 Thermodynamic Data

From the overall reaction of ethanol as shown in Eq. (2.9), the difference of the standard Gibbs function of formation and enthalpy of formation at 25°C, 1 atm can be calculated as follows:

$$\begin{aligned}\Delta G_f^o &= 3\left(\Delta G_f^o\right)_{H_2O} + 2\left(\Delta G_f^o\right)_{CO_2} - \left(\Delta G_f^o\right)_{C_2H_5OH} - 3\left(\Delta G_f^o\right)_{O_2} \\ &= 3\times(-237.2) + 2\times(-394.4) - (-174.9) - 3\times 0 \\ &= -1325.5 \quad \text{kJ.mol}^{-1}\end{aligned} \quad (2.10)$$

$$\begin{aligned}\Delta H_f^o &= 3\left(\Delta H_f^o\right)_{H_2O} + 2\left(\Delta H_f^o\right)_{CO_2} - \left(\Delta H_f^o\right)_{C_2H_5OH} - 3\left(\Delta H_f^o\right)_{O_2} \\ &= 3\times(-285.8) + 2\times(-393.5) - (-277.7) - 3\times 0 \\ &= -1366.7 \quad \text{kJ.mol}^{-1}\end{aligned} \quad (2.11)$$

Then, the equilibrium standard electromotive force (emf) can be calculated:

$$\begin{aligned}E_{eq}^o &= -\frac{\Delta G_f^o}{nF} \\ &= -\frac{(-1325.5)\times 1000}{12\times 96485} \\ &= 1.145 \text{ V}\end{aligned} \quad (2.12)$$

The theoretical energy density of ethanol can be evaluated as follows:

$$W_e = -\frac{\Delta G_f^o}{3600 \times MW} = -\frac{(-1325.5) \times 1000}{3600 \times 46} = 8\ \text{kWh.kg}^{-1} \quad (2.13)$$

Next, the theoretical efficiency of direct ethanol fuel cell can be computed by:

$$\varepsilon_{rev} = \frac{\Delta G_f^o}{\Delta H_f^o} = \frac{-1325.5}{-1366.7} = 0.969 \quad (2.14)$$

Overall efficiency (ε) at a working E_{cell} of 0.5 V is also evaluated as shown below.

$$\varepsilon = \frac{\varepsilon_{rev} \times E_{cell}}{E_{eq}^o} = \frac{0.969 \times 0.5}{1.145} = 0.423 \quad (2.15)$$

Similarly, thermodynamic calculation of the other fuels, hydrogen and methanol, are also done and the results are displayed in Table 2.1.

Table 2.1 Thermodynamic data of different fuels

Fuel	ΔG_f^o (kJ.mol^{-1})	E^o_{eq} (V)	W_e kWh.kg^{-1}	W_e kWh.m^{-3}	ΔH_f^o (kJ.mol^{-1})	ε_{rev}	ε
H_2	-237	1.229	32.9	2329	-286	0.830	0.338
CH_3OH	-702	1.213	6.1	4819	-726	0.967	0.398
C_2H_5OH	-1326	1.145	8.0	6312	-1367	0.969	0.423

It is noted that liquid hydrogen density at 20 K (70.8 kg.m^{-3}) [37] is used to calculate volumetric theoretical energy density of hydrogen (kWh.m^{-3}). As seen from Table 2.1, ethanol gives the overall efficiency at the working potential of 0.5 V higher than both methanol and hydrogen. In addition, the theoretical energy densities of ethanol are 8 kWh.kg^{-1} and 6312 kWh.m^{-3}, which are close to those of gasoline (13 kWh.kg^{-1} and 9620 kWh.m^{-3}) [38] as compared with the other fuels. As a result, it is reasonable to use ethanol as an alternative energy carrier for gasoline in the near future.

2.1.2 Kinetics Data

The oxidation kinetics of low-molecular weight alcohols such as methanol and ethanol are much slower than that of gaseous hydrogen at low working temperatures of 50-150^{o}C since it needs to break C-H and O-H bonds in methanol to complete 6 electrons released per methanol molecule. In addition, C-C bond in ethanol must be ruptured to

produce carbon dioxide, obtaining 12 electrons released per ethanol molecule finally. Difficulty of cleavage of those bonds is contributed to formation of several intermediate products during the oxidation of both methanol and ethanol. Therefore, knowledge of the adsorbed species, the reaction path, and rate determining step is crucial to increase in the overall reaction rate as well as decrease in the activation overpotential. There are two ways to attain the faster anodic kinetics of ethanol oxidation including increasing working temperature as well as looking for more active electrocatalysts (e.g. binary or ternary Pt-based catalysts). However, the former way is limited by degradation temperature of the membrane electrolyte. For example, the favorite membrane Nafion® type cannot work well if the temperature is above 120°C; thus other membrane types need to be discovered. It was reported that composite polymer membrane such as silica/Nafion films and a polybenzimidazole (PBI) membrane doped with phosphoric acid can be effectively used at a high temperature of 170°C [1].

2.2 Reaction Mechanism of Ethanol Oxidation

As mentioned earlier, the complete oxidation of ethanol gives carbon dioxide as the waste product. Thus, it needs two oxygen atoms which an oxygen atom comes from dissociation of ethanol molecule and the other one is obtained from activation of water molecule to generate the adsorbed H and OH species. Therefore, an active electrocatalyst for the ethanol oxidation must dissociate both of ethanol and water molecules. Due to containing C-C bond in ethanol's molecule, the reaction mechanism of the ethanol oxidation is so complicated, leading to formation of several adsorbed intermediates and by-products.

To understand such mechanism, electrochemical technique (cyclic voltammetry and rotating disc electrodes) has been combined with physicochemical technique including "in situ" spectroscopic methods (infrared [4,18,19,39,40,41,42,43,44] reflectance spectroscopy) to monitor the adsorbed intermediates and "on line" chromatographic technique [4,5,45,46,47] and differential electrochemical mass spectroscopy (DEMS) [6,39,44,48,49] to analyze products and by-products.

2.2.1 On Pt Electrode

As reported by Iwasita and Pastor [50] that two reactive sites, the OH group and the α-carbon atom, in ethanol molecule can interact with a platinum site during the adsorption process. The following reactions are displayed in Eq. (2.16) and Eq. (2.17).

$$Pt + CH_3 - CH_2OH \rightarrow Pt - OCH_2 - CH_3 + H^+ + e^- \quad (2.16)$$

$$Pt + CH_3 - CH_2OH \rightarrow Pt - CHOH - CH_3 + H^+ + e^- \quad (2.17)$$

Then, acetaldehyde can be formed at a potential lower than 0.6 V *vs.* RHE, and subsequently goes to the solution [4].

$$Pt - OCH_2 - CH_3 \rightarrow Pt + CHO - CH_3 + H^+ + e^- \quad (2.18)$$

$$Pt - CHOH - CH_3 \rightarrow Pt + CHO - CH_3 + H^+ + e^- \quad (2.19)$$

However, acetaldehyde can be re-adsorbed on the surface to form an acetyl residue, Pt-$(CO\text{-}CH_3)$, which is then interacted with the adsorbed OH species to produce acetic acid. Otherwise, the C-C bond in such adsorbed species is ruptured to form the adsorbed CO and methyl species [4,40] as seen in Eq. (2.23).

$$Pt + CHO - CH_3 \rightarrow Pt - (CO - CH_3) + H^+ + e^- \quad (2.20)$$

$$2Pt + H_2O \rightarrow Pt - H + Pt - OH \quad (2.21)$$

$$Pt - (CO - CH_3) + Pt - OH \rightarrow 2Pt + CH_3COOH \quad (2.22)$$

$$Pt + Pt - (CO - CH_3) \rightarrow Pt - CO + Pt - CH_3 \quad (2.23)$$

$$Pt - CO + Pt - OH \rightarrow 2Pt + CO_2 + H^+ + e^- \quad (2.24)$$

$$Pt - CH_3 + Pt - H \rightarrow 2Pt + CH_4 \quad (2.25)$$

It was reported that the dissociative adsorption of water on Pt electrode was occurred at a potential higher than 0.6 V *vs.* RHE and methane would be formed at low potential (E < 0.4 V *vs.* RHE) [40]. According to all those equations, the final products of the ethanol oxidation on Pt electrode consist of acetaldehyde, acetic acid, methane and carbon monoxide.

2.2.2 On PtM Electrode

Since water is activated by Pt to form the adsorbed OH residues at relatively high potential, Pt can be rapidly poisoned with the strongly adsorbed CO species. This would block the further adsorption of ethanol molecule on Pt active sites, resulting in deactivation of Pt. Thus, Pt is modified by introducing an oxophilic element, which can provoke adsorption/dissociation of water to form preferential oxygenated species like - OH_{ads} species at lower potential than pure Pt. It has been recognized that ethanol is adsorbed only on Pt sites while water will adsorb on the second metal site, referred to M [32,40]. Thus, M is involved in Eq. (2.21), (2.22) and (2.24) as follows.

$$M + H_2O \rightarrow M - OH + H^+ + e^- \quad (2.26)$$

$$Pt - (CO - CH_3) + M - OH \rightarrow Pt + M + CH_3COOH \quad (2.27)$$

$$Pt - CO + M - OH \rightarrow Pt + M + CO_2 + H^+ + e^- \quad (2.28)$$

From the previous studies, ethanol oxidation has been significantly enhanced on PtM rather than on pure Pt [5,11,19,40,51] because M helps to oxidize not only the strongly adsorbed CO but also the other C1 and C2 intermediate species to liberate the surface of Pt active sites at lower potential. As a result, PtM surface shows higher tolerance to those poisoning adsorbed residues. However, introducing the second metal to Pt have not changed product distribution of such reaction [5,51].

2.3 Electrocatalysts for Ethanol Electrooxidation

2.3.1 Supported Electrocatalysts

2.3.1.1 Pre-Treatment of Carbon Support

Since catalysis is a surface reaction, catalyst with high accessible surface area has superior activity. Thus, an active metal has been generally dispersed on a high surface area support. Carbon blacks, especially Vulcan XC-72R, have been widely used as a catalyst support in low-temperature fuel cells due to having high surface area, low cost and high availability [9]. It also is an electrically conductive material which facilitates electron flow from/to an electrode. Before their use, such supports have been normally pre-treated to modify their texture as well as their surface chemistry. This would affect metal dispersion, metal uptake and catalytic activity. The pre-treatment approach of the support can be categorized into chemical activation (oxidative treatment) and physical activation (thermal treatment).

I. Chemical Activation

As reported in the literature [52,53] that the oxidative treatments of carbons produced different acidic surface groups. Carboxylic and anhydrides are strong acid groups whereas lactones, phenols and carbonyl groups have weaker acid properties. Torres et al. [54] revealed that a high density of both strong and weak acid sites was found on the surface of the HNO_3-treated carbon while H_2O_2- and O_3-treated carbons had a large number of weak acid sites, but low content of strong acid sites. From the H_2PtCl_6 isotherms in liquid phase at 25^oC, an interaction between the chloroplatinic acid and the low acidity carbons, for example the carbons treated with H_2O_2 and O_3, is stronger which enhances Pt dispersion on those treated carbons, and subsequently the catalytic behavior. Fraga et al. [55] have also investigated effect of oxidation treatments of the support on the properties of carbon-supported platinum catalysts such as metal uptake and metal dispersion. The oxidation treatment of the support was carried out in both liquid (5 M HNO_3) and in gas phases (5% O_2/N_2 atmosphere). They found that an increase in the acidity of the support develops the surface concentration of acid groups, leading to the lower pH_{PZC} value of the support. This value implies the surface oxygen complexes and surface charge of carbon. The latter arises from the interaction between the carbon surface and the aqueous solution, and it will determine the strength of metal precursor-support interaction during deposition procedure. Increasing the pH_{PZC} reduces the total oxygen contents of the carbon surface, contributing to higher Pt uptake as well as Pt dispersion. As a result, it implies that the surface basic groups of the supports are anchoring sites for the strong adsorption of platinum when using chloroplatinic acid as the catalyst precursor. This was also confirmed by the results of Kim and Park [56] that the base-treated carbon-supported Pt catalyst has the smallest sizes of 2.65 nm and the highest Pt loading. However, the Pt uptake is much lowered when depositing chloroplatinic acid on the acid-treated carbon. From the electrochemical test, the activity of Pt/C for methanol oxidation would be enhanced in the case of base or neutral treatment rather than in that of acid treatment.

II. Physical Activation

Coloma et al. [57] have investigated heat-treated carbons as supports for platinum catalysts. Heat treatment of the supports was carried out under the inert atmosphere at the temperatures of 1273-2473 K for 1 h. The nitrogen adsorption showed that the

treatment of the carbon black at 1273 K increases BET surface area and slightly modifies the textural structure of the supports. However, at the higher temperatures both BET surface area and micropore volume of the supports are much decreased. As seen from the carbon pH_{slurry}, heat treatment shows basic property on the support surface, due to the pyrolysis of acidic oxygen surface complexes and subsequent the formation of pyrone-type groups when exposure to air at room temperature. The metal dispersion decreases when the pH_{slurry} of the supports becomes more acidic, demonstrating the weak adsorption of the anionic precursor ($PtCl_6^{2-}$) on the carbon surface. Heat treatment could also eliminate the less stable surface oxidized groups of the carbons. This was also found by the other work [58] that carboxylic anhydrides, most of the lactones and some phenol groups are removed by heating the carbon up to 873 K.

2.3.1.2 Preparation of Anode Electrocatalysts

For carbon-supported catalysts, there have been two main routes to prepare such catalysts, including colloidal method and impregnation method [59]. In the colloidal method, metal colloids are formed by adding stabilizer to the catalyst precursors. Such colloids are then deposited onto the carbon support, and the stabilizer is finally decomposed to access the active sites [60]. The other method includes impregnation of the support with the precursors, followed by reduction step in either liquid or gas phase [60]. Since this approach is relatively simple and does not require many types of equipment, it has been widely used for catalyst preparation.

I. Colloidal Method

- Bönnemann Method

In general, Bönnemann method consists principally of three steps as follows: preparing stabilizing agent, adsorbing the colloids on the support and removing the stabilizer by oxidative thermal treatment at 300^{o}C [5]. Tetra(alkyl)ammonium bromide ($(Nalk_4)^+ Br^-$) was firstly mixed together with triethylhydroborate ($K^+ (BEt_3H)^-$) in tetrahydrofuran (THF) solvent. Potassium bromide (KBr) was formed and was then precipitated from the solution of tetraalkylammonium triethylhydroborate ($(Nalk_4)^+ (BEt_3H)^-$). The resulting solution was used as the reducing agent. After reduction of the metal precursors, metal nanoparticles were stabilized by the long alkyl chain of $(Nalk_4)^+ Cl^-$, preventing agglomeration of the metallic particles. The colloid particles were, thereafter, added to the carbon suspension which the carbons were pre-treated for 4 h at 400^{o}C under nitrogen atmosphere. Finally, the stabilizer was removed by thermal treatment under air at 300^{o}C before employing the catalyst. Lamy et al. [19] prepared carbon-supported PtSn catalysts with different Pt:Sn ratios of 4:1 and 9:1. TEM images showed that thermal treatment at 300^{o}C did not cause sintering of the metallic particles with the mean particle size of 2.6±1.3 nm. It was also found by Oliveira Neto et al. [61] that PtRuMo/C (1:1:1) catalyst with thermal treatment in hydrogen gas at 300^{o}C showed superior electrocatalytic activity for both of methanol and ethanol oxidation reactions. This was due to completely removal of the surfactant covering on the Pt active sites to free for adsorption of alcohol molecules. X-ray diffractogram of PtSn/C disclosed that Pt diffraction peaks were not shifted, implying no alloy formation during the co-reduction process. In addition to PtSn/C, other binary Pt-based catalysts such as PtRh/C (4:1), PtRu/C (4:1) and PtRe/C (3:1) were prepared. From the result of linear sweep voltammetry, the onset potential of the ethanol oxidation of all the binary catalysts were negatively shifted as compared to Pt/C. Pt_9Sn_1/C catalyst showed the highest catalytic activity for ethanol oxidation. Furthermore, Rousseau et al. [5] synthesized ternary

$Pt_{86}Sn_{10}Ru_4$/C catalyst together with Pt_9Sn_1/C and Pt/C at the metal loading of 60 wt. %. From DEFC testing, introducing small amount of Ru to Pt_9Sn_1/C could increase nearly two times of the maximum power densities (51mW.cm^{-2} vs 27.5mW.cm^{-2}), but not modify the product distribution of ethanol oxidation.

- Polyol Synthesis

As reported in Bock et al. [62] that heat treatment as low as 220^{o}C was contributed to Pt and Ru phase separation in PtRu alloys, other approaches in which such stabilizer/surfactant is unnecessary are of interest. Polyol process is a technique in which a polyol (a viscous alcohol having at least two hydroxyl groups such as ethylene glycol, glycerol, triethanolamine and trihydroxymethylaminomethane) is preferably used as both solvent and reducing agent to minimize particle diffusion as well as inhibit particle growth [63,64]. Since glycolate obtained from an oxidation of ethylene glycol in Figure 2.2 acts as a stabilizer by forming chelate-type complexes via its carboxyl groups [62,65], such method does not require any types of stabilizer. In addition, the glycolate anion can be easily removed by heat treatment below 160^{o}C, resulting in liberation of the active sites without altering the properties of PtRu catalysts.

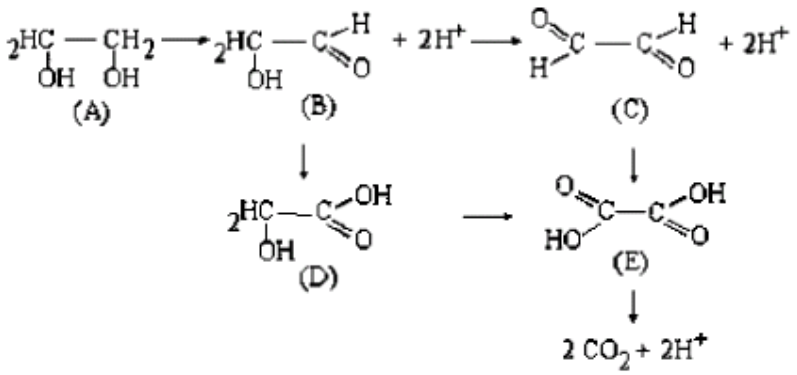

Figure 2.2 Oxidation mechanism of ethylene glycol (A=Ethylene glycol, B and C=Aldehyde, D=Glycolic acid, E=Oxalic acid)

It was also found that the concentration of glycolate anion increased in accordance with final pH of the solution between 2 and 6, but the size of PtRu/C particle was reduced from 4 nm to 0.7 nm [62]. Similarly, Oh et al. [65] disclosed that the concentration of glycolate anion, which is a function of pH, affects greatly not only controlling Pt particle size but also loading Pt on carbon. The Pt loading on the carbon support decreases with increasing concentration of NaOH in the colloid solution. As a result, pH of the colloid solution should be high sufficient to obtain small metal particle size as well as high metal loading on the support. Furthermore, effect of water content in ethylene glycol solution, pH value and reaction time of SnO_2 formation on the particle sizes of SnO_2 colloid was studied by Jiang et al. [66]. The result disclosed that particle sizes of SnO_2 colloid increases with increasing water content in ethylene glycol solution, decreasing pH of the colloid and increasing reaction time. XRD pattern of SnO_2 nanoparticles shows reflection peaks of SnO_2 (110), (101), (211) and (301) at the corresponding positions (PDF No. 411445).

The carbon-supported PtSn (2:1) catalyst was prepared by a modified polyol method with/without further reduction in H_2/Ar atmosphere at 600^{o}C for 2 h [13]. From XRD analysis, typical reflection peaks of a crystalline Pt with face-centered cubic (fcc)

structure were observed in both Pt_2Sn_1/C catalysts. However, further reductive treatment was contributed to great extent of PtSn alloy formation, as shown by three more peaks for PtSn (102), PtSn (110) and PtSn (202). This was also confirmed by the existence of Sn in zero-valence after reductive treatment in TPR analysis, possibly accelerating formation of the PtSn alloy. The mean particle size of Pt_2Sn_1/C catalyst estimated from TEM is 1.8 nm, but it is increased by 3.9 nm after the reduction owing to sintering of the metal atom at the high temperature. From cyclic voltammetry and single cell test, Pt_2Sn_1/C catalyst with reductive treatment showed interior activity of ethanol oxidation and DEFC performance. Thus, it can be suggested that Pt and multivalent Sn are the active species for ethanol oxidation. Song et al. [46] synthesized Pt_2Sn_1/C catalyst by direct decoration of Pt/C with Sn. XRD patterns revealed that reflection peaks of SnO_2 in addition to four typical diffraction peaks of fcc Pt structure were found remarkably. The Pt_2Sn_1 catalyst prepared by direct decoration of Pt/C with Sn has the mean particle size of 2.6 nm. In addition, it gives the maximum power density of 47 $mW.cm^{-2}$, which is smaller than that prepared by co-reduction (61.2 $mW.cm^{-2}$). It was because addition of Sn precursor to commercial Pt/C caused partial covering Pt active sites by the poor electrically conductive SnO_2. Jiang et al. [22] developed preparation of Pt_3Sn_1/C catalysts by a successive reduction method in comparison to by the conventional co-reduction method. From XRD result, both tetragonal structure of SnO_2 and fcc structure of Pt were found in Pt_3Sn_1 prepared by the successive reduction method, and the lattice parameter of Pt in the catalyst was nearly the same as that of pure Pt, implying no penetrating Sn atom into Pt lattice. Thus, PtSn alloy was not formed as confirmed by the existence of SnO_2 nanoparticles in the vicinity of Pt particles from HRTEM image. Table 2.2 shows the mean particle size estimated from XRD measurement, open circuit voltage and DEFC performance of the as-prepared PtSn catalysts by different preparation routes.

Table 2.2 Particle sizes, open circuit voltage and the maximum power density of DEFC of the Pt_3Sn_1/C catalysts

Synthesis route	Catalyst	Mean metal size (nm)	Open circuit voltage (mV)	Maximum power density ($mW.cm^{-2}$)
Co-reduction	Pt_3Sn_1/C	2.6	799	47.0
Successive reduction	Pt_3Sn_1/C	2.1	819	79.5

As seen from Table 2.2, the Pt_3Sn_1/C catalyst prepared by the successive reduction procedure has smaller particle sizes than that of the co-reduction method. The performance of fuel cell operating with ethanol disclosed that the as-prepared Pt_3Sn_1/C catalyst by a successive reduction method gave much higher maximum power density because SnO_2 sites could promote activation of water molecule to form the oxygen-containing species. Such species help to oxidize the adsorbed CO species to free Pt active sites, and consequently enhance adsorption/dehydrogenation of ethanol molecules. The atomic ratio of Pt:Sn in Pt/SnO_x/C catalysts was also varied by 5:5, 6:5, 7:3 and 8:2 [6]. Their particle sizes from TEM images are in the narrow range of 2.2 to 2.8 nm. From single DEFC evaluation, the binary PtSn (7:3) catalyst showed the highest maximum power density, which was 57 $mW.cm^{-2}$. Furthermore, an effect of reducing agents, which are ethylene glycol (EG), $NaBH_4$ and HCHO, on electrocatalytic activity of PtSn/C (3:1) catalyst was investigated through the co-reduction method [67]. The mean particle sizes of Pt_3Sn_1/C catalyst are ranked as follows: $NaBH_4$ (4.2 nm) > HCHO (2.3 nm) > EG (1.8 nm). Only fcc crystal structure of Pt was found in those three samples. The lattice parameter of Pt of PtSn/C(EG), PtSn/C(HCHO) and PtSn/C($NaBH_4$) was 0.3946 nm, 0.3937 nm and 0.3920 nm, respectively. It seems that

part of Sn enters the Pt lattice, and consequently the crystal lattice of Pt is modified in the case of using EG and HCHO as the reducing agent. TPR result revealed that the reduction of Sn^{2+} and Sn^{4+} in addition to that of Pt oxide was observed only in PtSn/C(EG). It indicates that part of Sn other than entering the Pt lattice exists in its oxide form. PtSn/C(EG) showed higher voltammetric current and DEFC performance than the other samples. The controversial result was found by Zhu et al. [47] that PtSn/C-$NaBH_4$ rather than PtSn/C-EG shows higher lattice parameter of Pt, which is 0.3997 nm as compared with 0.3961 nm. The enhanced activity for EOR as well as DEFC performance was seen in PtSn/C-$NaBH_4$. In addition, PtSn/C-EG exhibits superior performance of fuel cell to $PtSnO_2$/C from the successive reduction method. As a result, it can be deduced that non-alloyed SnO_2 oxidizes the adsorbed CH_3CO species to CH_3COOH via bi-functional mechanism while the PtSn alloy phase accelerates the rate of adsorption/dehydrogenation of ethanol to CH_3CHO, and hence promotes the efficiency of EOR by the electronic effect.

In addition to PtSn/C catalyst, other binary Pt-based catalysts including PtRu/C, PtW/C and PtPd/C were also examined by Zhou et al. [8]. All those catalysts were prepared by the modified polyol process with Pt:M atomic ratio of 1:1. The XRD patterns of these catalysts showed obviously characteristic structure of a crystalline Pt (fcc) phase without other diffraction peaks for the metallic or oxide phases of those corresponding metals. Introducing Ru and Pd to Pt was contributed to extraction of Pt lattice parameter, but the opposite result was found on PtSn/C and PtW/C. The results from TEM, XRD, CV and DEFC of these catalysts are illustrated in Table 2.3. The sizes of the binary Pt-based catalysts estimated by TEM and XRD techniques are nearly the same. Thus, the modified polyol process could prepare well-sized nanocatalysts. Pt_1Sn_1/C catalyst gave higher both peak current density and maximum power density than those other binary catalysts. For PtSn/C catalyst, atomic ratio of Pt:Sn was also investigated as shown in Table 2.3. Pt_2Sn_1/C catalyst showed the highest the maximum power density of 61.2 $mW.cm^{-2}$, probably due to supplying sufficient $–OH_{ads}$ species and having adequate Pt active sites for ethanol oxidation. Furthermore, Pt_1Ru_1/C catalyst was modified by introducing W, Mo and Sn [68]. It was observed that all those ternary catalysts had the enhanced DEFC performance; however their performance was still lower than the binary Pt_1Sn_1/C catalyst.

Table 2.3 Summary of TEM, XRD, CV and DEFC results of Pt-based catalysts

Catalyst	Mean particle size (nm)		a_{fcc} (nm)	Peak potential (mV *vs.* SCE)	Peak current density ($mA.cm^{-2}$)	OCV (mV)	MPD ($mW.cm^{-2}$)
	TEM	XRD					
Pt/C	2.7	2.6	0.3916	800	19.5	547	10.8
Pt_1Pd_1/C	3.0	2.8	0.3906	668	24.4	500	12.0
Pt_1W_1/C	3.4	3.2	0.3922	755	49.4	540	15.9
Pt_1Ru_1/C	1.9	1.8	0.3883	547	25.8	677	28.5
PtSn/C							
1:1 (50%)	2.3	2.1	0.3987	710	56.2	811	52.2
3:2 (40%)	2.2	1.9	0.3974	na	na	820	55.8
2:1 (33%)	3.0	2.6	0.3956	na	na	810	61.2
3:1 (25%)	2.2	1.9	0.3953	na	na	800	43.0
4:1 (20%)	2.3	1.9	0.3938			730	34.6
$Pt_1Ru_1W_1$/C	3.0	na	na	na	na	698	38.5
$Pt_1Ru_1Mo_1$/C	3.0	na	na	na	na	720	31.2
$Pt_1Ru_1Sn_1$/C	3.0	na	na	na	na	760	39.2

Remarks: a_{fcc} = Lattice parameter of Pt
OCV = Open circuit voltage
MPD = Maximum power density
na = non available

Spinace et al. [69] prepared binary PtSn/C electrocatalysts with various Pt:Sn ratios of 75:25, 50:50 and 25:75 and ternary $Pt_{50}Sn_{40}Ni_{10}$/C electrocatalyst by the alcohol-reduction process using ethylene glycol as both solvent and reducing agent. All these catalysts displayed Pt (fcc) diffraction peaks and cassiterite SnO_2 phase, except $Pt_{25}Sn_{75}$/C catalyst in which manifested reflection peaks of cassiterite SnO_2 phase remarkably. The particle sizes of $Pt_{75}Sn_{25}$/C, $Pt_{50}Sn_{50}$/C and $Pt_{50}Sn_{40}Ni_{10}$/C catalysts determined from XRD analysis are 2.4 nm, 2.0 nm and 2.4 nm, respectively. The actual composition of the corresponding metals in those catalysts obtained from EDX analysis was nearly the same as the intended values. As seen from cyclic voltammograms, $Pt_{50}Sn_{50}$/C catalyst shows higher electroactivity of ethanol oxidation in the binary catalysts, but less than ternary $Pt_{50}Sn_{40}Ni_{10}$/C catalyst due to the synergetic effect of Sn and Ni oxide species. Oliveira Neto et al. [21] also prepared $Pt_{50}Ru_{50}$/C, $Pt_{50}Sn_{50}$/C and PtSnRu/C with different Pt:Sn:Ru ratios of 50:40:10, 50:25:25 and 50:10:40 using the similar synthesis route. The metal compositions of all those catalysts from EDX were in agreement with the nominal values. The particle sizes of the Sn-rich samples, including $Pt_{50}Sn_{50}$/C, $Pt_{50}Sn_{40}Ru_{10}$/C and $Pt_{50}Sn_{25}Ru_{25}$/C, are in the range of 2.7-3.3 nm while the Ru-rich samples ($Pt_{50}Ru_{50}$/C and $Pt_{50}Sn_{10}Ru_{40}$/C) give bigger particle sizes of 4.0-4.7 nm. XRD result revealed that binary PtSn and PtRu alloys and ternary PtSnRu alloy are formed, as seen in the change of Pt-Pt distance. From chronoamperometric measurement, $Pt_{50}Sn_{50}$/C catalyst showed superior activity towards ethanol oxidation to the binary PtRu/C and even all ternary PtSnRu/C catalysts.

Liu et al. [11] developed a novel synthesis method of Pt/C and PtRu/C nanoparticles by a microwave-assisted polyol process, and transferred to a toluene solution of decanthiol. The carbon support is then added to the toluene solution to adsorb the thiolated Pt and Pt-Ru colloids. From XRD patterns, all Pt and PtRu catalysts, except $Pt_{23}Ru_{77}$, showed fcc lattice structure of crystalline Pt. Mean particle sizes of Pt/C and $Pt_{52}Ru_{48}$/C catalysts from TEM images were 4.7 nm and 4.5 nm, respectively with relative narrow size distribution of 3-6 nm. From single DEFC test, $Pt_{52}Ru_{48}$/C provided the highest maximum power density of 62 $mW.cm^{-2}$, which was two times greater than $Pt_{50}Ru_{50}$/C in the literature [8] owing to uniformity and speed of microwave heating.

II. Impregnation Method

Platinum based electrodes such as Pt/C, PtSn/C and PtRe/C were prepared using the co-impregnation-reduction method [45]. The powder was then calcined under air for 4 h at 300^{o}C and was reduced under hydrogen atmosphere at the same condition. The prepared Pt/C has the particle sizes of 1.5 nm and 5 nm. In the PtSn/C catalysts, Pt:Sn ratio of 100:20 seems to be the most active catalyst for EOR, and it gives a maximum power density of 35 $mW.cm^{-2}$, which is much higher than Pt/C and PtRe/C (100:20). Lima et al. [18] also synthesized carbon-supported Pt, Pt-Ru (1:1), Pt-Rh (1:1) and Pt-Ru-Rh (1:1:1) nanoparticles by impregnation, followed by treatment in a H_2 atmosphere at 500^{o}C for 1 h. With using Sherrer's equation, the averages crystallite sizes of the corresponding catalysts are 2.6 nm, 3.6 nm, 7.3 nm and 5.5 nm, respectively. The larger size in the Pt-Rh/C sample may be due to the alloy formation, as seen from a lattice contraction when introducing Rh to Pt. On the other hand, it has no evidence of the shift of Pt reflection peaks in both Pt-Ru/C and Pt-Ru-Rh/C samples. In addition to fcc

structure of crystalline Pt, reflection peaks due to metallic Rh or to their oxides were not found. Bi-metallic and tri-metallic Pt-Sn/C, Pt-Ir/C and Pt-Ir-Sn/C catalysts were also prepared by impregnation reduction method under hydrogen atmosphere [70]. It was noted that metal compositions in those catalysts were in the weight ratio. From TEM images, the mean particle sizes of the catalysts are 7.34 nm for Pt-Sn/C (20:20), 3.79 nm for Pt-Ir/C (20:20), 3.91 nm for Pt-Ir-Sn/C (10:15:15), 4.86 nm for Pt-Ir-Sn/C (20:10:10) and 6.54 nm for Pt-Ir-Sn/C (20:5:15). The maximum power density of the corresponding catalysts is 22.4 $mW.cm^{-2}$, 7.95 $mW.cm^{-2}$, 20.2 $mW.cm^{-2}$, 23.4 $mW.cm^{-2}$ and 29.13 $mW.cm^{-2}$, respectively, which is greater than that of Pt/C (4.56 $mW.cm^{-2}$).

Colmati et al. [71] prepared carbon-supported $Pt_{75}Sn_{25}$ catalyst by reduction with formic acid, and the resulting sample was thermally treated at 200^{o}C and 500^{o}C. The findings from XRD, TEM and fuel cell test are tabulated in Table 2.4. It was evidenced from lattice parameter of Pt that PtSn alloys were formed in those corresponding samples. The prepared $Pt_{75}Sn_{25}$/C catalyst has the average particle size of 4.5 nm in which its particle size does not change after heat treatment at 200^{o}C. However, heat treatment at 500^{o}C leads to increasing the particle size to 7.7 nm. The $Pt_{75}Sn_{25}$/C with heat treatment at 200^{o}C showed superior activity of ethanol oxidation and DEFC performance to those catalysts with/without heat treatment at 500^{o}C and even to commercial $Pt_{75}Sn_{25}$/C, probably owing to the smaller particle sizes and effective removal of impurities by the thermal treatment. The Pt_1Sn_1/C, Pt_1Ru_1/C, $Pt_1Sn_1Ru_{0.3}$/C and $Pt_1Sn_1Ru_1$/C were also produced by the same synthesis route [72]. The XRD patterns shows four characteristic peaks for Pt (fcc) structure and tetragonal SnO_2 phase in those Sn-containing samples. The mean particle size of Pt_1Sn_1/C is 6.6 nm, which is much bigger than those of ternary PtSnRu catalysts. From EDX analysis, the actual compositions of the Pt_1Sn_1/C and $Pt_1Sn_1Ru_{0.3}$/C are very close to the nominal one, but are lower than the expected values in Pt_1Ru_1/C and $Pt_1Sn_1Ru_1$/C. From linear sweep voltammetry and single DEFC evaluation, $Pt_1Sn_1Ru_{0.3}$/C exhibited higher catalytic activity for ethanol oxidation and DEFC performance. This was ascribed to the synergetic effect of Ru and Sn oxides. Furthermore, catalytic activities of binary Pt_1Rh_1/C and ternary $Pt_1Sn_1Rh_{0.3}$/C and $Pt_1Sn_1Rh_1$/C catalysts on ethanol oxidation were investigated [17]. From linear sweep voltammograms, the binary Pt-Sn catalyst gave higher catalytic activity for ethanol oxidation at the potentials lower than 0.45 V *vs.* RHE, but at the potentials higher than 0.45 V *vs.* RHE the superior activity EOR was observed on the ternary Pt-Sn-Rh catalysts.

Table 2.4 Summary of TEM, XRD and DEFC results of the catalyst of Colmati group

Sample	Lattice parameter (nm)	Mean particle size (nm)		Maximum power density ($mW.cm^{-2}$)
		XRD	TEM	
$Pt_{75}Sn_{25}/C$	0.3954	3.9	4.5±1.4	8.1
$Pt_{75}Sn_{25}/C$-200°C	0.4001	4.9	4.4±1.5	19.6
$Pt_{75}Sn_{25}/C$-500°C	0.4006	29	7.7±1.8	7.2
$Pt_{75}Sn_{25}/C$-ETEK	0.4002	4.1	4.2±1.3	12.1
Pt/C-ETEK	0.3915	2.9	3.0±1.2	4.7
** Cell operating temperature: 90°C				
Pt_1Sn_1/C	0.3973	3.1	6.6±1.7	28.0
$Pt_1Sn_1Ru_{0.3}/C$	0.3956	2.7	3.2	32.0
$Pt_1Sn_1Ru_1/C$	0.3939	2.3	3.2	21.0
Pt_1Ru_1/C	0.3909	4.6	na	na
Pt_1Ru_1/C-ETEK	0.3887	3.2	na	24.0
** Cell operating temperature: 110°C				
Pt_1Sn_1/C	0.3973	3.1	6.6±1.7	na
$Pt_1Sn_1Rh_{0.3}/C$	0.3965	2.4	3.8±1.0	na
$Pt_1Sn_1Rh_1/C$	0.3944	1.8	3.7±1.0	na
Pt_1Rh_1/C	0.3890	1.4	2.8±0.6	na

The Pt_1Ru_1/C and $Pt_6Ru_3Ni_1/C$ samples were synthesized via chemical reduction with $NaBH_4$ solution [12]. Only Pt (fcc) diffraction peaks are found in the XRD patterns of those catalysts. The lattice parameter of Pt is extracted when introducing Ru and Ni to Pt, implying that Ru and Ni atoms could enter Pt lattice. Both Pt_1Ru_1/C and $Pt_6Ru_3Ni_1/C$ electrocatalysts have the same particle sizes, which are about 4.5 nm. The EDX compositions of all those catalysts are almost similar to the intended values. Electrochemical test disclosed that $Pt_6Ru_3Ni_1/C$ showed slightly superior catalytic activity of ethanol oxidation to the Pt_1Ru_1/C. Similarly, Pt_1Ru_1/C and $Pt_6Ru_3Mo_1/C$ catalysts were also prepared [73]. It was confirmed by XRD analysis that binary and ternary alloys were formed in those samples. The mean diameter of Pt_1Ru_1/C and $Pt_6Ru_3Mo_1/C$ particles is 2.7 nm and 2.5 nm, respectively. The XPS analysis showed that Pt and Ru are in metallic state whereas Mo is in oxidation state. From electrochemical measurement, $Pt_6Ru_3Mo_1/C$ shows greater activity for ethanol oxidation as well as stronger CO tolerance than that of Pt_1Ru_1/C. This could be described by capability of water activation on Mo and also modification of Pt electronic states.

2.3.2 Unsupported Electrocatalysts

High surface area and small metal particles with 2-3 nm in size of Pt-based catalysts have been extensively used in solid polymer electrolyte fuel cell (SPEFC) [31,74]. With the limitation of electrode thickness for achieving high performance of fuel cell, unsupported catalysts are more favorable since they can make the catalyst layer thinner even at high metal loading of 40 wt.%, contributing to decrease in the electrode resistance. However, the conventional Pt black has small surface area of 20-26 $m^2.g^{-1}$ [24], which would give the low activity for oxidation of small organic molecules. Recently, great efforts have focused on preparation of highly ordered, porous nanostructured materials, which would be expected to be a new alternative catalyst particularly for SPEFC due to their characteristics such as high surface area and uniform pore diameter. Initially, Attard et al. [24] have prepared nanostructured Pt particles via chemical reduction of hexachloroplatinic acid in an aqueous domain of a hexagonal building block of a nonionic surfactant, octaethylene glycol monohexadecyl

ether ($C_{16}(EO)_8$). It is realized that this surfactant is a lyotropic liquid crystal material, and hence different nanostructures in hexagonal phase, cubic phase and lamellar phase are formed, depending on an amphiphile concentration and temperature. Such particles obtained have 3 nm in pore sizes separated by the wall thickness of 3 nm. Furthermore, mesoporous Pt film have been produced using electrodeposition of such platinum precursor from the liquid crystalline templating mixture onto a gold electrode [25]. Other metals such as tin [26] and nickel [27] have been also investigated by the same preparation route, but using different surfactants. Octaethylene glycol monohexadecyl ether was used in preparation of mesoporous tin film while inexpensive, commercial Brij surfactant was used in that of mesoporous nickel/nickel oxide electrodes.

For preparation of mesoporous precious metal catalysts in fuel cell application, Jiang and Kucernak have followed the synthesis route in Attard's work [24]. Beginning with production of Pt nanoparticle, they found that electrocatalytic activity for methanol oxidation reaction (MOR) was enhanced on the mesoporous Pt in comparison to a commercial unsupported Pt from Johnson-Matthey Plc [75]. This would result from having periodic nanostructure along with high surface area of the prepared Pt. Mesoporous PtRu and PtPdRuOs alloys have been therafter prepared, due to their ability to tolerate the strongly adsorbed CO species as a poison found during the oxidation reaction of methanol. The specific active surface area of the PtRu and PtPdRuOs alloy was 80 $m^2.g^{-1}$ [29] and 105 $m^2.g^{-1}$ [31], respectively, which was much higher than that of Pt (47 $m^2.g^{-1}$) [28]. Such nanoparticles have porous structure with their pore sizes of 2.4-3.6 nm in diameter. As a result, they suggested that those nanostructured materials are prospective catalysts for electro-oxidation of methanol and formic acid [30].

With the modified procedure of Jiang and Kucernak's work, Yamauchi et al. [76,77] have synthesized mesoporous Pt-Ni alloy particles in addition to mesoporous Pt. They revealed that the framework of hexagonally ordered mesoporous Pt particles consisted of the connected nanoparticles with an average size of ca. 3 nm. The mesoporous Pt-Ni alloys had small particles less than 100 nm in size with their specific surface area higher than 40 $m^2.g^{-1}$.

2.4 Electrocatalyst Characterization

2.4.1 X-ray Diffraction (XRD)

X-ray diffraction is a rapid, non-destructive technique. The widespread uses of this technique are in phase identification, crystallinity, lattice parameters and size and strain broadening [78]. The principle of X-ray diffractometer is illustrated in Figure 2.3. An X-ray beam, often produced from a Cu Kα source which has wavelength of 1.542 Å, is first filtered to produce a nearly monochromatic beam, and then hits a powder sample. This leads to emission, absorption, scattering or diffraction. A detector mounted on a goniometer is rotated around such sample with the same speed at the angle of 0 to 90^o, while the intensity of radiation is recorded as a function of diffraction angle.

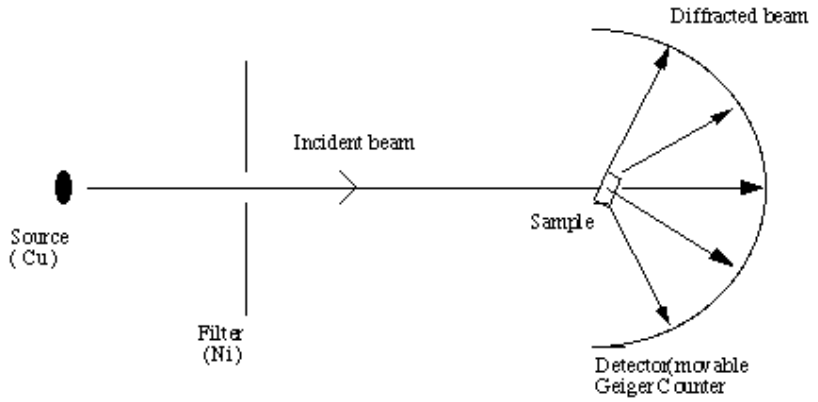

Figure 2.3 Principle of X-ray Diffractometer [79]

The diffraction of the X-rays beam is displayed in Figure 2.4 and also can be determined by using Bragg's law, as shown in Eq. (2.29).

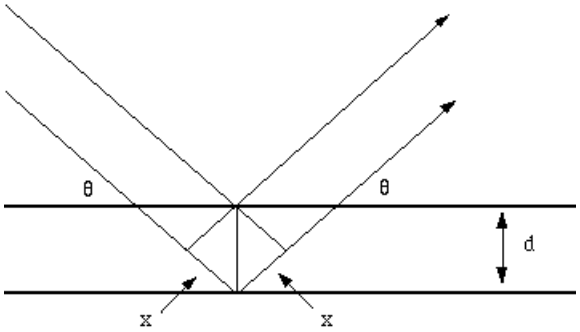

Figure 2.4 Schematic of the diffracted beam at the crystal plane [79]

$$n\lambda=2d\sin\theta \tag{2.29}$$

where λ = the wavelength of the X-rays
d = the distance between two lattice planes
θ = the angle between the incident X-rays and the normal lattice plane
n = an integer called the order of the reflection (i.e. 1, 2, 3,…)

In addition, the size and strain broadening of the crystallites can be calculated from combing the two equations known as the Hall-Williamson method.

$$\beta\cos\theta = \frac{K\lambda}{D}+\eta\sin\theta \tag{2.30}$$

From Eq. (2-30), the term of η represents the strain in the crystallites and the term of D is the size of the crystallites. As compared to the effect of size broadening, the effect of crystal strain can be normally negligible. The average particle size (D) is, therefore, estimated by the Debye-Scherrer formula in Eq. (2.31).

$$D = \frac{K\lambda}{\beta\cos\theta} \qquad (2.31)$$

where D = the average particle size
λ = the wavelength of the X-rays
K = a constant (typically ranges from 0.8-1.39)
β = width of the peak at the half height
θ = the angle between the incident X-rays and the normal lattice plane

2.4.2 Transmission Electron Microscope (TEM)

Transmission electron microscope is a favorable technique to measure particle sizes and size distribution of a catalyst. It uses electron beam, which has high energy and high intensity, as a light source. The principle of TEM is illustrated in Figure 2.5. The electron beam is first passed through a condenser to produce more intensity of electron beam. Then, the electron beam strikes the sample, resulting in a part of transmitted electron. The transmitted portion is, thereafter, focused by the objective lens into an image. Finally, the image hits the viewing screen and light is produced, allowing the user to see the image. The darker areas in the image present the fewer transmitted electrons incident on the screen; however the lighter areas in the image display the more transmitted electrons.

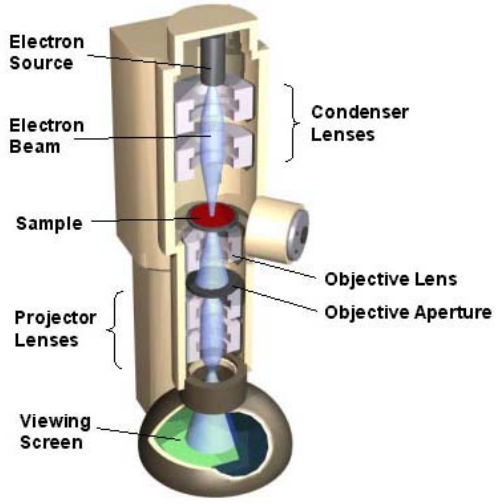

Figure 2.5 Main components of TEM [80]

2.4.3 Energy Dispersive X-ray Spectroscopy (EDX)

Energy dispersive X-ray spectroscopy is a simple, powerful technique used to determine the elemental compositions. This equipment can be coupled with several equipments such as Scanning Electron Microscopy (SEM), Transmission Electron Microscopy (TEM) and Scanning Transmission Electron Microscopy (STEM) [81], which act as an electron source. When an electron beam strikes a specimen, an electron in an inner shell may be excited and then be ejected from the shell, creating an electron hole. Thus, an electron from an outer shell fills the hole, and the difference between the higher and the lower energy shells may be released in the form of an X-ray, which is measured by an energy-dispersive spectrometer. The X-rays are characteristic of the elements in the

sample, forming peaks in the spectrum. The technique is non-destructive and has a sensitivity of >0.1% for elements heavier than C [82]. An example of spectrum from EDX analysis is displayed in Figure 2.6.

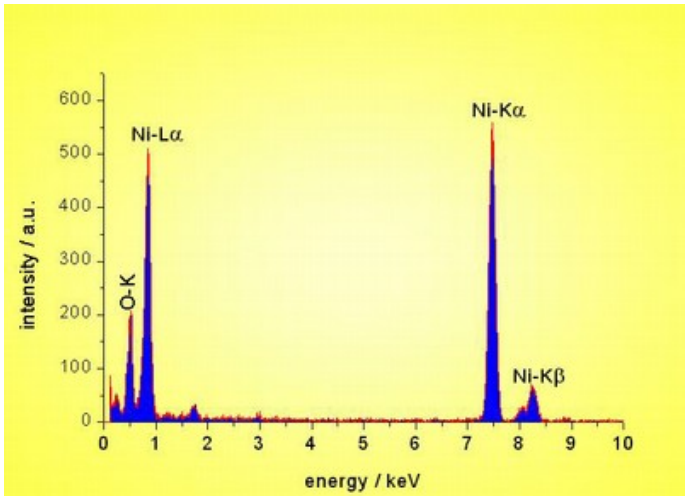

Figure 2.6 Example of EDX spectrum [83]

2.4.4 Inductively Coupled Plasma-Atomic Emission Spectroscopy (ICP-AES)

Atomic Emission Spectroscopy, which uses inductively coupled plasma (ICP) as an energy source, is called Inductively Coupled Plasma-Atomic Emission Spectroscopy. This technique is used to determine elemental compositions in trace analysis. A sample is supplied by an energy source, and consequently electrons in ground state are moved to an excited state, which is unstable. The electrons are then moved down to their ground state or less energetic energy level, leading to emission of energy in the form of photon as shown below.

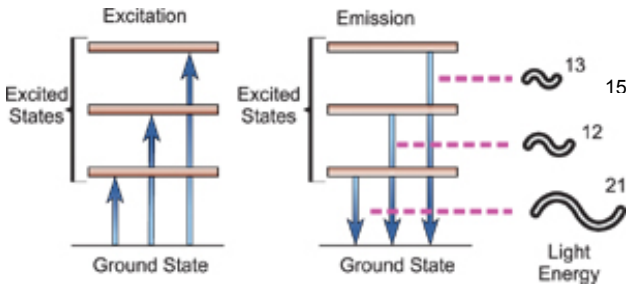

Figure 2.7 Emission of a characteristic wavelength of light [84]

Due to unique electronic structure of individual element, the wavelength of emitted light is characteristic of the element. To know compositions of the element, the intensity of light emitted at the wavelength of the element is measured.

2.5 Electrochemical Measurement

2.5.1 Cyclic Voltammetry (CV)

Cyclic voltammetry is a type of potentiodynamic electrochemical measurement [85]. This technique is used to study a redox system. A potential is supplied to the system, and the current response due to a redox reaction is measured. In the forward scan, the reduced species are oxidized, producing the anodic current from the oxidation reaction. Therefore, the current measured will increase exponentially as increasing the potential until depletion of the analyte concentration. The product generated during the forward scan is available at the electrode surface for the reverse scan. The oxidized species are then reduced in the reverse scan, producing the cathodic current from the reduction reaction. A typical cyclic voltammogram is displayed in Figure 2.8.

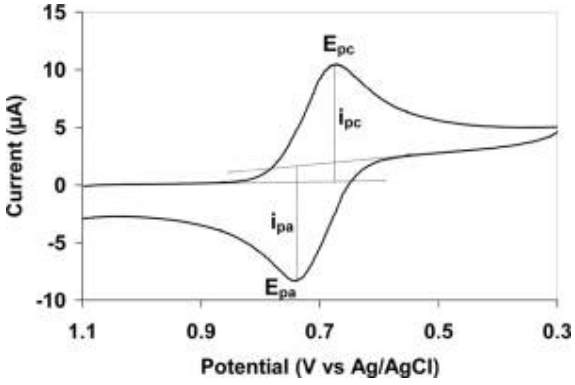

Figure 2.8 Typical cyclic voltammogram [85]

At the anodic peak as shown in Figure 2.8, the potential is sufficiently high to oxidize all of the reduced species that reach the electrode surface. Thus, the anodic current depends significantly on the diffusion of the analyte from the bulk solution to the electrode surface. Three electrodes including reference electrode, working electrode, and counter electrode are preferable to use in cyclic voltammetry. The potential is measured between the reference electrode and the working electrode while the current is measured between the working electrode and the counter electrode.

2.5.2 Chronoamperometry (CA)

Chronoamperometry is one of the potential step techniques which are used to examine kinetics of heterogeneous reactions. The potential of the working electrode is changed instantaneously from a value at which no faradaic current occurs, E_{start}, to a potential, E_{end}, at which any electrode reaction occurs. The profile of the potential-time for a single potential step of chronoamperometry experiment is displayed in Figure 2.9.

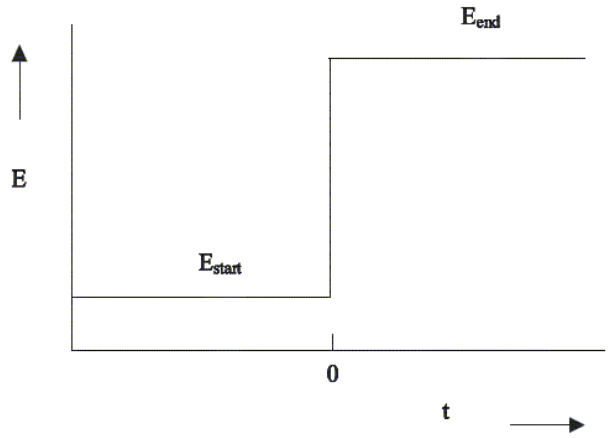

Figure 2.9 Potential-time profile for a single potential step

The current response is monitored as a function of time shown in Figure 2.10. It can be seen from Figure 2.10 that there are three types of the current-time transient. The reaction in curve (a) is diffusion controlled, as given by the Cottrell equation:

$$I = \frac{nFD^{1/2}c_0^{\infty}}{\pi^{1/2}t^{1/2}} \qquad (2.32)$$

In this case, the stationary working electrode and the unstirred solution are used. It is assumed to be linear diffusion to a planar electrode. The curve (b) is obtained when the rate constant of such reaction is very small, and consequently diffusion does not play an important role in determining the rate. In the case of mixed control where the rate of diffusion is comparable to that of electron transfer, the *I-t* response has the form as shown in curve (c).

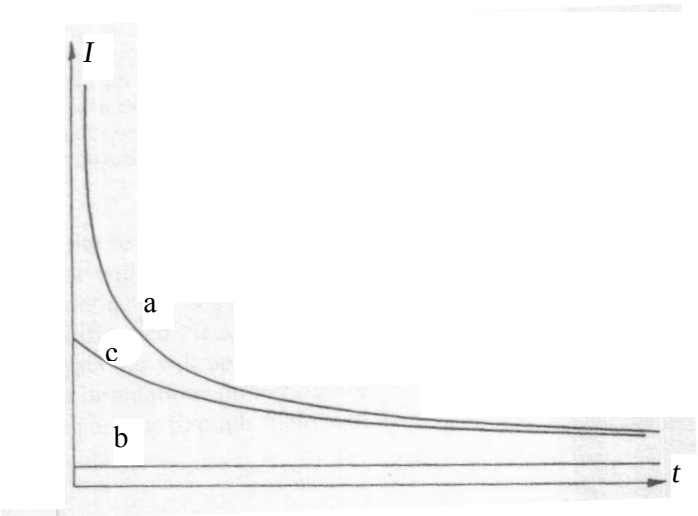

Figure 2.10 *I-t* response for a potential step experiment [86]: (a) the reaction is diffusion controlled, (b) the reaction is kinetically controlled, (c) there is mixed control

CHAPTER 3 METHODOLOGY

3.1 Chemicals

The main chemicals used to prepare both supported and unsupported catalysts are as follows:
For supported catalysts,
- Support: Vulcan XC-72R (Cabot Corp.)
- Catalyst precursors: chloroplatinic acid hexahydrate ($H_2PtCl_6.6H_2O$, ACS reagent, ≥37.5% Pt basis) and tin (II) chloride dehydrate ($SnCl_2.2H_2O$, ACS reagent, 98%) from Sigma-Aldrich, Inc.
- Solvent and reducing agent: ethylene glycol ($C_2H_6O_2$, ReagentPlus®, ≥99%) from Sigma-Aldrich, Inc.
- pH adjuster: sodium hydroxide (NaOH) from Carlo Erba Reagenti

For unsupported catalysts,
- Catalyst precursors: chloroplatinic acid hexahydrate ($H_2PtCl_6.6H_2O$, ACS reagent, ≥37.5% Pt basis), tin (II) chloride ($SnCl_2$, reagent grade, 98%), ruthenium (III) chloride ($RuCl_3.xH_2O$, ReagentPlus) and osmium (III) chloride hydrate ($OsCl_3.xH_2O$) manufactured from Sigma-Aldrich, Inc.
- Surfactant: polyethylene glycol hexadecyl ether (Brij® C10) from Sigma-Aldrich, Inc.
- Reducing agent: Zinc (ACS reagent, -30-+100 mesh, ≥99.8%, granular) from Sigma-Aldrich, Inc.

3.2 Electrocatalyst Preparation

3.2.1 Supported Electrocatalysts

Vulcan XC-72R carbon black was first pre-treated by chemical/thermal treatment. For chemical treatment, 5 M HNO_3 was added to the fresh carbon, which was then heated at its boiling point for 5 h. Afterwards, the solution was centrifuged, washed with copious amounts of deionized water, and dried at 150°C overnight. For thermal activation, the virgin carbon was heated at 600°C under N_2 atmosphere for 30 min [10]. The HNO_3-treated and heat-treated carbon supports were denoted as NA-C and HT-C, respectively.
The PtSn/C electrocatalysts were prepared by a successive reduction procedure as described in the literature [22]. In brief, SnO_2 colloid was initially prepared by dissolving tin (II) chloride dihydrate in analytical grade ethylene glycol. Then, the slurry was heated up to 190°C and kept at this temperature until the solution became a light-yellow colloid. The required amount of SnO_2 colloid was added to chloroplatinic acid hexahydrate with continuous stirring for 15 min. Afterwards, the pH of the solution was adjusted above 11 with 1 M NaOH. The mixture was heated to 160°C and kept at this temperature for 2 h while passing N_2 through the system to eliminate oxygen and organic byproducts. The dispersed Vulcan XC-72R pre-treated with the different methods was then added to the solution; and was further stirred for 2 h. Finally, the solution was centrifuged, washed with copious amounts of deionized water until no detection of chloride anion remained, and dried in an air oven at 120°C overnight. The ratio of platinum to tin taken for the catalyst preparation was 3:1. The metal content of

all catalysts was 20 wt.%. The as-prepared catalysts were designated as PtSn/C where C referred to F-C for fresh, NA-C for HNO_3-treated and HT-C for heat-treated Vulcan XC-72R.

3.2.2 Unsupported Electrocatalysts

Mesoporous Pt-based catalysts were prepared through liquid crystalline templating technique as described thoroughly in Jiang and Kucernak's work [36]. In the modified procedure, 25 wt.% of metal salt, 25 wt.% of water and 50 wt.% of Brij® C10 surfactant were mixed together, and then were subjected to three heating/cooling cycles between 25°C and 45°C until obtaining homogeneous mixture. Afterwards, the mixture was equilibrated at 40°C overnight to form a gel which was subsequently added by granular Zn to reduce the metal complexes to their metallic states as indicated by fully black in color. Before use, the surfactant and the excess Zn in the black gel were removed by washing with several times of acetone, deionized water, 3 M HCl, deionized water and acetone, respectively. Finally, the solid materials were dried at 80°C. In addition to Pt, the other catalysts such as PtSn, PtRu, PtSnRu and PtSnOs were prepared by using the same procedure. The intended atomic ratio of the metals in those binary and ternary catalysts was 1:1 and 1:1:0.5, respectively.

3.3 Characterization

3.3.1 Supports

The fresh and treated supports were characterized using an Autosorb-1 (QuantaChrome Co. Ltd.) to determine their specific surface areas (S_{BET}) and textural properties. The physical adsorption was conducted at -196°C using N_2 as an adsorbent. The pH at the point of zero charge (pH_{PZC}) of the supports was estimated by a mass titration method explained in detail by Reymond et al. [87]. Three different initial pH solutions of 0.1 M KNO_3 used were 4, 6 and 9. Varying amounts of the support, i.e. 0.05, 0.5, 5, 10 and 15% by weight, were subsequently added to those initial pH solutions. The equilibrium pH was measured after 24 h by a pH meter, model 59003-25 (Cole-Parmer Instrument Co.). The surface functional groups of the fresh and pre-treated Vulcan XC-72R were carried out by a Spectrum One FT-IR Spectrometer (Perkin Elmer Co.). The solid samples were first milled with potassium bromide (KBr), and then compressed into thin pellets. A frequency range between 500 and 4000 cm^{-1} with a resolution of 4 cm^{-1} was used. The acid and base sites on the support surfaces were determined by titrating with NaOH and HCl, respectively [56]. In details, 0.1 g of sample was added to 50 mL of either 0.1 M NaOH or 0.1 M HCl. The solution was then shaken at room temperature for 24 h. Thereafter, the suspension was filtered and titrated with either 0.1 M HCl or 0.1 M NaOH.

3.3.2 Electrocatalysts

The characterization of the particle size and the crystalline structure of the as-prepared catalyst samples was carried out by an X-Ray Diffractometer (Bruker AXS Model D8 Discover) using a Cu Kα radiation source. The XRD patterns were recorded from 15° to 90° at the scan rate of 0.03° min^{-1}. Metal composition in the catalysts was obtained using

inductively coupled plasma-atomic emission spectrometry (ICP-AES) technique with an OPTIMA 3000 (Perkin Elmer Co.). Transmission electron microscope (TEM) technique was used to examine morphology and metal particle sizes. The sample was dispersed in ethanol and then deposited on the copper grid. TEM images were taken using a JEOL JEM-2010 electron microscope at the operating voltage of 200 kV. More than 300 particles were counted to obtain the average metal particle sizes and size distribution of the catalysts. The energy dispersive X-ray spectrometer (EDX) analysis was conducted using an X-ray detector in a scanning electron microscope (JSM-6400 attached with EDX Oxford Link ISIS series 300, JEOL) with the working voltage held at 20 kV.

3.4 Electrochemical Tests

For the supported catalysts, electrochemical measurements of the catalysts were carried out by cyclic voltammetry and chronoamperometry techniques using a potentiostatic/cyclic voltammetry (Solartron SI 1287). A working electrode was prepared by ultrasonically dispersing the synthesized catalysts in a solution of 5 wt.% Nafion ionomer (Electrochem Inc.,) and analytical grade isopropanol for 1 h. 25 μL of the suspension was then dropped, at 100 $\mu g_{cat}.cm^{-2}$ loading, on a clean glassy carbon electrode with a diameter of 3 mm (BAS Inc.,). The same electrochemical measurement was also carried out for all the electrocatalysts but with the same Pt loading in all the electrodes. Pt gauze of 1 cm^2 was used as a counter electrode while a saturated calomel electrode (SCE) was used as a reference electrode. The electrolytes for hydrogen and ethanol oxidation were a 0.5 M H_2SO_4 and a 0.5 M H_2SO_4 containing 1 M C_2H_5OH solution, respectively. Before performing the measurement set at a constant temperature of 25^oC, the electrolytes were saturated with high purity Ar for 30 min to expel oxygen in the solutions. All cyclic voltammograms were recorded versus SCE. Electrochemical surface area (ESA) of the Pt-based catalysts evaluated from hydrogen adsorption or desorption area normally represents available Pt active sites, which could be calculated using the following equation [88]:

$$ESA = 0.1 \times \frac{Q_{ads}}{Q_{ref} \times L_{Pt}} \tag{3.1}$$

where Q_{ads} is the charge of hydrogen adsorption, commonly equivalent to hydrogen desorption ($mC.cm^{-2}$), Q_{ref} refers to the hydrogen desorption charge of the Pt single crystallite (0.21 $mC.cm^{-2}$) and L_{Pt} is the Pt loading ($mg.cm^{-2}$).

For the unsupported catalysts, electrochemical measurements of the prepared Pt-based catalysts were carried out using a potentiostat/galvanostat/ZRA instrument (Gamry Reference 600). A working electrode was prepared by polishing a 50 μm gold microelectrode to the catalyst sample. A Pt wire counter electrode and a reversible hydrogen reference electrode (RHE) were also involved. For ethanol oxidation, the cyclic voltammetric (CV) experiment was performed in the supporting electrolyte of 0.5 M H_2SO_4 containing 1 M C_2H_5OH over the potential window of 0.05-0.8 V *vs.* RHE at both temperatures of 20^oC and 60^oC. In chronoamperometric test, the potential considered was kept at 0.3, 0.4, 0.5 and 0.6 V *vs.* RHE for 25 min each. The amount of metal deposited on the 50 μm gold microelectrode was estimated by conducting CV experiment on 0.071 cm^2 glassy carbon (BAS Inc.) in 0.5 M H_2SO_4 with the same sweep rate. The catalyst loading on the glassy carbon electrode was 0.5 $mg_{cat}.cm^{-2}$. It was recognized that the ratio of the charge for hydrogen desorption region to the amount

of metal on the electrode must be constant for such catalyst. From this relation, the amount of metal on the microelectrode was then obtained. In CO stripping experiment, CO was adsorbed on the electrode surface at 0.09 V *vs.* RHE [36] for 20 min in 0.5 M H_2SO_4 electrolyte solution. The excess CO dissolved in the sulfuric acid solution was then purged out by bubbling high purity Ar through the solution for another 30 min. Thereafter, the adsorbed CO on the electrode surface was stripped by positive-going scanning from 0.09 to 1 V *vs.* RHE at the sweep rate of 0.02 $V.s^{-1}$. To make sure that CO was completely stripped from the electrode surface, CV was done until obtaining the base voltammogram.

3.5 MEA Preparation and Single Cell Evaluation

The anode electrodes were prepared using the synthesized PtSn/C catalysts. First the catalyst was suspended in a mixture of 5 wt.% Nafion® solution (Electrochem Inc.) and isopropanol for 2 h. The Nafion content of 33 wt.% was used for all catalysts. The slurry was then applied onto the commercial carbon cloth based ELAT@ (E-TEK) by painting method. A commercial GDE with Pt/C catalyst (E-TEK) was used for the cathode side. To remove organic impurities as well as to promote a protonic form, the Nafion® 115 membrane (DuPont) was treated in the following solutions: deionized water, 3 wt.% H_2O_2, deionized water, 0.5 M H_2SO_4, and deionized water, respectively as described in the previous work [88]. The membrane electrode assembly (MEA) was fabricated by hot-pressing at 150^oC and 6.9×10^6 Pa for 150 s. A single cell was assembled with the prepared MEA and graphite bipolar plates and placed in a commercial single cell housing (5 cm^2 purchased from ElectroChem Inc.). A solution of 1 M C_2H_5OH was fed to the anode at the flow rate of 1 $mL.min^{-1}$. Unhumidified O_2 at the flow rate of 100 $mL.min^{-1}$ and 2×10^5 Pa was the oxidant supplied to the cell. The cell temperature was set at 90^oC.

CHAPTER 4 RESULTS AND DISCUSSION

4.1 Carbon-Supported Pt-Based Electrocatalysts

In this part of study, Vulcan XC-72R carbon was pretreated using acid and thermal activation methods, and the carbons obtained were then used as supports for a PtSn/C catalyst, which was prepared by a successive reduction process. Surface characteristics of the supports, including BET surface area, pH_{PZC} and functional group, were analyzed using physical N_2 adsorption, mass titration, acid-base titration, and Fourier transform infrared (FTIR) spectroscopy technique, respectively. The prepared PtSn/C catalysts were characterized by X-ray diffraction (XRD), energy dispersive X-ray spectrometry (EDX), inductively coupled plasma atomic emission spectrometry (ICP-AES), and transmission electron microscope (TEM) techniques, and then were examined for their behavior under ethanol oxidation as well as for their performances in a single direct ethanol fuel cell. Furthermore, the performance of fuel cell feeding with ethanol of three platinum electrodes, PtSn/HT-C, and commercial Pt/C and Pt_3Sn_1/C manufactured by E-TEK, were examined. In the preparation of the heat-treated carbon-supported PtSn catalysts, the effect of metal loading order, in which the platinum precursor was either co-deposited with tin oxides on the heat-treated carbon or consecutively deposited on the heat-treated carbon-supported tin oxides, and solution pH was also investigated to increase metal content in the catalysts.

4.1.1 Effect of Pre-Treatment Approach of a Carbon Support on Activity of PtSn/C Catalysts for Ethanol Oxidation

I. Physical Characterization of Pre-treated Supports

Table 4.1 Some characteristics and adsorption parameters of supports

Support	S_{BET} ($m^2.g^{-1}$)	Pore radius (Å)	V_{total} ($mL.g^{-1}$)	V_{micro} ($mL.g^{-1}$)	V_{meso} ($mL.g^{-1}$)	pH_{PZC}	Acid value ($meq.g^{-1}$)	Base value ($meq.g^{-1}$)
F-C	193	38.8	0.374	0.16	0.214	7.05	2319	1222
NA-C	202	39.9	0.403	0.16	0.243	2.47	3415	798
HT-C	265	34.1	0.452	0.22	0.232	8.99	2021	1639

** $meq.g^{-1}$ = miliequivalents per gram

Specific surface area (S_{BET}) and pore volume of the supports before and after pre-treating with the different activation approaches are summarized in Table 4.1. It can be seen from Table 4.1 that these activation methods affected the specific surface areas and textural characteristics of the supports differently. The HNO_3 treatment did not alter the surface area of the supports, which is in accordance with what was reported in previous literature [89,90]. This treatment also hardly modified the pore structure of the Vulcan XC-72R; however, it increased the meso-pore volume. In contrast, thermal treatment improved the BET surface area by approximately 37% and generated micro-pores, resulting in reduction of the average pore radius. This reduction could have been due to the removal of inorganic matter on the support surface at high temperature, a result that was also found by Coloma et al. [57].

Table 4.1 also shows the pH value at the point of zero charge (pH_{PZC}) of the supports. The pH_{PZC} indicates the surface oxygen complexes and surface charges of the support. The latter determines the strength of the interaction between the metal precursors and the support surface during the deposition procedure. The complex species on the support surface can generally be classified as acidic groups (carboxylic, anhydride, and lactone), neutral or weakly acidic groups (phenolic, carbonyl, quinones, and ether), and basic groups (pyrone and chromene) [89]. The surface of the fresh carbon (F-C) was considered to be amphoteric with pH_{PZC} of 7.05, meaning that it can adsorb either anionic or cationic species depending on the pH of the solution. The HNO_3 treatment introduced acidic property in NA-C whereas HT-C showed the basic property.

The acidity of NA-C may result from the acidic groups generated from an oxidized complex species of HNO_3. As a result, the pH_{PZC} of the nitric-treated carbon was lower. The basic characteristic of HT-C was attributed to the pyrolysis of acidic oxygen surface groups to form pyrone-type groups when exposed to air at room temperature [57]. In addition, the acid-base surface values shown in Table 4.1 confirmed that the base functional groups on F-C and HT-C are higher than that of NA-C. It can be clearly seen that the pretreatment method could alter functional groups as well as the microstructure of the carbon. Consequently, the Pt adsorption capacity of the heat-treated support was affected.

The surface functional groups of the Vulcan XC-72R before and after HNO_3/thermal treatment processes were characterized using FTIR technique. Their FTIR spectra are illustrated in Figure 4.1. It can be seen that there were two obvious characteristic peaks at 3430 and 1630 cm^{-1} present on the surfaces of F-C. These two bands are assigned to phenolic groups and quinones, respectively [14,56,58,91]. Heating up to 600^{o}C under an inert atmosphere could remove some of less stable oxygen complexes, as shown by the slight decrease in the intensity of the characteristic FTIR bands of HT-C [58]. In contrast, the HNO_3 activation approach increased a large number of the phenolic groups and quinones on the support surfaces. In addition, a sharp absorption peak at 1380 cm^{-1} associated with carboxyl-carbonates and nitrate groups was observed [90]. Thus, it can be deduced that several functional groups such as phenolic, quinones, carboxyl-carbonates, and nitrate groups were produced on the carbon surface by HNO_3 treatment. The results are in agreement with the pH_{PZC} and the acid values of the supports.

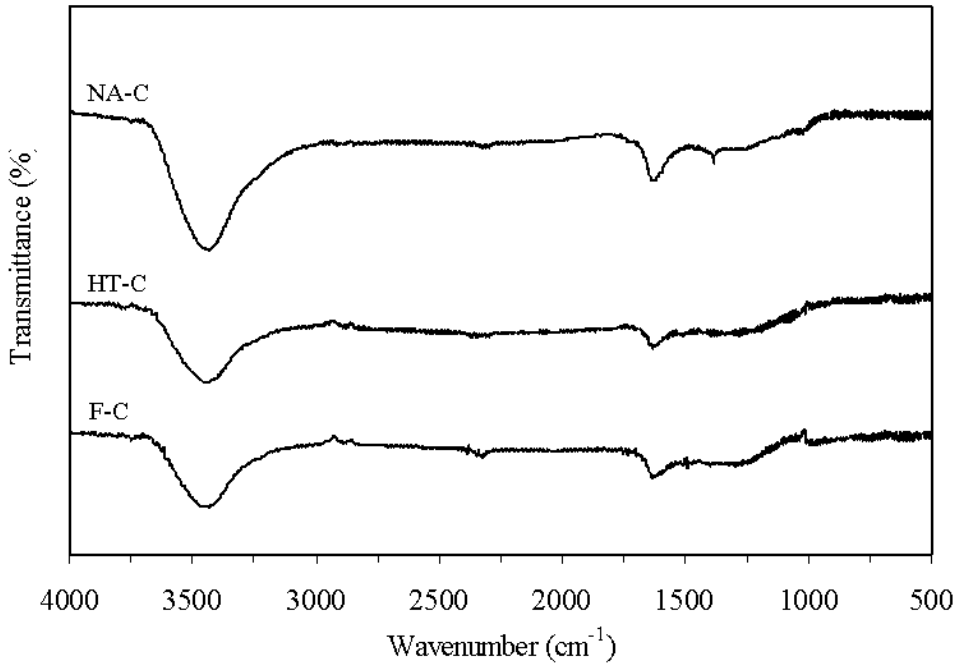

Figure 4.1 FTIR spectra of the various supports

II. Physical Characterization of PtSn/C Catalysts

The XRD patterns of all the as-prepared PtSn/C catalysts and the commercial Pt/C catalyst supplied by E-TEK are shown in Figure 4.2. The broad diffraction peak at around 25°, assigned to the graphite (002) plane of the hexagonal structure of Vulcan XC-72R, was observed in all diffractograms. Four typical diffraction peaks of a crystalline Pt face-centered cubic (fcc) phase including Pt(111), Pt(200), Pt(220) and Pt(311) obviously appeared at about 39°, 46°, 67° and 81°, respectively. Neither the diffraction peaks of tin metallic nor those of tin oxides were found in the prepared PtSn/C catalysts (See curves b, c, d). Previous literatures [6,22] reported that SnO_2 diffraction peaks at around 34° and 52° were present in PtSn/C catalysts prepared by successive reduction method, but at low SnO_2 content, the peaks could not be observed [6]. However, in this study, the non-alloyed PtSn was formed as indicated by the unchanged positions of the Pt diffraction peaks (See especially Pt(111)) from those of the Pt/C catalyst [22]. Considering the ratio of Pt:Sn of all catalysts obtained from EDX analysis as shown in Table 4.2, it was in the range of 4.74-7.53. The Pt:Sn ratio of the prepared samples are higher than the intended values of 3:1, indicating that they contain small Sn content as also found in the XRD results.

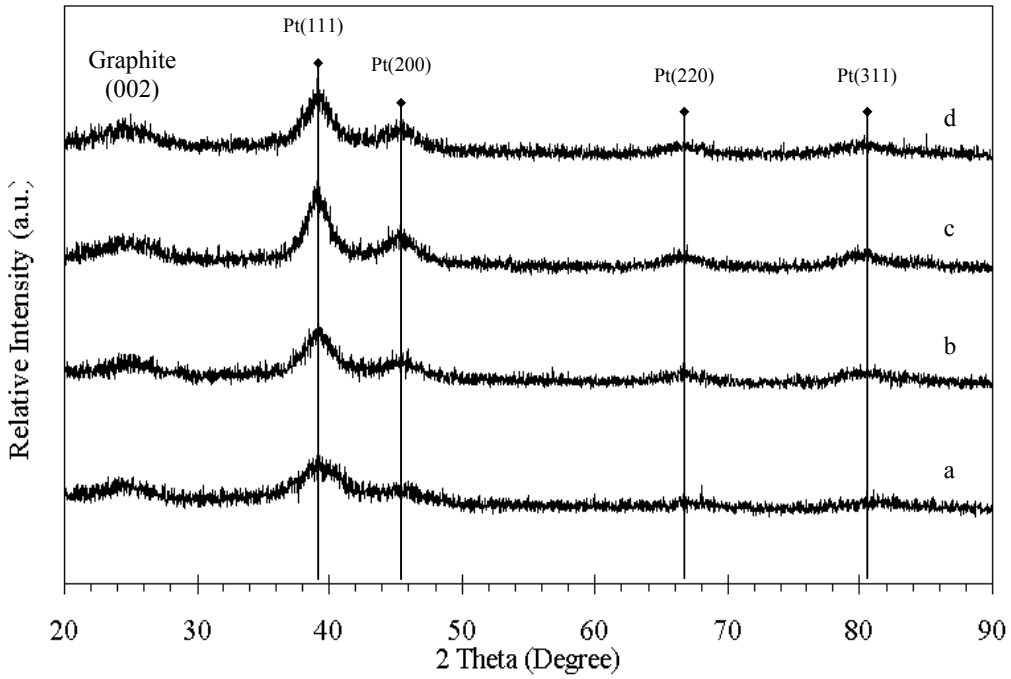

Figure 4.2 X-ray diffractograms of the Pt-based catalysts: a Pt/C (E-TEK), b PtSn/F-C, c PtSn/NA-C, d PtSn/HT-C

Table 4.2 TEM mean particle sizes, Pt:Sn rations and Pt content of various PtSn-based catalysts

Sample	Mean particle size (nm)	Pt:Sn from EDX	Pt content from ICP (wt.%)
PtSn/F-C	2.6 ± 0.7	7.53	13.05
PtSn/NA-C	2.5 ± 0.6	4.74	9.05
PtSn/HT-C	2.2 ± 0.5	5.46	10.17

The TEM images of all the synthesized PtSn/C catalysts, where metal particles are identified by black spots, are shown in Figure 4.3. The effects of the support pre-treatment methods on Pt particle sizes of the PtSn/C catalysts and their size distribution can be estimated. The PtSn/HT-C catalyst gave the smallest metal sizes as compared with the other prepared PtSn/C catalysts, owing to higher surface area of heat-treated support. However, some aggregation of the metal particles, possibly leading to bigger metal sizes and wider size distribution (1.5-6.0 nm), was clearly observed in the PtSn/F-C catalyst. Pt size distribution of PtSn/NA-C and PtSn/HT-C catalysts was narrower with the particle size range of 1.5-4.5 nm. The mean particle sizes of Pt calculated from the TEM images of all catalysts are displayed in Table 4.2. The average diameters of PtSn/F-C, PtSn/NA-C and PtSn/HT-C catalysts were 2.6 nm, 2.5 nm, and 2.2 nm, respectively. Additionally, the pre-treatment approaches of the support affected metal dispersion in these as-prepared PtSn/C catalysts. In comparison to PtSn/F-C and PtSn/NA-C catalysts, Pt particles of the PtSn/HT-C catalysts are uniformly well-dispersed on the support as shown in Figure 4.3c.

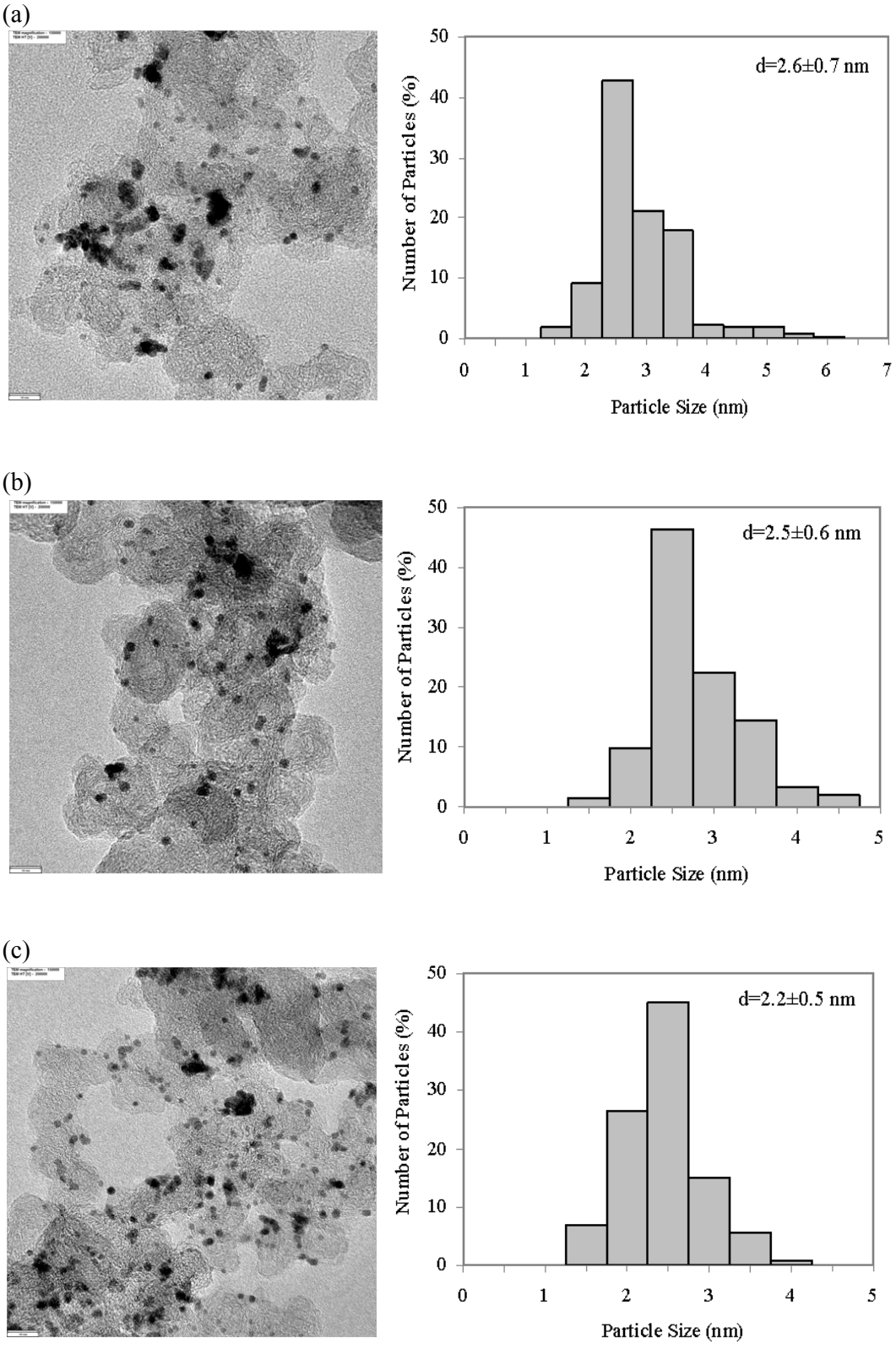

Figure 4.3 TEM images and size distribution of the as-prepared PtSn/C catalysts: a PtSn/F-C, b PtSn/NA-C, c PtSn/HT-C

As already mentioned, functional groups on support surface could manipulate the Pt adsorption of the support surface, leading to different Pt contents in the prepared PtSn/C catalysts. The results from ICP analysis in Table 4.2 showed that the adsorbed Pt contents in PtSn/F-C, PtSn/NA-C and PtSn/HT-C catalysts were 13.05 wt.%, 9.05 wt.%, and 10.17 wt.%, respectively. Higher amounts of Pt adsorbed on the basic HT-C and amphoteric F-C than that on the acid NA-C could be attributed to the surface charge of the support. The higher base values of both F-C and HT-C than that of NA-C shown in Table 4.1 indicated higher base functional groups on the surfaces of the supports. The Pt deposition to the support surface was enhanced by the base functional groups where Pt reduction can occur. It was reported in other work that base condition was preferable in the preparation of Pt nanoclusters-deposited supports because the reduction process of the Pt precursor was best affected under base condition [56]. Furthermore the small Pt nanocluster size for PtSn/HT-C might have originated with well distributed base functional groups. The reason why F-C could adsorb Pt more than HT-C is that the surface oxygen groups presented on F-C can act as anchoring centers for the metal precursors and these complex surface oxygen species was subsequently decomposed to form pyrone-type groups after the heat treatment.

III. Electrochemical Characterization and Activity of PtSn/C towards EOR

Cyclic voltammograms of the as-prepared PtSn supported on the different pre-treated supports in 0.5 M H_2SO_4 electrolyte are illustrated in Figure 4.4. The current responses in the potential range of -200 to 800 mV *vs.* SCE for all voltammograms were normalized by the actual Pt contents evaluated from ICP analysis as being in the unit of $mA.mgPt^{-1}$. In the absence of ethanol solution, only the adsorption and desorption of hydrogen and oxygen were appeared. The hydrogen ad/desorption regions of all the Pt-based catalysts were seen in the potential range of -200 to 100 mV *vs.* SCE. A larger double-layer charging current of PtSn/NA-C than that of the untreated and heat-treated PtSn/C catalysts was observed. This is attributed to the presence of the surface oxygen complexes formed from the dissociation of water on the Sn sites as well as the oxidation of the support by the acid treatment, thereby increasing the electrode capacitance [32]. It was believed that the preferential oxygen-containing species facilitated the removal of the strongly CO-adsorbed species to free Pt active sites. As a result, PtSn/NA-C catalyst was expected to provide the highest catalytic activity for ethanol oxidation. On the other hand, in regard to the electrochemical surface area (ESA), the catalysts could be ranked in the following sequence: PtSn/HT-C (52.9 $m^2.g^{-1}$) > PtSn/F-C (14.4 $m^2.g^{-1}$) > PtSn/NA-C (9.3 $m^2.g^{-1}$). PtSn/HT-C had the highest amount of available Pt active sites, inferring the better Pt dispersion in the PtSn/HT-C. Similarly, the much lower ESA of PtSn/F-C and PtSn/NA-C could be attributed to an inadequate Pt active sites dispersed on the untreated/acid-treated supports as well as the bigger Pt particle sizes in those catalysts obtained from TEM. As a result, the PtSn/HT-C showed higher catalytic activity than the others did.

Figure 4.5 presents the cyclic voltammograms of the as-prepared PtSn/C catalysts toward ethanol oxidation. As can be seen, there are two oxidation peaks in the potential window of -200 to 900 mV *vs.* SCE. The first oxidation peak appears during the forward scan, and the other one shows in the reverse scan. No hydrogen ad/desorption peaks can be observed, due to prominence of ethanol adsorption. The inset in Figure 4.5 displays the onset potential of PtSn/F-C, PtSn/NA-C and PtSn/HT-C, which are 220, 175 and 160 mV *vs.* SCE, respectively. As reported in the other work [92], the onset potential of the commercial Pt/C was 510 mV *vs.* SCE. Thus, the addition of Sn to Pt

led to the negative onset potential, approximately 300 mV, indicating easier and faster ethanol oxidation in those binary catalysts. The peak potential of the as-prepared PtSn/C catalysts was in the range of 650-690 mV *vs.* SCE during the positive potential scanning and 510-540 mV *vs.* SCE for their reverse scanning, respectively. The activity of the catalysts for ethanol oxidation is normally determined by the maximum current density of the positive scan peak [8]. From the voltammograms, the maximum current density of all those binary catalysts was ranked as follows: PtSn/HT-C (179.5 $mA.mg_{Pt}^{-1}$) > PtSn/NA-C (116.6 $mA.mg_{Pt}^{-1}$) > PtSn/F-C (81.3 $mA.mg_{Pt}^{-1}$). As a result, the PtSn/HT-C catalyst provided the highest electrochemical activity for ethanol oxidation, possibly resulting from its highest ESA.

It was also observed that the maximum current density obtained from PtSn/HT-C was about 1.5 times that from PtSn/NA-C although the ESA of the PtSn/HT-C was five times that of the PtSn/NA-C. This is because the Pt:Sn ratio and the oxide form of Sn play important roles for ethanol oxidation. This result is similar to the finding in the previous work carried out by Spinacé et al. [69]. The presence of Sn can promote ethanol oxidation not only by an electronic effect in the Pt-based electrode material but also by an activation of the interfacial water molecules necessary to promote CO and acetaldehyde oxidation reactions [4,6]. The Pt:Sn ratio in PtSn/NA-C was about 4.74:1 which is closer to 3:1 than that of PtSn/HT-C. The optimum ratio of Pt:Sn giving the best DEFC performance previously reported was 3 or approaching 3 [6,14]. In addition, Zhou et al. [8] presented that the DEFC anode catalyst containing lower Pt:Sn ratio showed better cell performance than that with higher Pt:Sn ratio.

To confirm the catalytic activity of the as-prepared PtSn/C catalysts towards ethanol oxidation, chronoamperometric experiment was conducted by holding the potential at 600 mV *vs.* SCE for 30 min in 0.5 M H_2SO_4 containing 1 M C_2H_5OH; and the result shows in Figure 4.6. As seen from Figure 4.6, the current of all binary catalysts drops rapidly within 5 min, and then decays slowly. After holding the potential for 30 min, the final current density of PtSn/F-C, PtSn/NA-C and PtSn/HT-C catalysts were 23.1, 28.2 and 47.5 $mA.mg_{Pt}^{-1}$, respectively. This result indicated that PtSn/HT-C catalyst had stronger tolerance to the poisoning adsorbed CO species, implying better catalytic activity for ethanol oxidation as compared to the other PtSn/C catalysts. The results are in agreement with those of cyclic voltammetry measurements.

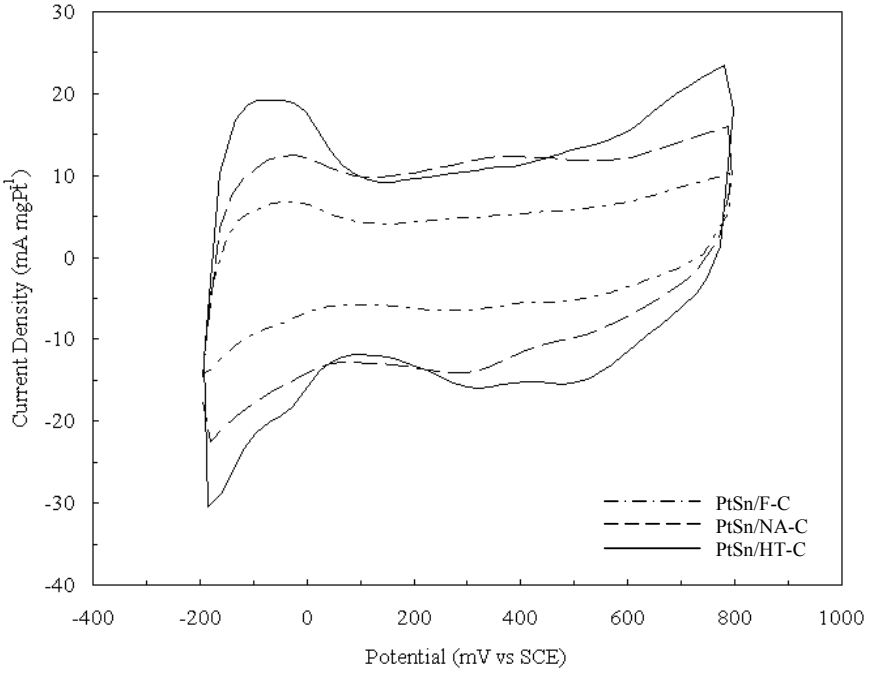

Figure 4.4 Cyclic voltammograms of the synthesized PtSn/C catalysts in 0.5 M H_2SO_4 solution with a scan rate of 0.05 $V.s^{-1}$ at 25°C

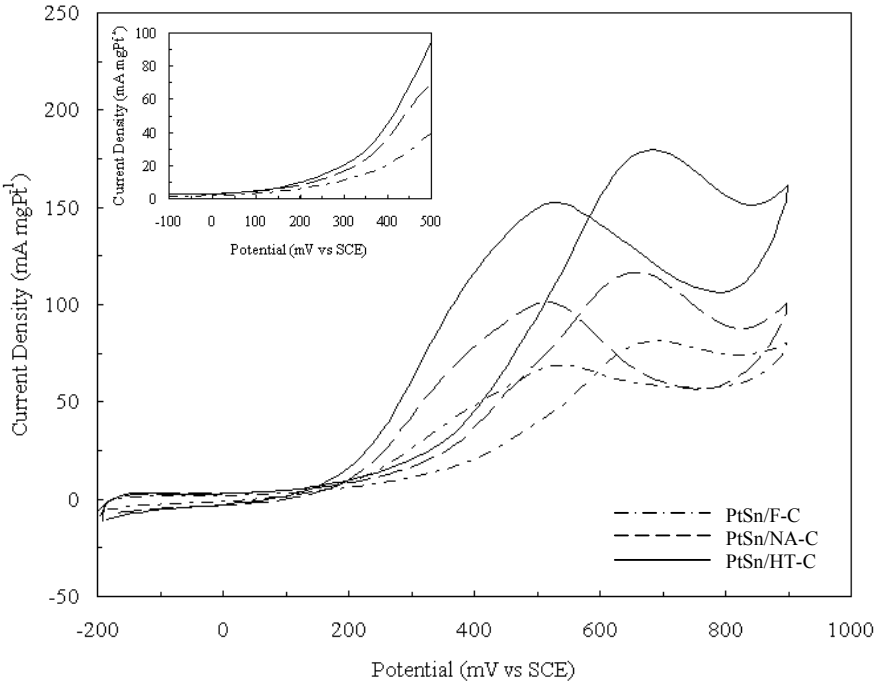

Figure 4.5 Cyclic voltammograms of the synthesized PtSn/C catalysts in 0.5 M H_2SO_4 containing 1 M C_2H_5OH solution with a scan rate of 0.02 $V.s^{-1}$ at 25°C

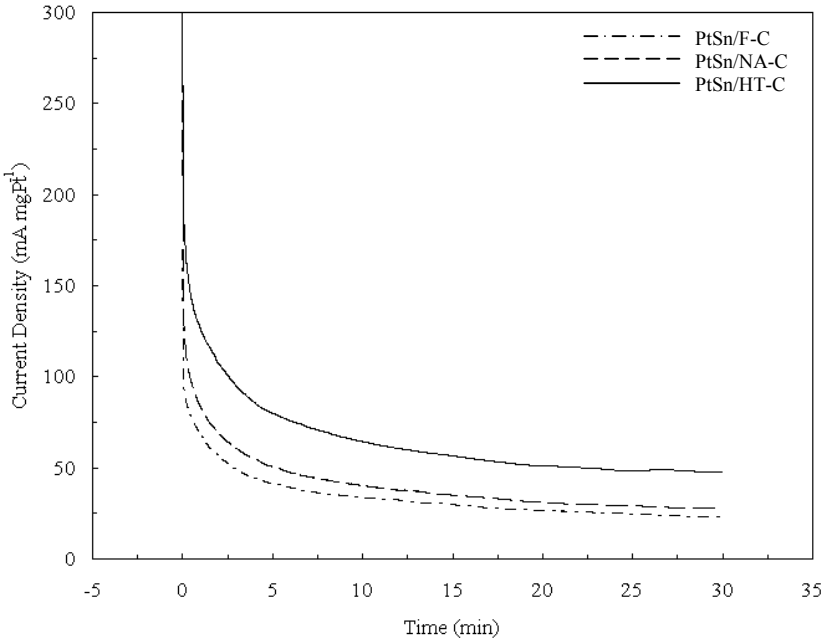

Figure 4.6 Chronoamperometric curves of the as-prepared PtSn/C catalysts in 0.5 M H_2SO_4 containing 1 M C_2H_5OH solution at 600 mV *vs.* SCE for 30 min

IV. Electrochemistry Test for EOR at the Same Pt Loading

To verify the effect of pre-treatment method of the support towards an EOR, the electrochemical characterization of the as-prepared PtSn on the different pretreated supports were performed again by keeping the same amount of Pt loaded onto a glassy carbon substrate. The voltammograms in 0.5 M H_2SO_4 with/without 1 M C_2H_5OH and the chronoamperometric curves in 0.5 M H_2SO_4 containing 1 M C_2H_5OH are illustrated in Figure 4.7. As seen from Figure 4.7a, PtSn/HT-C catalyst provided a larger hydrogen desorption area. As a consequence, it would have a higher ESA. The ESA of PtSn/HT-C was 57.4 $m^2.g^{-1}$, which is much higher than those of PtSn/NA-C and PtSn/F-C. PtSn/HT-C also showed superior ethanol oxidation and CO tolerance to the other as-prepared PtSn/C catalysts as displayed the results in Figure 4.7b, c respectively. By comparing between the results at the constant catalyst loading and the constant Pt loading, PtSn/HT-C still gave higher performance than PtSn/NA-C, while PtSn/F-C had the lowest performance in ethanol oxidation. This is a compromise effect of Pt dispersion and Pt:Sn ratio. PtSn/NA-C contained higher Sn:Pt ratio while PtSn/HT-C had higher Pt dispersion.

(a)

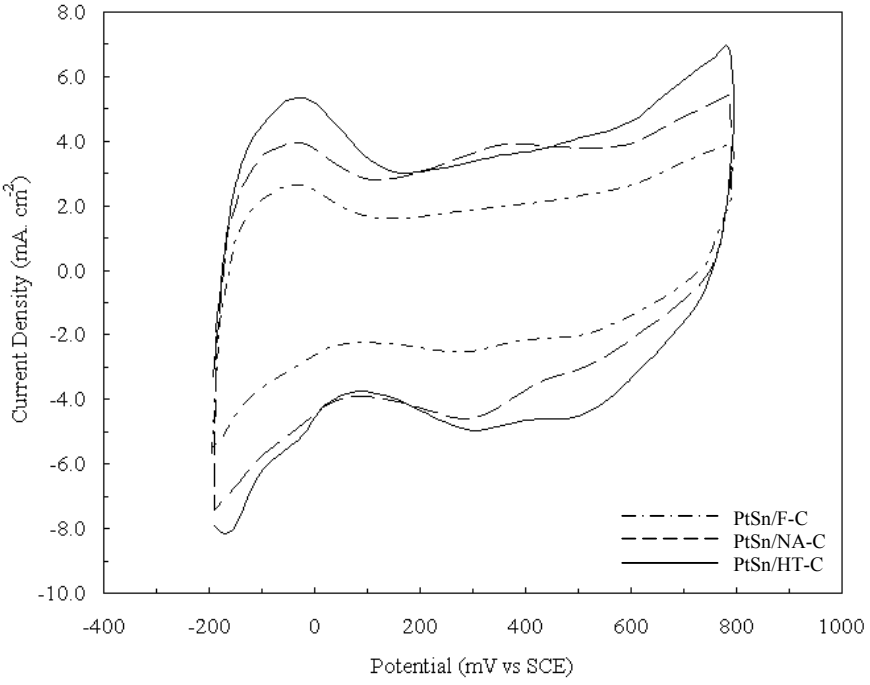
Current Density (mA. cm-2)
Potential (mV vs SCE)
PtSn/F-C
PtSn/NA-C
PtSn/HT-C

(b)

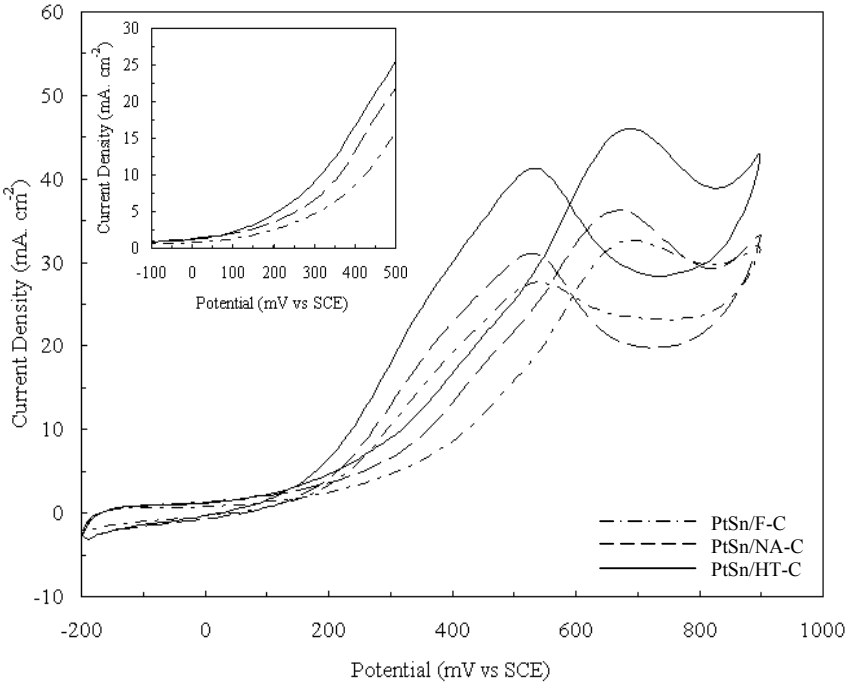
Current Density (mA. cm-2)
Potential (mV vs SCE)
PtSn/F-C
PtSn/NA-C
PtSn/HT-C

(c)

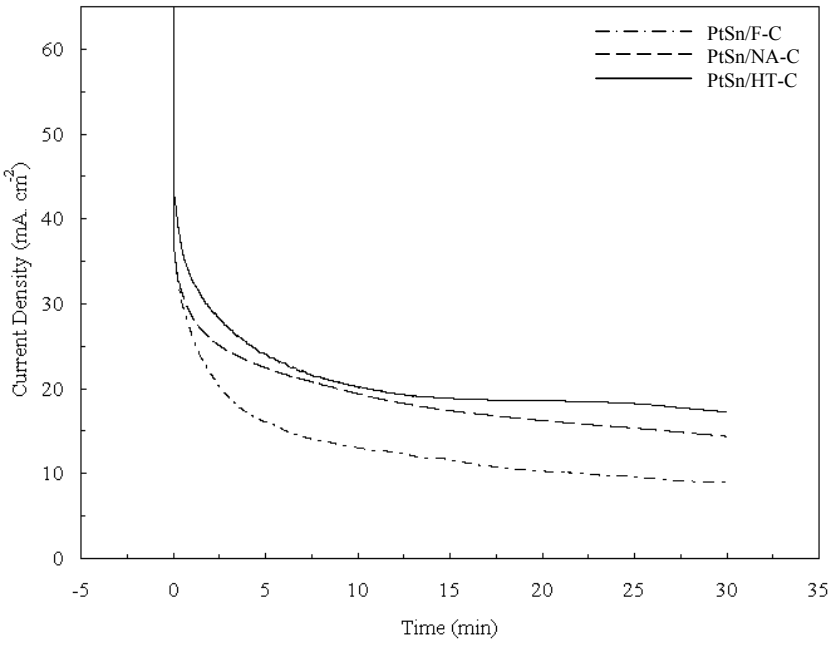

Figure 4.7 Electrochemistry curves of the PtSn/C catalysts loaded at the same amount of Pt on a glassy carbon at 25°C: a Voltammograms in 0.5 M H_2SO_4 with a scan rate of 0.05 $V.s^{-1}$, b Voltammograms in 0.5 M H_2SO_4 + 1 M C_2H_5OH with a scan rate of 0.02 $V.s^{-1}$, c Chronoamperometric curves in 0.5 M H_2SO_4 + 1 M C_2H_5OH at 600 mV *vs.* SCE for 30 min

V. Direct Ethanol Fuel Cell Test

The DEFC performances of the cell, prepared from the as-prepared PtSn/C catalysts employed as the anode catalyst, are displayed in Figure 4.8. Since the Pt amounts deposited on the pre-treated and untreated supports were not the same as previously mentioned, the polarization and power density curves of these electrodes were calculated, based on the weight of Pt in the unit of $mA.mgPt^{-1}$ instead of $mA.cm^{-2}$ to account for the effect of different amounts of Pt. To verify the role of Sn in the binary catalysts, polarization and power density curves of the commercial Pt/C were used for comparison. The I-V curves show that the open circuit voltages of all the binary catalysts were about 720 mV, which is noticeably higher than that of Pt/C by approximately 300 mV. The I-V curves of Pt/C showed that the voltage sharply dropped as the current density increased, demonstrating much faster poisoning of the Pt active sites in Pt/C than the as-prepared PtSn/C catalysts. In contrast, the enhanced performance of all the binary catalysts was attributed to the incorporation of Sn into Pt, promoting oxidative removal of the poisoning CO species by the so-called bi-functional mechanism.

The maximum power density of all the catalysts is ranked from the highest to the lowest as follows: PtSn/HT-C > PtSn/NA-C > PtSn/F-C > Pt/C, which is in reasonable agreement with the activity of these catalysts towards the EOR that was obtained from cyclic voltammetry and chronoamperometry techniques. In the low current density region (< 75 $mA.mgPt^{-1}$), slightly better performance of PtSn/NA-C than PtSn/HT-C and PtSn/F-C was observed, which might have been due to the contribution of the higher Sn:Pt ratio obtained from PtSn/NA-C catalyst preparation. It was also observed

that the performance of PtSn/NA-C was diminished by the higher current density region but was still better than that of PtSn/F-C. It was believed that the HNO_3 pretreatment of support could generate significant surface oxygen complexes, which had enhanced the hydrophillicity of the carbon [10]. This could have prevented the gas (CO_2) product from being released from the catalyst layer, resulting in inhibition of fuel accessibility to the active sites [93]. As a result, PtSn/HT-C enhanced both DEFC performance as well as catalytic activity towards ethanol oxidation. It could be explained that the thermal pre-treatment approach of support improved metal dispersion, as seen in the TEM images, and could have led to a high electrochemical surface area for ethanol oxidation. Overall, our results indicated that considerable increase in the ethanol oxidation reaction (EOR) over the PtSn/C catalyst can be achieved by thermal pre-treatment method of support, and the PtSn/HT-C electrode showed the best performance in a direct ethanol fuel cell.

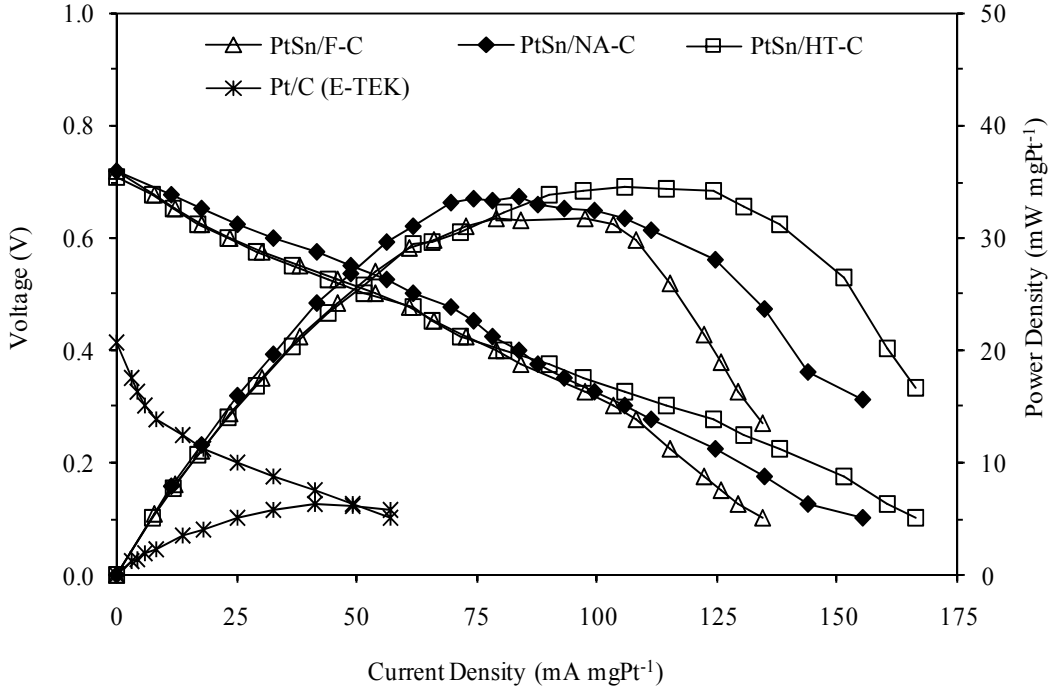

Figure 4.8 Normalized DEFC performance curves by actual amount of Pt noble metal

4.1.2 Performance in DEFC of PtSn/HT-C Electrode in Comparison to Commercial Pt/C and Pt_3Sn_1/C Electrodes

Figure 4.9 shows the XRD patterns of the catalyst samples in the 2θ scan range of 15°-90°. The broad peak at around 25° as seen in all the samples is the reflection peak of graphite (002) plane of the hexagonal structure of Vulcan XC-72R. The characteristic peaks of fcc crystalline Pt structure including Pt(111), Pt(200), Pt(220) and Pt(311) were also found. From Figure 4.9, shift of all Pt reflection peaks to a lower position could be observed in both Sn-containing samples (See curve b and c compared to curve a). However, PtSn/HT-C catalyst showed the fewer shifts of those peaks. The lattice parameter of Pt calculated from (220) plane for Pt/C (E-TEK), prepared PtSn/HT-C and Pt_3Sn_1/C (E-TEK) is 0.3924 nm, 0.3937 nm and 0.3973 nm, respectively. The small

dilation of lattice parameter of Pt in PtSn/HT-C sample implies separation of Pt and SnO_2 phase [22].

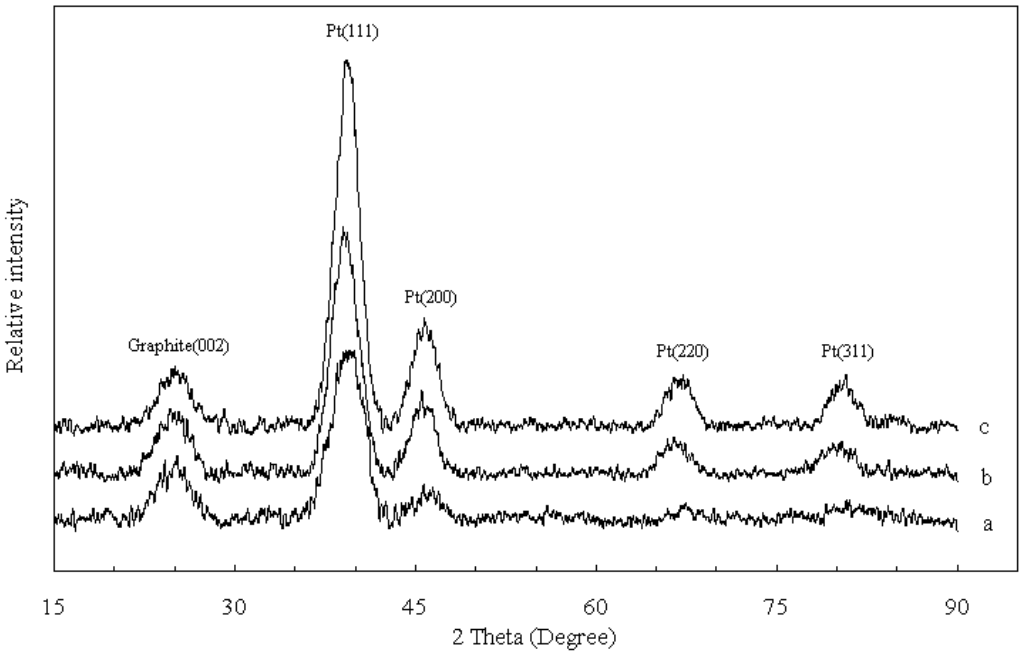

Figure 4.9 X-ray diffractograms of the samples: a Pt/C (E-TEK), b Pt_3Sn_1/C (E-TEK), c PtSn/HT-C

As can be seen from TPR profiles of the catalysts in Figure 4.10, there were two obvious peaks for all samples at around 200°C and 670°C, which were ascribed to the reduction of platinum oxide and the reaction of C-H interaction, respectively [13]. The Pt_3Sn_1/C (E-TEK) and PtSn/HT-C samples would also have small other peaks at 420°C and 530°C. These peaks would be the reduction peaks of SnO and SnO_2, respectively [14,94,95]. However, the SnO_2 reduction peak of the prepared PtSn/HT-C was much larger than that of the commercial one, demonstrating higher tin oxides contained in PtSn/HT-C catalyst.

For a practical point of view, the performance in the direct ethanol fuel cell fabricated from all the Pt-based catalysts was investigated in 5 cm^2 single cell housing and their polarization and power curves are illustrated in Figure 4.11. From I-V curves, Pt_3Sn_1/C (E-TEK) electrode has the same open circuit voltage as PtSn/HT-C electrode that is 0.72 V. But, it is much larger than that of Pt/C electrode. As the current density increased, the voltage rapidly dropped in the Pt/C electrode, due to accumulation of the CO poisoning species on the Pt surface. The binary catalysts showed much better performance in both low and high current density regions than the pure Pt. In binary catalysts, the activated-controlled region was nearly the same. However, as the current density was greater than 40 $mA.mgPt^{-1}$ the prepared PtSn/HT-C electrode exhibited the enhanced performance better than the commercial one. The maximum power density of PtSn/HT-C was 34 $mW.mgPt^{-1}$, which was higher than those of commercial Pt_3Sn_1/C (27 $mW.mgPt^{-1}$) and Pt/C (6 $mW.mgPt^{-1}$), respectively. This is because more tin oxides contained in PtSn/HT-C sample help to dissociate water molecules to form hydroxyl species sufficient for oxidative CO removal.

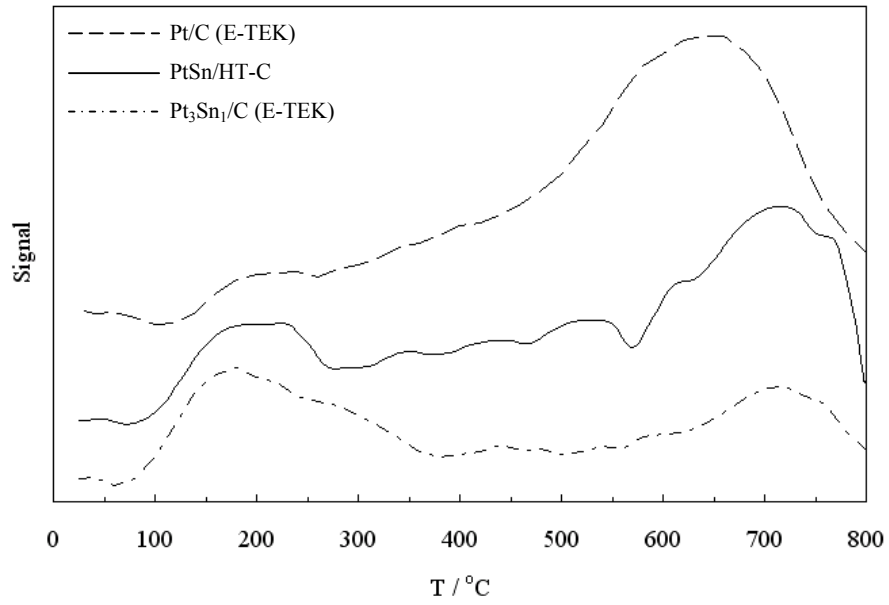

Figure 4.10 TPR curves of the Pt-based catalysts at the temperature between 25°C and 800°C with the ramp rate of 10°C.min^{-1}

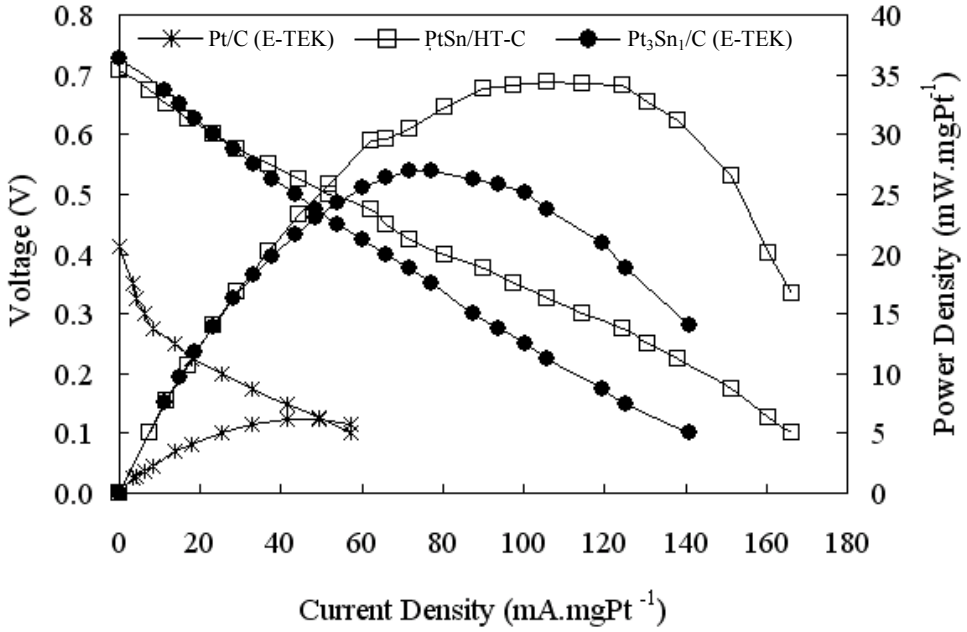

Figure 4.11 I-V and I-P performance curves of the electrodes with anode Pt loading of 1.5 $mg_{Pt}.cm^{-2}$ and commercial GDE at cathode side. T_{cell}: 90°C, Ethanol flow rate: 1 mL.min^{-1}, Oxidant flow rate: 100 mL.min^{-1}, P_{O2}: 2 bar

4.1.3 Effect of Metal Loading Order and Solution pH in PtSn/HT-C Preparation on Ethanol Oxidation

Table 4.3 Metal composition of various PtSn/HT-C samples

Sample	Metal composition from EDX (wt.%)		Pt:Sn ratio
	Pt	Sn	
PtSn/HT-C	7.35±1.07	0.83±0.15	5.46
Pt/Sn/HT-C	12.82±0.07	1.65±0.05	4.73
Pt/Sn/HT-C+HCl	16.54±3.91	2.00±0.58	5.11

Table 4.3 displays metal composition of metallic Pt and Sn in the PtSn/HT-C catalysts. It could be seen from Table 4.3 that co-deposition of platinum precursor and tin oxides on the heat-treated carbon, labeled as PtSn/HT-C, yielded 7.35 wt.% of Pt and 0.83 wt.% of Sn which were much lower than the intended values (16.63 wt.% for Pt and 3.37 wt.% for Sn). Consecutive deposition of platinum precursor on the heat-treated carbon-supported tin oxides (Pt/Sn/HT-C) increased both Pt and Sn contents in the catalyst sample. It was also found that further adjusting solution pH to around 3 by hydrochloric acid (Pt/Sn/HT-C+HCl) induced more Pt deposition on the support, and consequently Pt content in such catalyst was pretty good with the expected value. This was because acidity of the solution destroyed stabilization of Pt ions and accelerated deposition of Pt on the support. However, it might cause larger deviation of Pt content in Pt/Sn/HT-C+HCl than PtSn/HT-C and Pt/Sn/HT-C. As considering the ratios of Pt:Sn in the corresponding samples which were in the narrow range of 4.73-5.46, it implied that metal loading order and solution pH in PtSn/HT-C preparation hardly affected Pt:Sn ratio.

Ethanol oxidation study of all the catalysts was then performed in the electrolyte solution of 0.5 M H_2SO_4/1 M C_2H_5OH at 25^oC. As seen from Figure 4.12, the Pt/Sn/HT-C catalyst gave greater voltammetric current than the other catalysts, implying more active Pt/Sn/HT-C catalyst for the oxidation of ethanol. It was also confirmed by chronoamperometric curves of the corresponding catalysts shown in Figure 4.13 that Pt/Sn/HT-C showed higher final current after holding the potential at 0.8 V *vs.* RHE for 30 min, meaning stronger ability to tolerate the poisoning species formed during ethanol oxidation. It might result from higher metal content of Pt and Sn than PtSn/HT-C together with a well dispersion of Pt in Pt/Sn/HT-C rather than in Pt/Sn/HT-C+HCl. The combination of these effects would, therefore, lead to the excellent activity of Pt/Sn/HT-C catalyst towards ethanol oxidation.

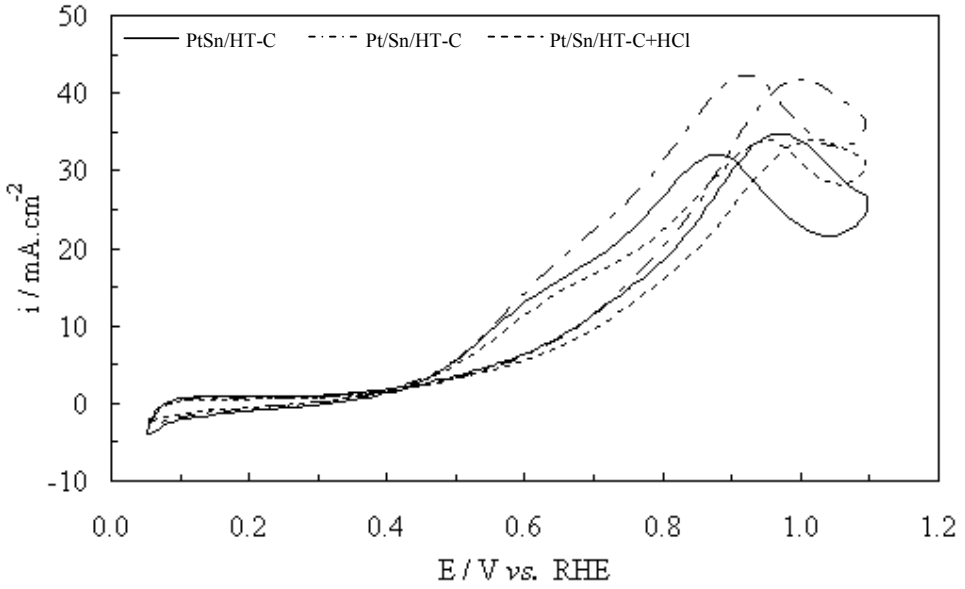

Figure 4.12 Cyclic voltammograms of the PtSn/HT-C samples in 0.5 M H_2SO_4 containing 1 M C_2H_5OH solution with a scan rate of 0.02 $V.s^{-1}$ at 25°C

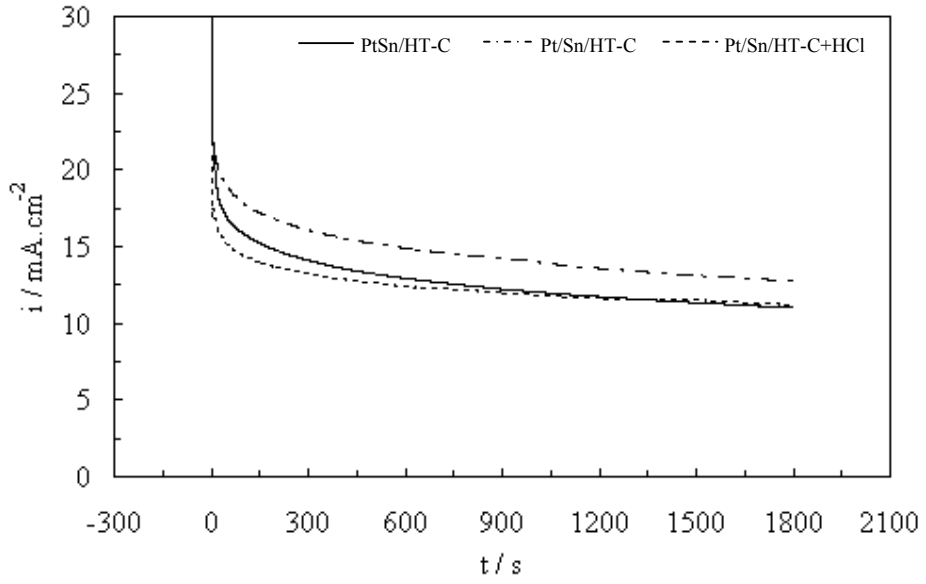

Figure 4.13 Chronoamperometric curves of various PtSn/HT-C samples in 0.5 M H_2SO_4 containing 1 M C_2H_5OH solution at 0.8 V *vs.* RHE, 25°C

4.2 Unsupported Electrocatalysts

In this study, unsupported catalysts were prepared via chemical co-reduction of the catalyst precursors in the aqueous domain of liquid crystal template of a nonionic surfactant. Mesoporous Pt and PtSn were initially produced and their catalytic activities for ethanol oxidation were then carried out using popular electrochemical techniques including cyclic voltammetry and chronoamperometry. Furthermore, a third metal including Ru and Os was introduced to such PtSn catalyst in order to promote not only

electrocatalytic ethanol oxidation but also oxidation of adsorbed CO species. To clarify promotion role of Ru and Sn for ethanol oxidation, preparation of mesoporous PtRu and PtRuSn was also done.

4.2.1 Activity of Mesoporous Pt and PtSn for Ethanol Oxidation

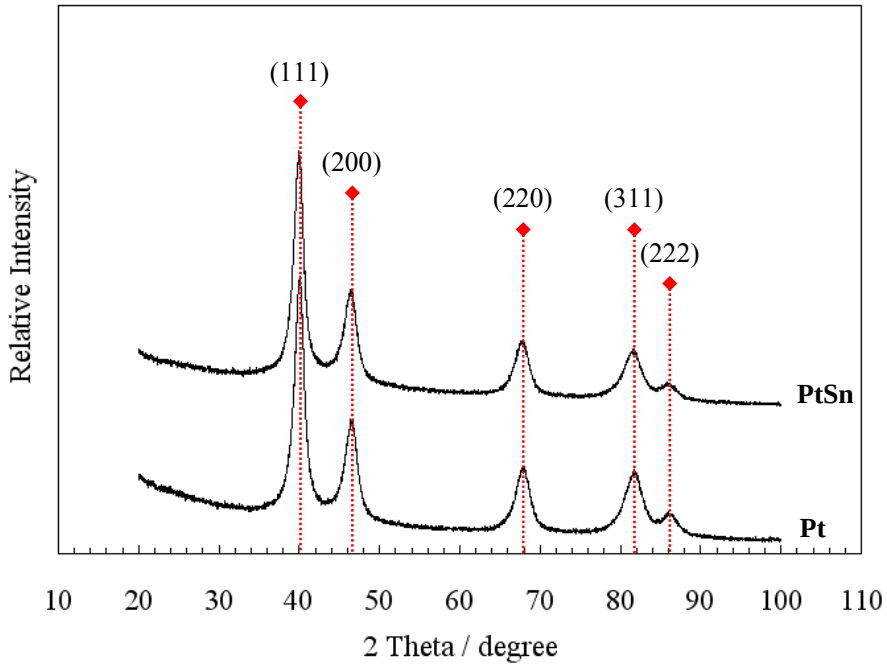

Figure 4.14 X-ray diffractograms of mesoporous Pt and PtSn catalysts

The XRD patterns of both mesoporous Pt and PtSn samples scanned from 20° to 100° are depicted in Figure 4.14. All those diffractograms show a face-centered cubic (fcc) lattice of crystalline Pt structure (JCPDS 04-0802) assigned to (111), (200), (220), (311) and (222) at the corresponding reflection positions. The typical characteristics peaks of tin oxide according to JCPDS 41-1445 normally found in the Sn-containing catalyst [6,32] could not be observed herein. It might result from the formation of their amorphous oxides and/or the presence of small amount of tin oxides which were limited by XRD detection. As seen from Figure 4.14, all the Pt reflection peaks were hardly shifted to lower position when Sn was incorporated into Pt. Therefore, it was expected that tin oxides would be formed and present in the vicinity of Pt particles instead of entering into the fcc lattice of Pt. In order to prove this, the Pt (220) peak was fitted a Gaussian to estimate the lattice parameter of Pt by the equations in Radmilovic et al.'s work [96], which was subsequently used to calculate atomic fraction of Sn in the alloy and alloying degree of Sn in the catalyst by the following equations [72].

$$x = \left[\frac{a-a_0}{a_s-a_0}\right] \times x_s \qquad (4.1)$$

$$Sn_{al} = \frac{x}{(1-x)(Sn/Pt)_{EDX}} \qquad (4.2)$$

where a_0 (0.3905 nm) and a_s (0.4002 nm) are the lattice parameter of mesoporous Pt and Pt_3Sn catalysts at the Sn atomic fraction (x_s) of 0.25, respectively. Also, $(Sn/Pt)_{EDX}$ is the atomic Sn/Pt ratio from EDX measurement. Besides, the crystallite size of particle can be determined by the Scherrer formula [96]; and all the calculated values are then listed in Table 4.4. The metal compositions in the prepared catalysts are also included. From Table 4.4, the amount of Sn in the alloy is about 1.5 at.% which is much less than that found in the bulk compositions (9 at.%). As a result, only some of Sn could take part in the Pt lattice while the unalloyed Sn must exist in its amorphous oxide form. Both mesoporous Pt and PtSn samples have the same mean particle sizes of approximately 4.3 nm.

Table 4.4 Element composition and structural analysis of all the Pt-based samples

Catalyst	Atomic ratio from EDX (Pt:Sn)	Lattice parameter (nm)	Sn atomic fraction in the alloy	Alloying degree of Sn in the catalyst (%)	Metal size from XRD (nm)
Pt	1.00:0.00	0.3905	0	0	4.4
PtSn	0.91:0.09	0.3911	0.015	14.9	4.3

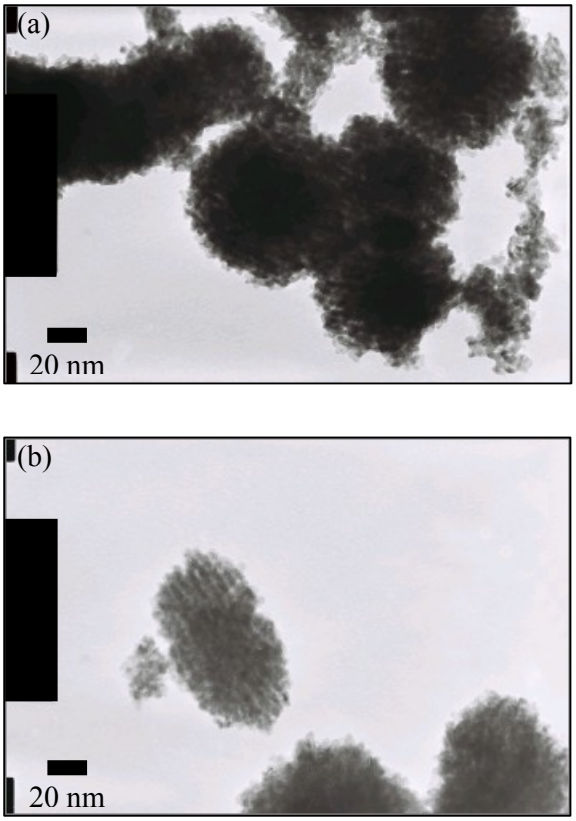

Figure 4.15 TEM images of the prepared catalysts: a mesoporous Pt, b mesoporous PtSn

Figure 4.15 illustrates TEM images of mesoporous Pt and PtSn catalysts. As seen from Figure 4.15a, mesoporous nanostructure of Pt could not be well-defined as also found in

the other works [28,76]. However, the PtSn sample showed ordered mesoporosity partially with 4 nm in diameter of crystallite size, which was in agreement with that from XRD analysis. The active surface area determined by CO adsorption (not shown) of Pt and PtSn samples is 41 $m^2.g^{-1}$ and 51 $m^2.g^{-1}$, respectively. The surface area of Pt obtained is as high as that of the highly ordered mesoporous Pt in the literature [25]. The reason why porous structure could not be clearly seen in the prepared Pt is that the images of neighboring pores are superimposed if the pores are not exactly parallel to the beam axis.

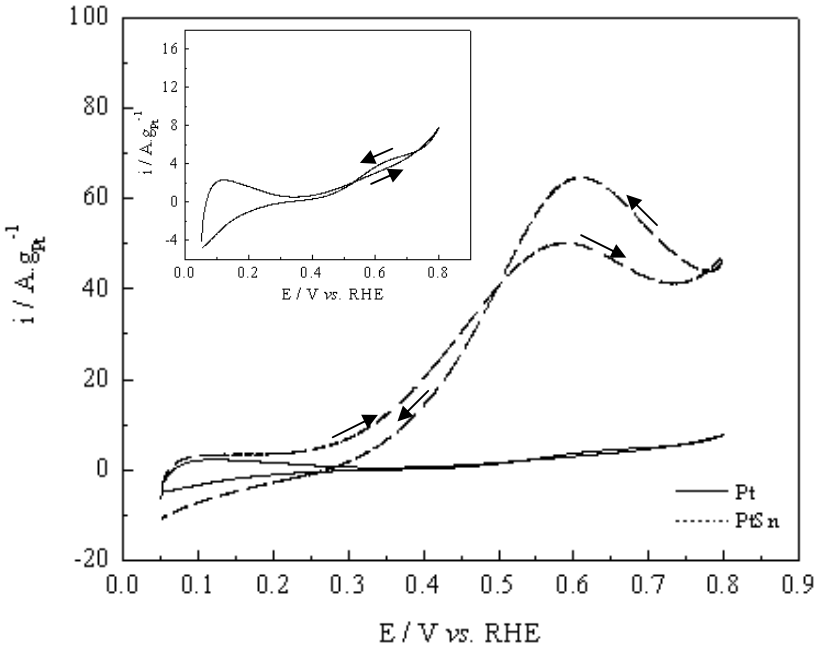

Figure 4.16 Cyclic voltammograms of the mesoporous Pt and PtSn catalysts in 0.5 M H_2SO_4/1 M C_2H_5OH with a sweep rate of 0.05 $V.s^{-1}$ at 20°C

An electrochemically catalytic behavior of all the prepared catalysts towards EOR was also investigated by means of cyclic voltammetry technique. The experiment was conducted in the supporting electrolyte of 0.5 M H_2SO_4 containing 1 M C_2H_5OH at 20°C with a sweep rate of 0.05 $V.s^{-1}$ and the result is then shown in Figure 4.16. The inset displays the enlarged voltammogram of the mesoporous Pt. It is noticeably observed that there are no any oxidation peaks during the potential window scanned, probably due to offering the sufficient oxygenated species for the rate of EOR occurred. By contrast, two oxidation peaks are presented in the mesoporous PtSn. The EOR for the Pt catalyst commences at 0.4 V *vs.* RHE; however the onset potential of the EOR is negatively shifted to lower potential of 0.2 V *vs.* RHE when adding 9 at.% Sn in the PtSn catalyst. Thus, an oxophilic element, namely Sn, in the binary sample could catalyze the EOR at the lower potentials, and consequently the current measured would significantly rise in the mesoporous PtSn but not in the pure Pt.

The plot between time and current of the mesoporous Pt and PtSn at the different potentials of 0.3, 0.4, 0.5 and 0.6 V *vs.* RHE is depicted in Figure 4.17. From all those curves, the current drops quickly at the short time and then decays slowly in the longer period and finally approaches the pseudo-steady state. This is because all the active sites

are initially vacant for ethanol adsorption; and as the time proceeds, the rate of EOR decreases greatly due to the increase of occupied active sites from the intermediate adsorbed species. Therefore, the stronger poisoning-tolerance catalyst would provide higher pseudo-steady state current. As seen from Figure 4.17, after holding the potential for 25 min each, the final current of the mesoporous PtSn catalyst was much higher than that of pure Pt in the whole potentials interested. The reason was that tin oxides could easily promote adsorption/dissociation of water to form the oxygenated species at lower potential, which could further oxidize the C1 and C2 intermediate adsorbed species to free Pt sites for re-adsorption of ethanol. As a result, the EOR would be enhanced by Sn.

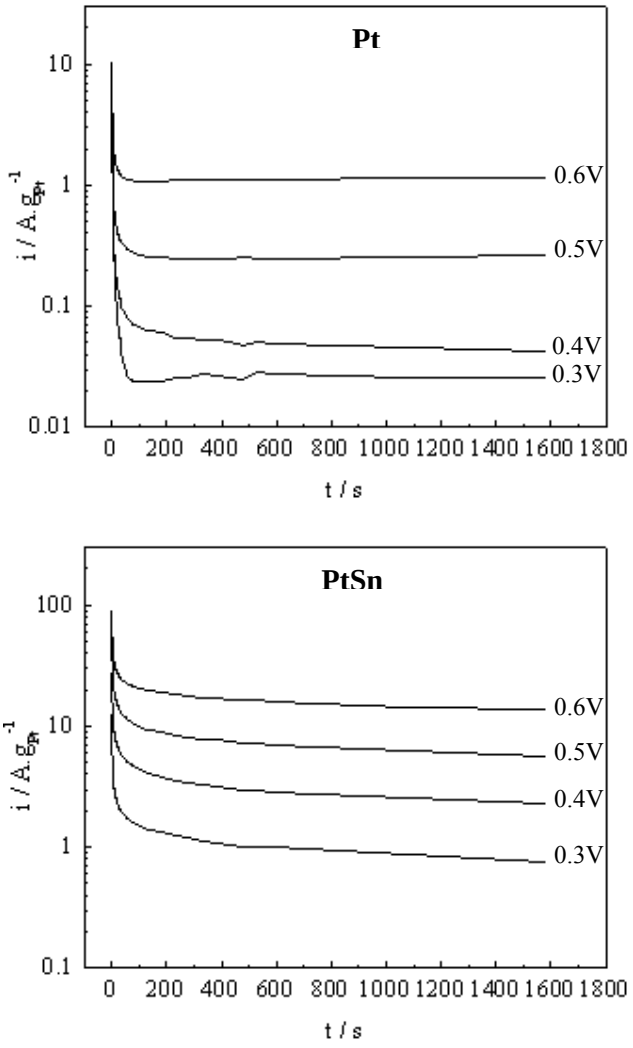

Figure 4.17 Current-time relationship of the prepared Pt-based catalysts in 0.5 M H_2SO_4/1 M C_2H_5OH at 20^oC

4.2.2 Effect of a Third Metal (Ru, Os) in Mesoporous PtSn-Based Catalysts on Their Activities for Ethanol Oxidation

Table 4.5 Element composition of the prepared PtSn-based catalysts

Sample	Solution composition (at.%)				Metal composition from EDX (at.%)			
	Pt	Sn	Ru	Os	Pt	Sn	Ru	Os
PtSn	50	50	-	-	91±1	9±0	-	-
PtSnRu	40	40	20	-	71±1	13±0	16±1	-
PtSnOs	40	40	-	20	72±1	21±3	-	7±1

Table 4.5 shows the intended composition of catalyst precursor solution and metal composition of the prepared Pt-based catalysts, which the latter values were obtained from EDX analysis. The measured Sn and Os contents in all prepared catalysts were much less than the expected ones; however the Ru content from EDX measurement of PtSnRu sample was nearly close to the intended value. Incomplete Os reduction was also found by the other groups [31,97,98]. They mentioned that the formation of an inactive Os oxide phase could be responsible for this manner. On the contrary, the difference of Sn content would be attributed to the ineffective reduction of its corresponding precursor by Zn granule to its metallic state, due to much lower reduction potentials of Sn than those of Pt and Ru (See Eq. (4.3) and (4.4) compared with Eq. (4.5), (4.6) and (4.7)).

$$Sn^{2+} + 2e^- \rightarrow Sn \qquad E^o = -0.14\,V \tag{4.3}$$

$$Zn^{2+} + 2e^- \rightarrow Zn \qquad E^o = -0.76\,V \tag{4.4}$$

$$[PtCl_6]^{2-} + 2e^- \rightarrow [PtCl_4]^{2-} + 2Cl^- \qquad E^o = 0.68\,V \tag{4.5}$$

$$[PtCl_4]^{2-} + 2e^- \rightarrow Pt + 4Cl^- \qquad E^o = 0.73\,V \tag{4.6}$$

$$RuCl_3 + 3e^- \rightarrow Ru + 3Cl^- \qquad E^o = 0.68\,V \tag{4.7}$$

It was also observed from these results that introducing the third metal (Ru and Os) to the catalyst could induce more Sn deposit. The maximum Sn content (at.%) was obtained with PtSnOs catalyst.

Figure 4.18 displays the x-ray diffraction pattern of all prepared catalysts along with that of sample holder which shows small reflections at low 2θ scan range (20-50^o). After subtracting from those peaks, all the prepared Pt-based catalysts would, therefore, show only a face-centered cubic (fcc) lattice of crystalline Pt structure as indicated by the red triangle symbol. However, it should be mentioned that all the reflection peaks of Pt in PtSnOs sample had much lower intensities than those of the others since the amount of PtSnOs sample used in XRD experiment was very small. The Pt (220) reflection peak was then selected to fit a Gaussian for calculating lattice constant of Pt as well as crystallite size of particles using the equations found in the literature [96].

The lattice constant of Pt in PtSn, PtSnRu and PtSnOs samples obtained was 0.3911 nm, 0.3899 nm and 0.3905 nm, respectively. Those values are comparable to that of the pure Pt catalyst (0.3905 nm) prepared by the same procedure. From the lattice constant of Pt estimated, atomic fraction of Sn in the alloy and degree of Sn alloyed in the catalysts were, thereafter, determined by Eq. (4.1) and Eq. (4.2), respectively. The corresponding values are shown in Table 4.6. Only 1.5-1.6 at.% Sn was found in the alloy phase of both PtSn and PtSnRu catalysts; but there was no Sn alloyed in the Os-containing sample. In addition, the alloying degree of Sn in the binary catalyst was much greater than those of ternary catalysts since introducing a third non-alloyed element such as Ru and Os could lower the degree of Sn alloyed in the binary PtSn catalyst as also found in the other studies [72,99]. Therefore, the non-alloyed Sn, Ru and Os would be in the form of their amorphous oxide phases and would exist in the vicinity of fcc Pt structure separately. As seen from Table 4.6, the particle size of PtSn catalyst was 4.3 nm; however, addition of Ru and Os as the third metal to the PtSn sample could decrease in the sizes of those solid particles to 3.6 nm and 3.4 nm, respectively. This might be a role of tin oxide that would act as a stabilizer to inhibit the agglomeration of Pt particles during the synthesis procedure as also found by Jiang et al. [6].

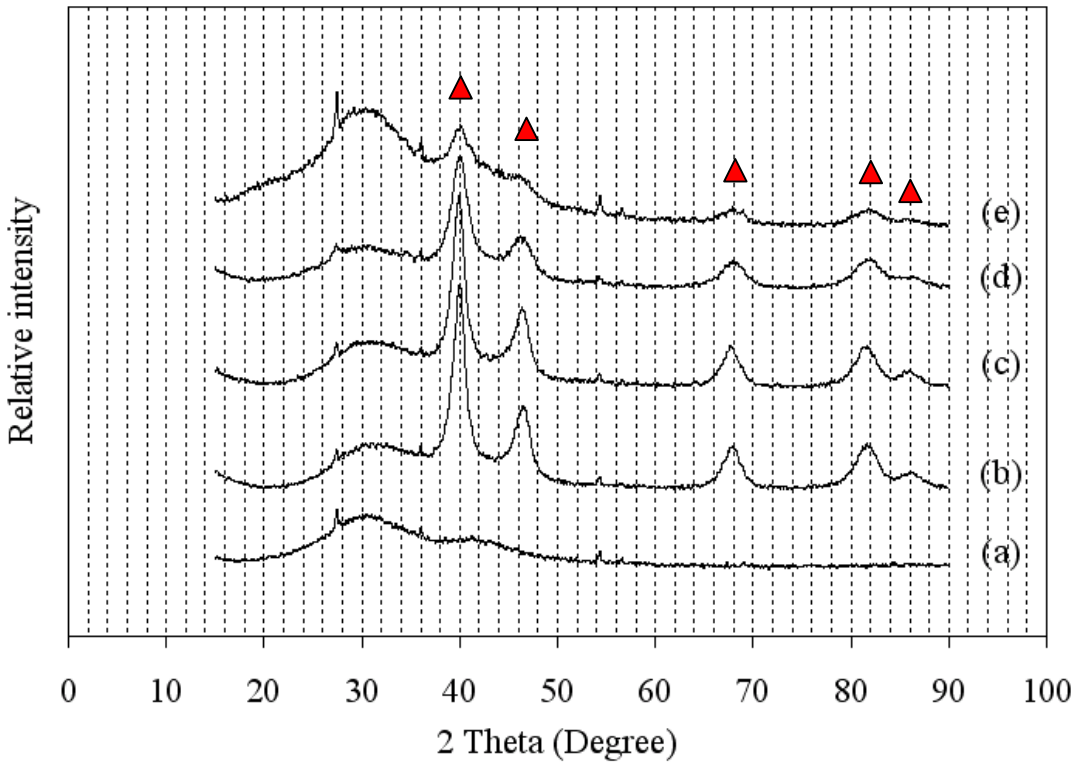

Figure 4.18 XRD patterns of the samples: a Sample holder, b Pt, c PtSn, d PtSnRu, e PtSnOs

Table 4.6 Structural analysis of PtSn, PtSnRu and PtSnOs catalysts

Sample	Lattice Parameter (nm)	Sn atomic fraction in the alloy	Alloying degree of Sn in the catalyst (%)	Crystallite size from XRD (nm)
PtSn	0.3911	0.015	14.9	4.3
PtSnRu	0.3899	0.016	8.6	3.6
PtSnOs	0.3905	0	0	3.4

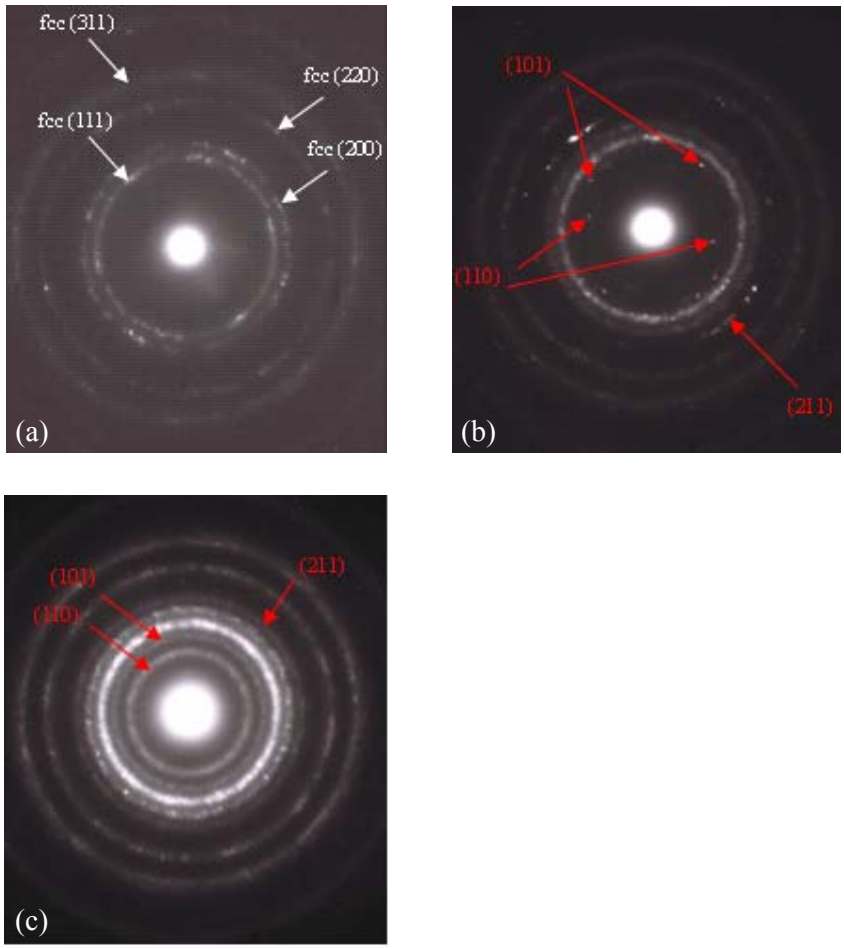

Figure 4.19 Electron diffraction patterns of the Pt-based catalysts: a PtSn, b PtSnRu, c PtSnOs with the camera length of 100 cm

Since the detection of amorphous oxides has been generally limited by XRD technique [29], electron diffraction through TEM analysis was then applied in order to confirm higher amount of Sn in PtSnOs sample. The electron diffractograms of all the in-house Pt-based catalysts with the camera length of 100 cm are illustrated in Figure 4.19. Broad, continuous ring patterns ascribed to fcc Pt structure of (111), (200), (220) and (311) crystal facets (JCPDS 04-0802) were found in all the samples, demonstrating the polycrystalline grains [77]. Beside the presence of Pt crystalline structures, tetragonal (110), (101) and (211) planes of cassiterite SnO_2 according to JCPDS 41-1445 were

also existed in both the PtSnRu and PtSnOs catalysts. Nevertheless, the ring pattern of SnO_2 structure is much favorable in the latter catalyst, indicating larger amount of Sn content in the Os-containing sample which is corresponding to the finding obtained from EDX measurement.

The microstructure of PtSnOs catalyst was, thereafter, studied using TEM technique. From Figure 4.20a, light color regions are the pores left after the building blocks of the surfactant were removed whereas the deposited metals are indicated by black color regions as seen remarkably in the red rectangle region. Thus, PtSnOs sample prepared by liquid crystalline templating technique showed mesoporous structure [24,28]. The HRTEM micrograph of PtSnOs catalyst is also illustrated in Figure 4.20 (b). From this observation, the d-spacing of 0.196 nm and 0.228 nm was attributed to Pt (200) and Pt (111) planes, respectively. These values are the same as those found in the pure Pt prepared by the same procedure, demonstrating the formation of unalloyed PtSnOs. In addition, the 0.264 nm spacing assigned to tetragonal SnO_2 (101) facet could also be evident. It implies the existence of SnO_2 nanoparticles in the vicinity of Pt particles [22].

(a)

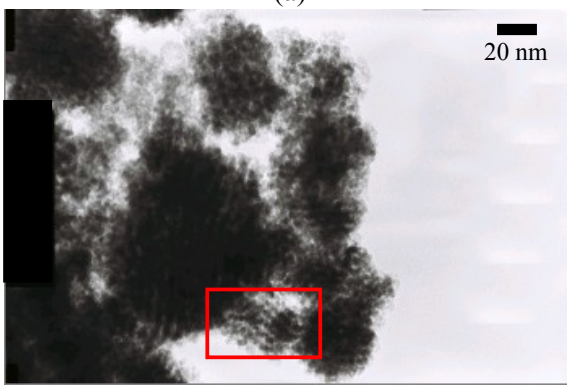

(b)

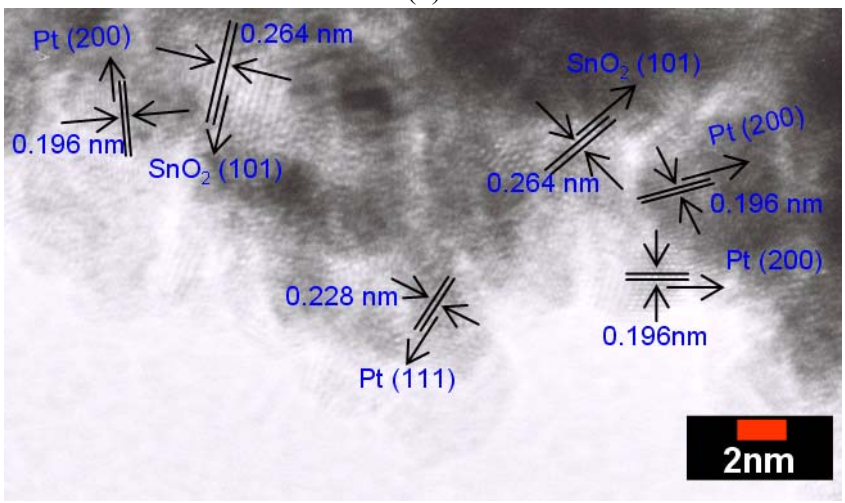

Figure 4.20 TEM (a) and HRTEM (b) images of PtSnOs sample

Figure 4.21 shows base cyclic voltammograms and CO stripping curves of the prepared Pt-based catalysts in 0.5 M H_2SO_4 with a scan rate of 0.02 $V.s^{-1}$. As seen from Figure 4.21, the second cycle of all the samples revealed the base cyclic voltammograms, meaning that the pre-adsorbed CO was oxidatively removed within the first sweep. To prevent the dissolution of the second/third metal into the supporting electrolyte, the upper potential was limited to 1 V [100,101] at which the complete CO stripping was occurred. The hydrogen desorption normally found during the positive-going scan from 0.05 to 0.4 V *vs.* RHE [102,103] was disappeared in all the samples, implying the blocking of their active sites by pre-adsorption of CO. For Pt, when the potential scanned was reached at 0.43 V *vs.* RHE, the weakly adsorbed CO was oxidized instantaneously [99] as indicated by the small shoulder in the potential range of 0.43-0.62 V *vs.* RHE, which was also observed in the other studies [104,105]. Besides, there was a strong peak found at higher overpotential with its peak potential of 0.77 V *vs.* RHE, which was assigned to the oxidation peak of the strongly adsorbed CO. Morimoto et al. [104] has found that the adsorbed CO at lower overpotential is bridge-adsorbed CO (CO_B) while that at higher overpotential is mainly linearly-adsorbed CO (CO_L) together with small portion of CO_B. For PtSn catalyst, the CO oxidation commences at 0.29 V *vs.* RHE, which is much lower than 0.43 V *vs.* RHE for pure Pt. Three oxidation peaks, centered at 0.45, 0.73 and 0.79 V *vs.* RHE were also existed in the binary catalyst [100]. Addition of Sn to Pt was contributed to the negative shift of the small pre-peak by *ca.* 0.1 V; but it had small influence on that of the strong oxidation peak. Thus, Sn adjacent to Pt sites helps to oxidize the bridge-adsorbed CO effectively [104]. The different result was found in PtSnRu sample that the strongly adsorbed CO was oxidized at the lower potential of 0.66 V *vs.* RHE; however PtSnRu catalyst showed the same onset potential of CO oxidation as PtSn catalyst. In Os-containing sample, the oxidation of CO starts at 0.26 V *vs.* RHE, which is the lowest onset potential among those prepared Pt-based catalysts. As a result, Os could promote CO oxidation rather than Sn and Ru could.

Electrochemically active surface area of all the prepared catalyst was then estimated by the following equation [12].

$$S_{ESA} = \frac{Q_{CO}}{420 \times G} \tag{4.8}$$

where Q_{CO} is the adsorbed CO charge on the electrode by assuming a monolayer CO oxidation charge of 420 $\mu C.cm^{-2}$ and G is the amount of the active metal for adsorption of CO. It was discovered from the other works that CO was adsorbed on a Pt-group metal such as Pt [40,100,102], Ru [102] and Os [106], but not on Sn sites as found by Shubina et al. [107]. From the above relationship, the electrochemically active surface area of the prepared catalyst is as follows: 41 $m^2.g^{-1}$ for Pt, 51 $m^2.g^{-1}$ for PtSn, 54 $m^2.g^{-1}$ for PtSnRu and 43 $m^2.g^{-1}$ for PtSnOs. It could be observed that the active surface of the ternary catalysts was comparable to that of PtSn and pure Pt even though their crystallite sizes measured by XRD analysis were much smaller. This was because of the higher amount of tin oxide in those ternary catalysts that could cover more Pt active sites, resulting in less electrochemical surface area for CO adsorption.

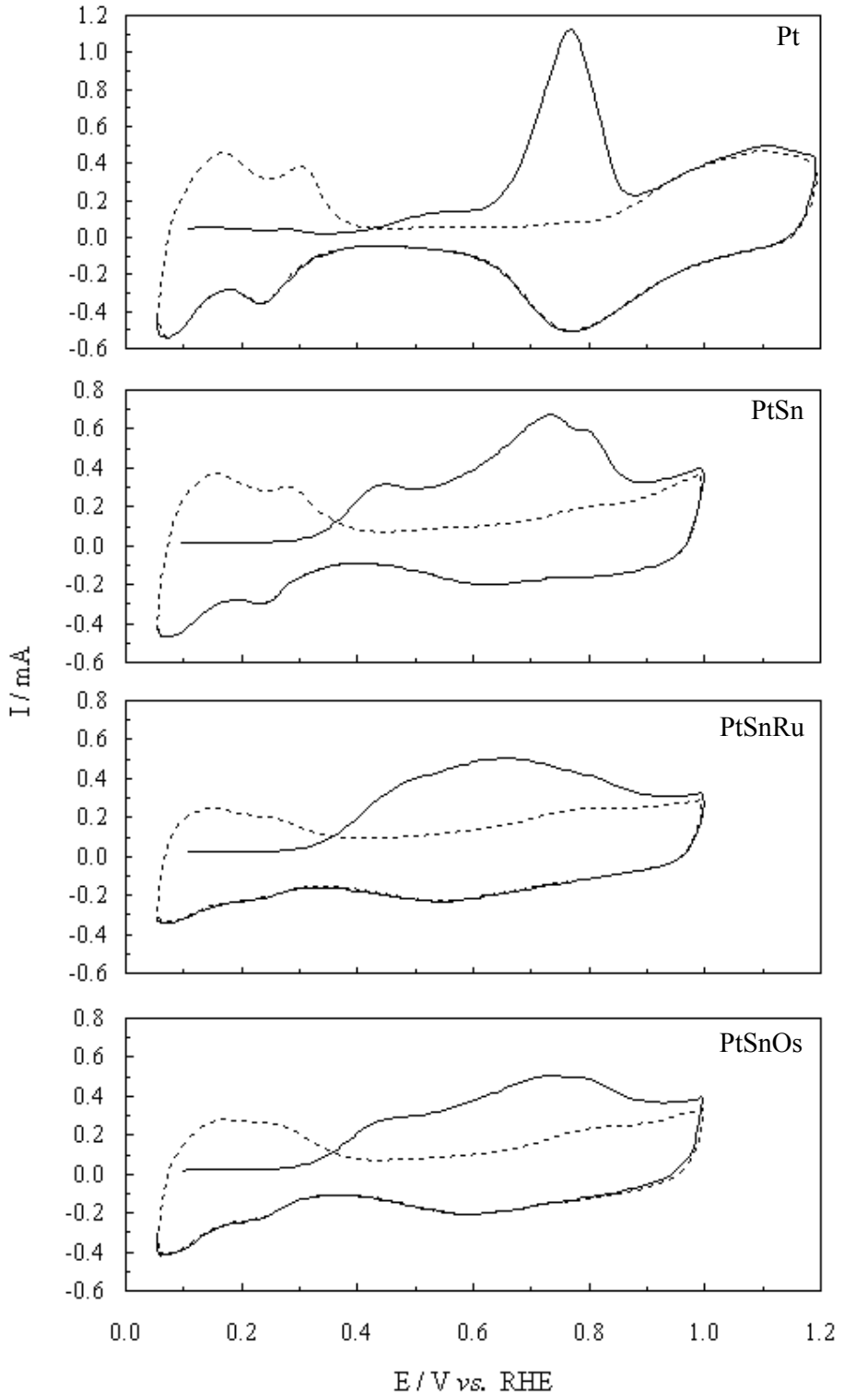

Figure 4.21 Cyclic voltammograms of the prepared Pt-based catalysts in 0.5 M H_2SO_4 with a scan rate of 0.02 $V.s^{-1}$ at 20°C. (——) first cycle; (- - - -) second cycle

In order to study the catalytic activity of the prepared Pt-based catalysts for ethanol oxidation reaction (EOR), cyclic voltammetric experiment was conducted in the

electrolyte solution of 0.5 M H_2SO_4/1 M C_2H_5OH at 20°C and 60°C as shown in Figure 4.22a and 4.22b, respectively. With the hypothesis of adsorption of ethanol on Pt sites, the currents measured were then normalized by Pt weight obtained from EDX measurement. The inset displays the onset potential of all the corresponding samples. From Figure 4.22a, PtSnOs catalyst showed the lowest onset potential, which was 0.15 V *vs.* RHE compared to 0.17 V *vs.* RHE for PtSnRu and 0.22 V *vs.* RHE for PtSn catalysts. Thus, the EOR could be catalyzed by PtSnOs better than the others. With considering the direction of the potential scan indicated by the arrows, the forward oxidation peak was clearly found in PtSn catalyst. However, introducing either Ru or Os into the PtSn sample affects the voltammograms differently. That oxidation peak was not observed in those samples during the positive-going scan since these oxophilic metals, namely Ru and Os, could promote water dissociation for oxidative removal of C1 and C2 adsorbed intermediates at the lower potentials than Sn could. This would liberate the active sites of Pt for further adsorption of ethanol. As compared Ru with Os, the Ru-containing sample gave small shoulder starting at 0.58 V *vs.* RHE but the other one did not. This gave the higher Faradaic current during the negative-going scan for PtSnOs sample. Besides, it was found that the reaction temperature influenced the activity of the corresponding samples in EOR. As seen from Figure 4.22a and 4.22b, an increase in the temperature from 20°C to 60°C lowered their onset potentials as well as increased their oxidation current considerably. In conclusion, PtSnOs is the most effective catalyst for EOR at both low and high temperatures.

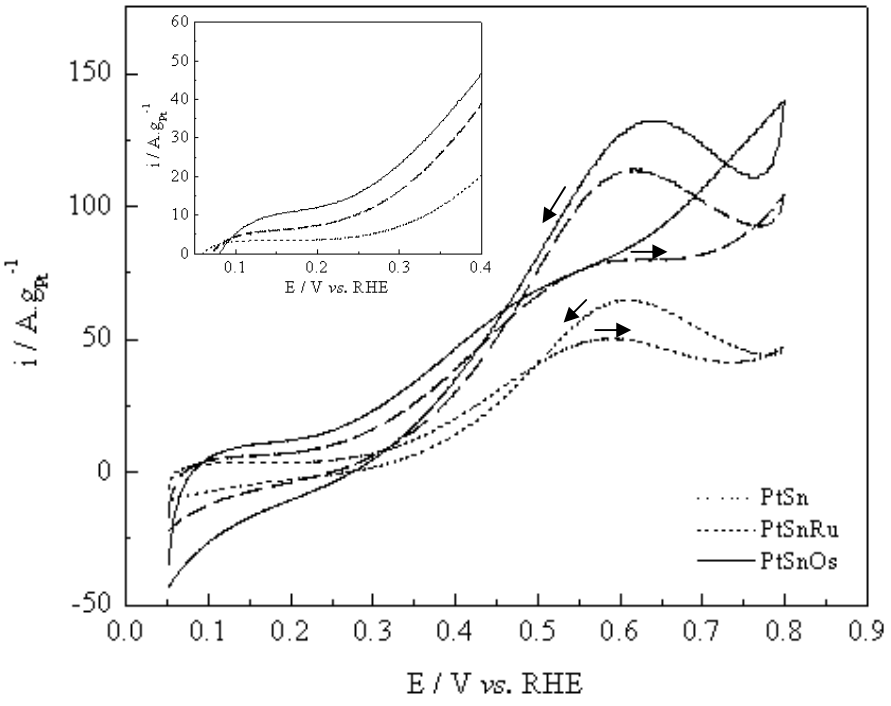

(a)

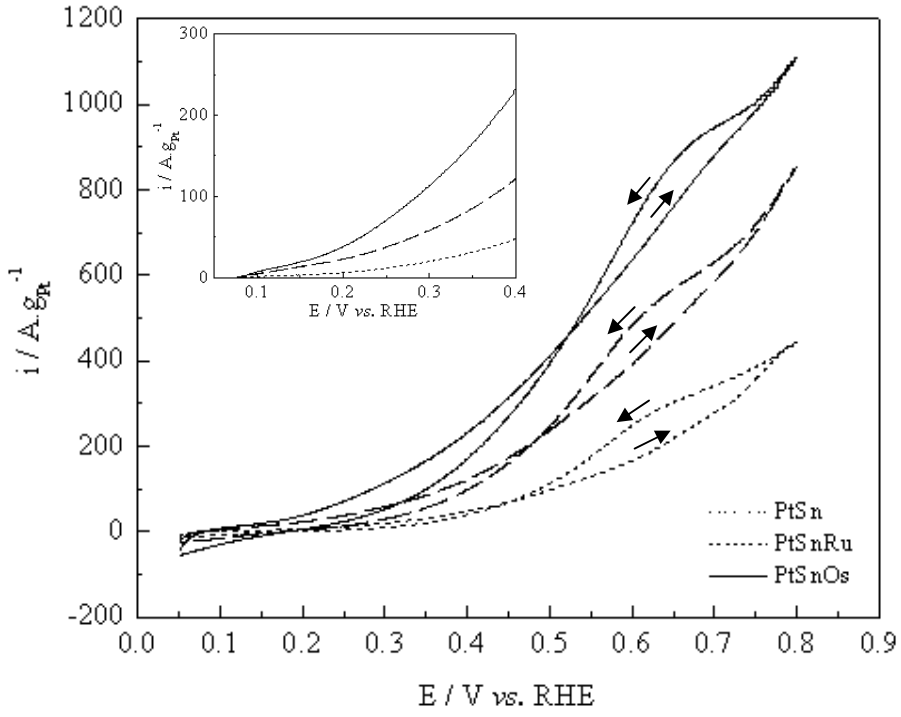

(b)

Figure 4.22 Voltammetric curves of the catalysts in 0.5 M H_2SO_4/1 M C_2H_5OH with a scan rate of 0.05 $V.s^{-1}$ at different temperatures: a 20°C, b 60°C

To know the detailed mechanistic information of the EOR, chronoamperometric measurement of all those samples is then performed in the same electrolyte solution. However, only current-time curves of PtSnOs sample at 60°C with the different potentials are shown here in Figure 4.23. For each potential of 0.3 to 0.6 V *vs.* RHE, the current measured drops rapidly at early stage, and then decays gradually until approaching a pseudo-steady state. The long-term poisoning rate of all the Pt-based catalysts (δ) is, thereafter, calculated by the following equation [108];

$$\delta = \frac{100}{I_0} \times \left(\frac{dI}{dt} \right)_{t \geq 500\ s} \tag{4.9}$$

where I_0 and $(dI/dt)_{t\geq 500s}$ are the current at y-intercept and the slope of the linear regression line, respectively. The relationship between the potential considered and the corresponding poisoning rate is then plotted as displayed in Figure 4.24. As seen from Figure 4.24a, the poisoning rate of PtSn sample was less than those of PtSnRu and PtSnOs samples, especially at the lower potentials; but at 0.6 V *vs.* RHE the poisoning rates of all the catalysts were approximately the same at 0.015 $\%.s^{-1}$. At elevated temperatures (i.e., 60°C), all the corresponding samples gave the same poisoning rate at the potentials of less than or equal to 0.5 V *vs.* RHE. However, at 0.6 V *vs.* RHE the lowest poisoning rate was found with PtSnOs catalyst. It was assumed that the mechanism of ethanol oxidation on Pt-based catalysts was the same as methanol oxidation reaction (MOR). The rate-determining step (rds) of the EOR at 25°C and/or lower potentials is ethanol adsorption/dehydrogenation whereas at elevated temperatures and/or higher potentials activation of water molecule to form $–OH_{ads}$ became the rds [32,34]. As a result, the former reaction would be pronounced in PtSn sample while PtSnOs sample showed superior activity for the latter reaction, which was

confirmed by the easier oxidation of CO. From all the findings found in the electrochemical measurements, PtSnOs catalyst could significantly enhance the EOR due to not only containing more Sn content but also having optimum Os-O bond strength [34]. The latter reason would directly affect ability to oxidatively adsorb water available for reacting with the C1 and C2 intermediates and forming CO_2 and CH_3COOH final products.

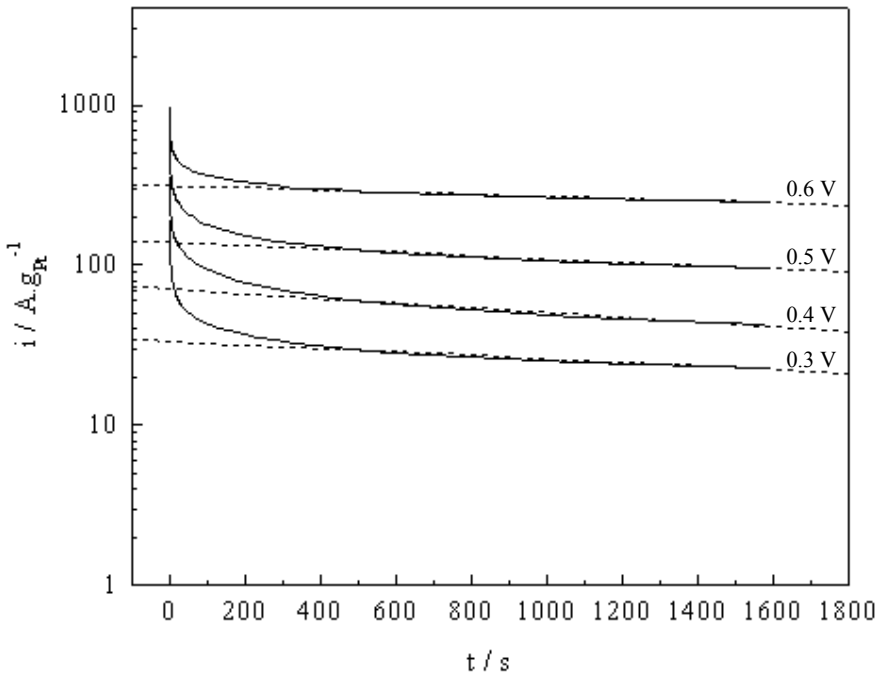

Figure 4.23 Time-current curves of PtSnOs catalyst in 0.5 M H_2SO_4/1 M C_2H_5OH at different potentials, 60°C

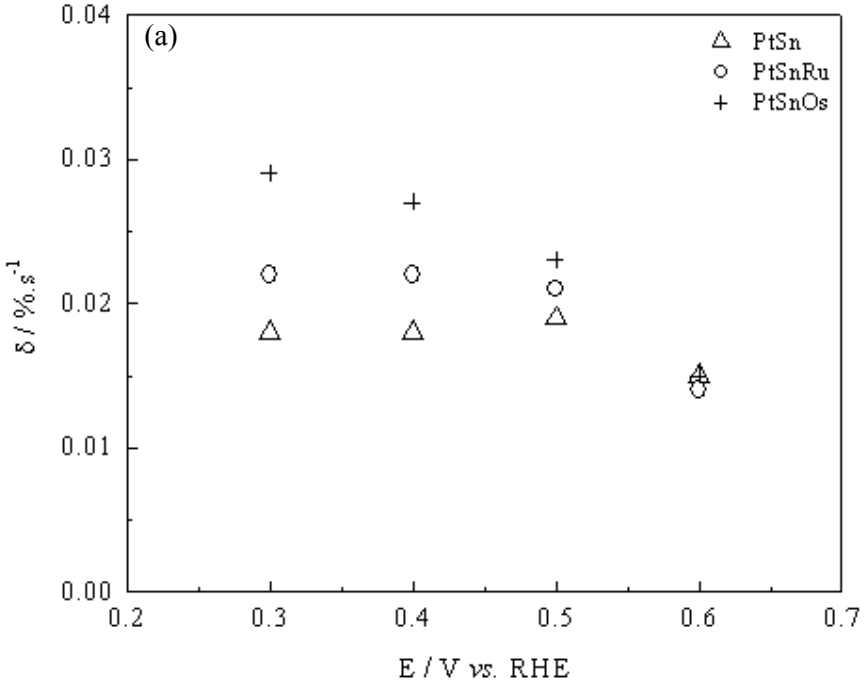

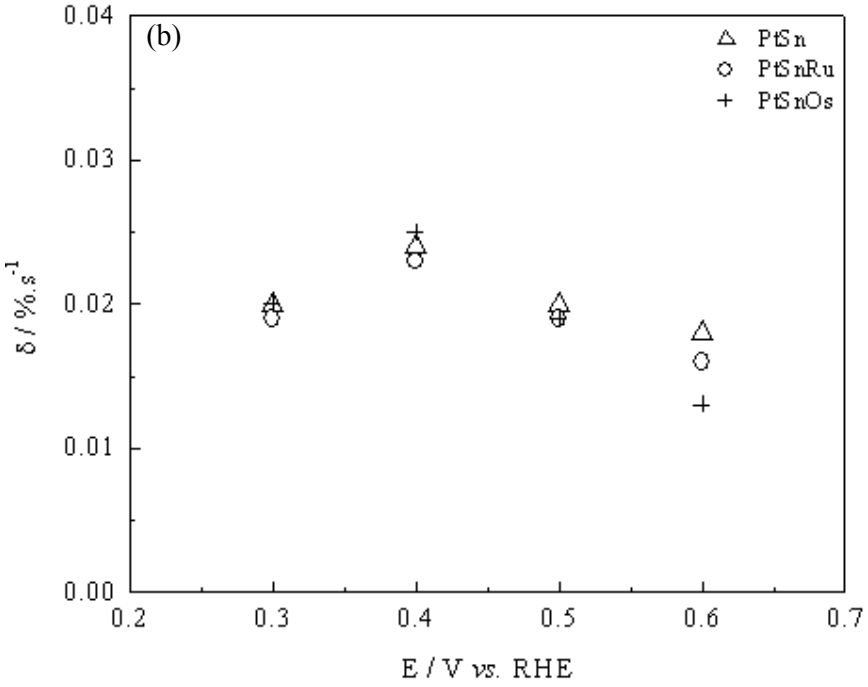

Figure 4.24 Relationship between potential and poisoning rate of the prepared samples at different temperatures: a 20°C, b 60°C

4.2.3 Promotion Role of Ru and Sn in Mesoporous PtRu and PtRuSn towards Ethanol Oxidation

Figure 4.25 manifests XRD patterns of mesoporous PtRu and PtRuSn samples. Besides, the reflection peaks of a sample holder during 2θ scan range of 20-50° are also shown. Without consideration of those peaks, a typical face-centered cubic (fcc) character of Pt crystal structure pointed by the red star could be clearly seen in both catalysts. There are no other diffraction peaks of metallic or oxide form of Ru and Sn, probably due to small amount of those metals contained or their amorphous oxide phases formed in the catalysts which could not be detected by XRD technique. The (220) reflection peak fitted a Gaussian is also displayed in the inset. According to the equation in the other work [96], the crystallite size of mesoporous PtRu and PtRuSn samples calculated was around 3.6 nm. The lattice constant of Pt was 0.3882 nm for PtRu sample; however addition of Sn to PtRu would extend it to 0.3899 nm which was very close to that of the prepared Pt (0.3905 nm). The degree of Ru alloyed in PtRu and PtRuSn samples calculated by the equation found in the literature [29] was 31% and 22%, respectively, demonstrating that Ru oxide would be favorably formed in PtRuSn better than in PtRu. As a result, those Ru and Sn oxides would not enter into the fcc lattice, leading to the unchanged lattice parameter of Pt when adding both metals to Pt. The atomic composition of PtRu and PtRuSn obtained from EDX technique was $Pt_{57}Ru_{43}$ and $Pt_{71}Ru_{16}Sn_{13}$, respectively.

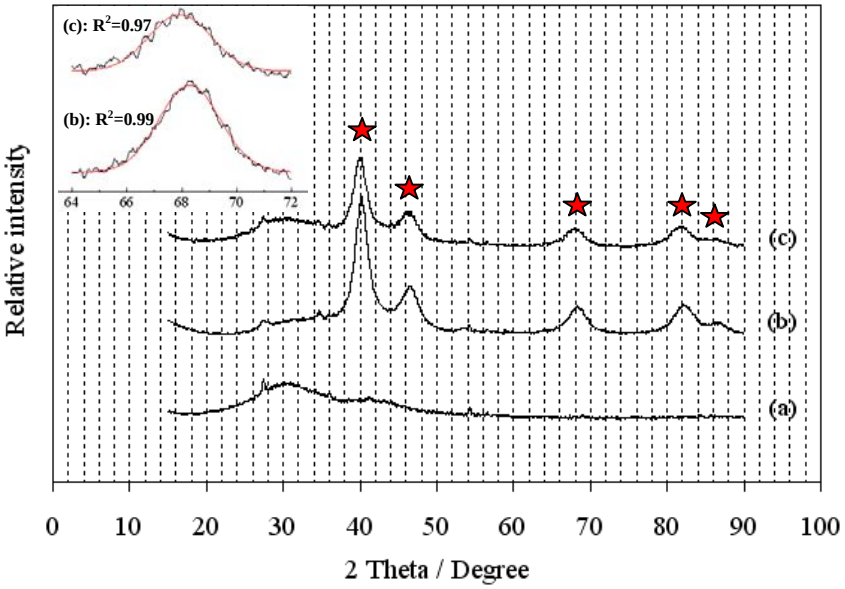

Figure 4.25 X-ray diffractograms of the samples: a Sample holder, b mesoporous PtRu, c mesoporous PtRuSn

Figure 4.26 displays cyclic voltammograms of all the prepared catalysts after pre-adsorption of CO at 0.09 V *vs.* RHE in 0.5 M H_2SO_4 solution at 20^oC. The upper potential of the prepared Pt, PtRu and PtRuSn was set at 1.2 V, 0.8 V and 1 V *vs.* RHE, respectively, in order to completely oxidize the adsorbed CO without the dissolution of these metals into the electrolyte solution [101,109]. The entire pre-adsorbed CO was stripped from the electrode surface at the first cycle which was confirmed by the base voltammogram in sulfuric acid solution at the second cycle as shown by the dash line. It can be seen from Figure 4.26 that pure Pt exhibits small shoulder between 0.43 and 0.62 V *vs.* RHE and a strong peak at 0.77 V *vs.* RHE. Those are ascribed to the oxidation peaks of weakly and strongly adsorbed CO, respectively [110]. The oxidation of CO on PtRu commences at 0.38 V *vs.* RHE which was shifted to lower potential in comparison to pure Pt (0.43 V *vs.* RHE). In addition, only one strong peak was found at 0.60 V *vs.* RHE, meaning that PtRu could oxidize the strongly adsorbed CO at lower potential than Pt could [104]. As Sn was incorporated to PtRu, the onset potential of the CO oxidation was negatively shifted to 0.28 V *vs.* RHE; and the peak potential of the broad oxidation peak was seen at 0.66 V *vs.* RHE. As a result, PtRuSn showed the highest activity for the oxidation of CO because not only Ru promotes the oxidation of the strongly adsorbed CO but also Sn helps to oxidize the weakly adsorbed CO found in the low potential region [104]. Furthermore, the electrochemically active surface area of the the corresponding catalysts was calculated by using Eq. (4.8). The prepared mesoporous Pt and PtRu have their active surface areas of 41 $m^2.g^{-1}$ and 84 $m^2.g^{-1}$, respectively, which are in good agreement with those samples in the other studies [28,29]. However, introducing Sn into PtRu would remarkably reduce the active surface area of PtRuSn to 54 $m^2.g^{-1}$ although it had the same particle size as the binary catalyst. It might result from tin oxide contained in PtRuSn would cover the active Pt sites as also found by the literature [6].

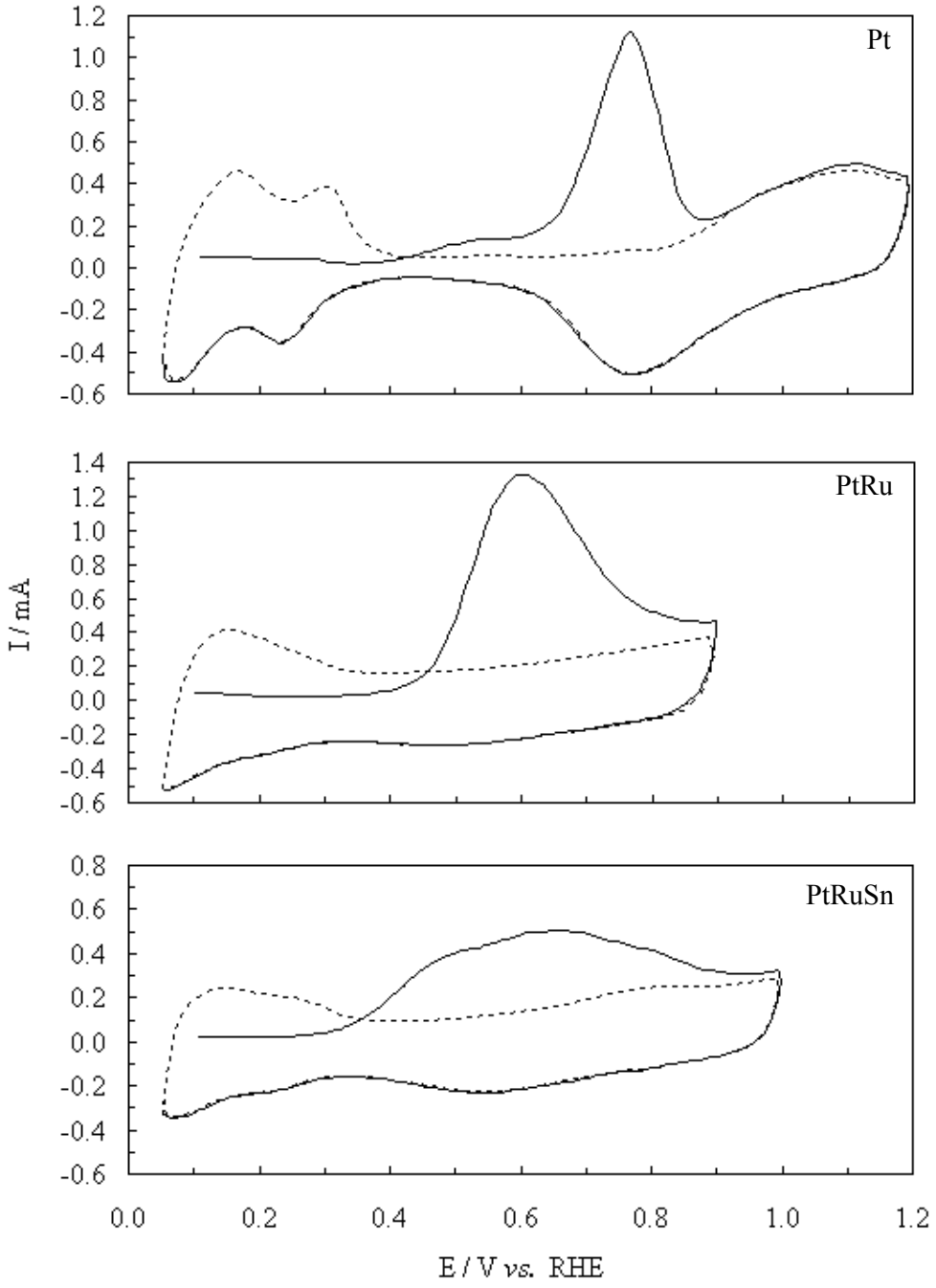

Figure 4.26 CO stripping curves of the prepared catalysts in 0.5 M H_2SO_4 with a sweep rate of 0.02 $V.s^{-1}$ at 20°C. (——) first cycle; (- - - - -) second cycle

In ethanol oxidation study, cyclic voltammograms of mesoporous PtRu and PtRuSn for was carried out in 0.5 M H_2SO_4 containing 1 M C_2H_5OH solution and the voltammograms obtained are depicted in Figure 4.27. The experiment was conducted at 60°C with a scan rate of 0.05 $V.s^{-1}$. The applied potential was scanned from 0.05 to 0.8 V vs. RHE. The oxidation current response was then normalized to the actual amount of Pt since it was hypothesized that ethanol molecule would adsorb only on Pt sites [40]. It

could be seen from the inset of Figure 4.27 that the EOR commences at about 0.225 V vs. RHE on PtRu; however, addition of Sn to PtRu led to the negative shift of the onset potential by approximately 0.1 V. There are no oxidation peaks during positive/negative-going scan, indicating no accumulation of the poisons on the surface [36]. It was also observed that the voltammetric current of PtRuSn was much greater than that of PtRu over the potential range of 0.3-0.8 V vs. RHE. From all the above results, the ternary catalyst could promote EOR better than PtRu could.

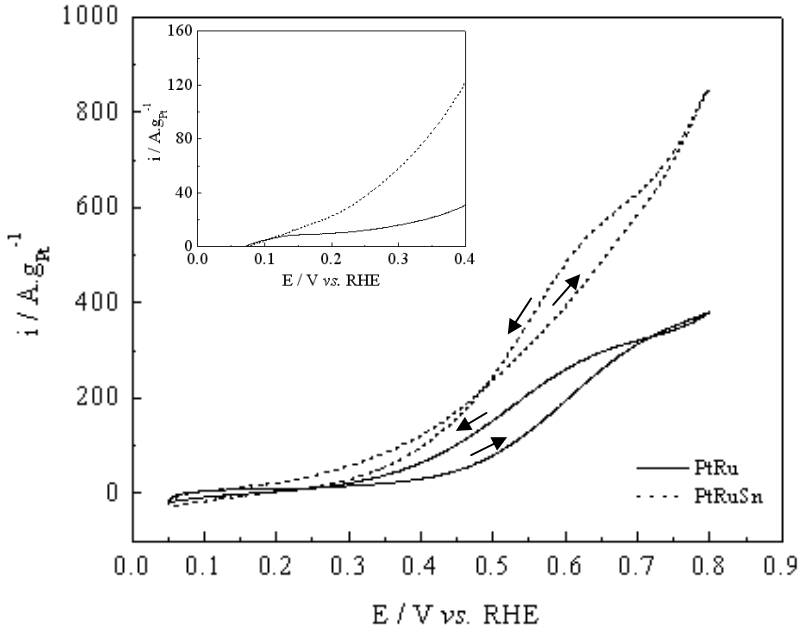

Figure 4.27 Cyclic voltammograms of mesoporous PtRu and PtRuSn catalysts in the electrolyte solution of 0.5 M H_2SO_4/1 M C_2H_5OH with a scan rate of 0.05 V.s^{-1} at 60^{o}C

Furthermore, chronoamperometric measurement was conducted in the same electrolyte solution in order to clarify the poison-tolerance ability of the catalyst for EOR. The curves shown in Figure 4.28 were collected by varying the potentials over 0.3-0.6 V *vs.* RHE for 1580 sec each. The red curves designated as R refer to those of PtRu while the blue ones labeled by RS belong to PtRuSn. The dashed lines in all the current-time curves are linear regression lines from 500 to 1580 s. It could be seen from Figure 4.28 that the current in all those curves decreases quickly at short time, followed by a slow decay rate at longer times and approaches a steady current finally. PtRuSn produces much higher current in the whole range of time interested and the potential considered than PtRu, implying stronger ability to tolerate the adsorbed ethanolic residues on PtRuSn surface rather than on PtRu surface. In addition, the long-term poisoning rate of the prepared catalysts is calculated using Eq. (4.9) and is then plotted as a function of potential shown in Figure 4.29. As seen from Figure 4.29, the surface of PtRu rather than that of PtRuSn was seriously poisoned by the adsorbed C1 and C2 intermediate species at the lower potential region (≤ 0.4 V *vs.* RHE); but, the poisoning rate of PtRu was dropped rapidly as increasing the applied potential over 0.5-0.6 V *vs.* RHE. At the high potential of 0.6 V *vs.* RHE, PtRu showed stronger poison-tolerance than the PtRuSn. As mention before that dissociative adsorption of ethanol is the rate-determining step (rds) in the low potential region; but at higher potentials the rds is

water activation. As a consequence, the former reaction would be severely deteriorated by the contraction of Pt lattice in PtRu sample in comparison to the elongated lattice of Pt in PtRuSn. By contrast, the latter reaction was enhanced by PtRu as seen from the lower poisoning rate in the high potential. As a result, Sn and Ru show different promotion effects for EOR. Sn promotes the adsorption/dehydrogenation of ethanol molecules on the active Pt sites while Ru activates water molecules to form the hydroxyl species ($-OH_{ads}$). It was also confirmed by the result from CO oxidation that Ru helps to oxidize the strongly adsorbed CO at lower potential. The synergetic roles of Sn and Ru would, therefore, give rise to the overall EOR on the mesoporous PtRuSn catalyst.

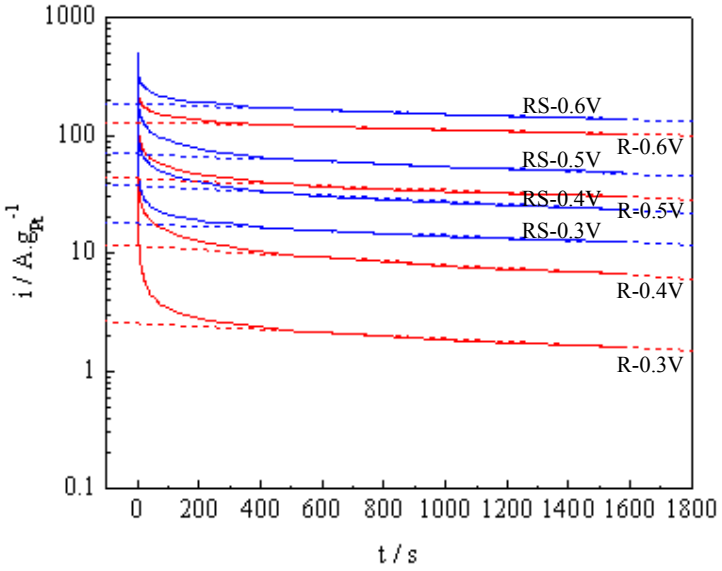

Figure 4.28 Chronoamperometric curves of the prepared catalysts in the electrolyte solution of 0.5 M H_2SO_4/1 M C_2H_5OH at 60°C

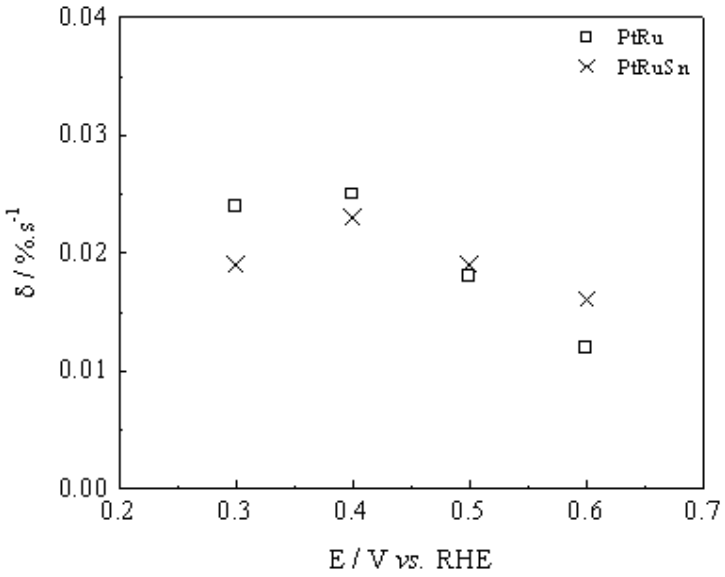

Figure 4.29 Long-term poisoning rate of the prepared catalysts at different potentials, 60°C

CHARTER 5 CONCLUSIONS AND RECOMMENDATIONS

5.1 Conclusions

5.1.1 Carbon-Supported PtSn Electrocatalysts

In this part of study, the effect of pre-treatment methods of carbon supports for PtSn on catalytic activity of the prepared PtSn/C catalysts was investigated. Both acid and thermal activation methods affected surface characteristics of the supports differently, including specific surface area, pore size, surface functional groups and surface charge. The surface characteristics of the supports determined metal loading and interaction between the metal precursor and the support surface during the deposition step. FTIR spectra showed that the HNO_3 pre-treatment had produced various oxygenated functional groups such as phenol, quinone, carboxyl-carbonates and nitrate groups on the support surface, which promote acidic property. The high acidic functional groups on NA-C could hinder Pt reduction, but promote Sn deposition leading to lower Pt:Sn ratio. By contrast, thermal activation enhanced the specific surface area of the carbon and increased base functional groups. The base functional groups acted as the sites for Pt nanocluster deposition, and consequently provided smaller metal particle sizes and higher metal dispersion. The cyclic voltammograms in sulfuric acid and chronoamperometric results revealed that PtSn/HT-C catalyst had yielded the highest electrochemical surface area and electrochemical activity for ethanol oxidation, respectively. As a result, heat treatment of carbon had enhanced catalytic activity for ethanol oxidation as well as DEFC performance, of the PtSn/C catalyst better than nitric acid treatment would have done, owing to a combination of high metal dispersion and suitable Pt:Sn ratio. In comparison to commercial Pt-based catalysts manufactured by E-TEK, the electrode fabricated from PtSn/HT-C catalyst showed the better performance in the direct ethanol fuel cell than those from commercial Pt/C and Pt_3Sn_1/C catalysts because PtSn/HT-C sample contained tin oxides sufficient for accelerating CO oxidation to free Pt active sites for further ethanol adsorption. In the study of metal loading order and solution pH in PtSn/C preparation, it was found that consecutive deposition of platinum precursor on heat-treated carbon-supported tin oxides increased metal content as well as dispersion of metal on the supports, contributing to the enhanced efficiency of ethanol oxidation.

5.1.2 Unsupported Electrocatalysts

Initially, mesoporous Pt and PtSn catalysts have been prepared successfully through liquid crystalline templating technique. The prepared catalysts gave the same average particle sizes of 4.3 nm with high active surface area of 40-50 $m^2.g^{-1}$. The results from electrochemical measurement disclosed that addition of 9 at.% Sn to Pt could promote ethanol oxidation at lower potential of 0.2 V *vs.* RHE. The effect of a third metal (Ru, Os) added in mesoporous PtSn-based catalysts on their activities for ethanol oxidation was then investigated. The results from XRD showed that introducing both Ru and Os into the PtSn sample led to the reduction in their average crystallite sizes; but their electrochemical active surface areas, which were 54 $m^2.g^{-1}$ for PtSnRu and 43 $m^2.g^{-1}$ for PtSnOs, was comparable to that of PtSn (51 $m^2.g^{-1}$). This was because more tin oxides

in those ternary catalysts acted as a barrier preventing Pt agglomeration during the synthesis procedure and also could cover on the active Pt sites. Electrochemical test disclosed that PtSnOs was the most effective catalyst for ethanol oxidation as compared to PtSnRu and PtSn catalysts due to high tin oxides contained and more oxophilicity of Os. Especially at higher temperature and potential, PtSnOs could actively promote the overall ethanol oxidation as well as CO oxidation by catalyzing water molecule to form hydroxyl species for the oxidative removal of the C1 and C2 intermediates, yielding lower poisoning rate. Furthermore, the role of Ru and Sn in mesoporous PtRu and PtRuSn for ethanol oxidation was examined. The alloying degree of Ru in the PtRu sample was 31%, but it was reduced to 22% as Sn was incorporated into PtRu. It implied that the non-alloyed Ru oxides would be preferably formed in PtRuSn and could accelerate adsorption/dissociation of water. The results from electrochemical measurements confirmed that the synergetic roles of Ru and Sn enhanced the oxidation of ethanol in PtRuSn catalyst because not only Sn promotes dissociative adsorption of ethanol on the Pt sites but also Ru accelerates water activation for the oxidation of the strongly adsorbed CO and other C1 and C2 intermediate species.

5.2 Recommendations

For supported electrocatalysts, osmium should be introduced as a third metal to Pt/Sn/HT-C. In addition, solution pH in the preparation of ternary supported catalyst should be adjusted to obtain high metal loading together with high metal dispersion on the supports.

For unsupported electrocatalysts, a stronger reducing agent, $NaBH_4$, should be applied instead of granular Zn to increase tin content in PtSnOs sample. Suitable condition for PtSnOs preparation without a formation of osmium oxide should also be sorted out to achieve the intended Os content. The products and by-products collected during the oxidation reaction of ethanol should be further monitored by chromatographic techniques such as gas chromatography (GC) and high-performance liquid chromatography (HPLC) to understand the reaction mechanism. For a practical point of view, the modified PtSnOs catalyst should be employed as the anode catalyst for MEA preparation, and subsequently will be evaluated the performance in ethanol feed fuel cell.

REFERENCES

1. Lamy, C., Lima, A., LeRhun, V., Delime, F., Coutanceau, C. and Léger, J.M., 2002, "Recent Advances in the Development of Direct Alcohol Fuel Cells (DAFC)", **Journal of Power Sources**, Vol. 105, pp. 283-296.
2. Song, S. and Tsiakaras, P., 2006, "Recent Progress in Direct Ethanol Proton Exchange Membrane Fuel Cells (DE-PEMFCs)", **Applied Catalysis B: Environmental**, Vol. 63, pp. 187-193.
3. Song, S., Zhou, W., Liang, Z., Cai, R., Sun, G., Xin, Q., Stergiopoulos, V. and Tsiakaras, P., 2005, "The Effect of Methanol and Ethanol Cross-Over on the Performance of PtRu/C-Based Anode DAFCs", **Applied Catalysis B: Environmental**, Vol. 55, pp. 65-72.
4. Simões, F.C., dos Anjos, D.M., Vigier, F., Léger, J.M., Hahn, F., Coutanceau, C., Gonzalez, E.R., Tremiliosi-Filho, G., de Andrade, A.R., Olivi, P. and Kokoh, K.B., 2007, "Electroactivity of Tin Modified Platinum Electrodes for Ethanol Electrooxidation", **Journal of Power Sources**, Vol. 167, pp. 1-10.
5. Rousseau, S., Coutanceau, C., Lamy, C. and Léger, J.M., 2006, "Direct Ethanol Fuel Cell (DEFC): Electrical Performances and Reaction Products Distribution under Operating Conditions with Different Platinum-Based Anodes", **Journal of Power Sources**, Vol. 158, pp. 18-24.
6. Jiang, L., Colmenares, L., Jusys, Z., Sun, G.Q. and Behm, R.J., 2007, "Ethanol Electrooxidation on Novel Carbon Supported Pt/SnO_x/C Catalysts with Varied Pt:Sn Ratio", **Electrochimica Acta**, Vol. 53, pp. 377-389.
7. Wang, J., Wasmus, S. and Savinell, R.F., 1995, "Evaluation of Ethanol, 1-Propanol, and 2-Propanol in a Direct Oxidation Polymer-Electrolyte Fuel Cell", **Journal of The Electrochemical Society**, Vol. 142, pp. 4218-4224.
8. Zhou, W., Zhou, Z., Song, S., Li, W., Sun, G., Tsiakaras, P. and Xin, Q., 2003, "Pt Based Anode Catalysts for Direct Ethanol Fuel Cells", **Applied Catalysis B: Environmental**, Vol. 46, pp. 273-285.
9. Antolini, E., 2009, "Carbon Supports for Low-Temperature Fuel Cell Catalysts", **Applied Catalysis B: Environmental**, Vol. 88, pp. 1-24.
10. Tian, J.H., Wang, F.B., Shan, Z.Q., Wang, R.J., and, Zhang, J.Y., 2004, "Effect of Preparation Conditions of Pt/C Catalysts on Oxygen Electrode Performance in Proton Exchange Membrane Fuel Cells", **Journal of Applied Electrochemistry**, Vol. 34, pp. 461-467.
11. Liu, Z., Ling, X.Y., Su, X., Lee, J.Y. and Gan, L.M., 2005, "Preparation and Characterization of Pt/C and PtRu/C Electrocatalysts for Direct Ethanol Fuel Cells", **Journal of Power Sources**, Vol. 149, pp. 1-7.
12. Wang, Z.B., Yin, G.P., Zhang, J., Sun, Y.C. and Shi, P.F., 2006, "Investigation of Ethanol Electrooxidation on a Pt-Ru-Ni/C Catalyst for a Direct Ethanol Fuel Cell", **Journal of Power Sources**, Vol. 160, pp. 37-43.
13. Jiang, L., Sun, G., Zhou, Z., Zhou, W. and Xin, Q., 2004, "Preparation and Characterization of PtSn/C Anode Electrocatalysts for Direct Ethanol Fuel Cell", **Catalysis Today**, Vol. 93-95, pp. 665-670.
14. Guo, Y., Zheng, Y. and Huang, M., 2008, "Enhanced Activity of PtSn/C Anode Electrocatalyst Prepared by Formic Acid Reduction for Direct Ethanol Fuel Cells", **Electrochimica Acta**, Vol. 53, pp. 3102-3108.
15. Neto, A.O., Farias, L.A., Dias, R.R., Brandalise, M., Linardi, M. and Spinacé, E.V., 2008, "Enhanced Electro-Oxidation of Ethanol Using PtSn/CeO_2-C

Electrocatalysts Prepared by an Alcohol-Reduction Process", **Electrochemistry Communications**, Vol. 10, pp. 1315-1317.

16. dos Anjos, D.M., Kokoh, K.B., Léger, J.M., de Andrade, A.R., Olivi, P. and Tremiliosi-Filho, G., 2006, "Electrocatalytic Oxidation of Ethanol on Pt-Mo Bimetallic Electrodes in Acid Medium", **Journal of Applied Electrochemistry**, Vol. 36, pp. 1391-1397.
17. Colmati, F., Antolini, E. and Gonzalez, E.R., 2008, "Preparation, Structural Characterization and Activity for Ethanol Oxidation of Carbon Supported Ternary Pt-Sn-Rh Catalysts", **Journal of Alloys and Compounds**, Vol. 456, pp. 264-270.
18. Lima, F.H.B. and Gonzalez, E.R., 2008, "Ethanol Electro-Oxidation on Carbon-Supported Pt-Ru, Pt-Rh and Pt-Ru-Rh Nanoparticles", **Electrochimica Acta**, Vol. 53, pp. 2963-2971.
19. Lamy, C., Rousseau, S., Belgsir, E.M., Coutanceau, C. and Léger, J.M., 2004, "Recent Progress in the Direct Ethanol Fuel Cell: Development of New Platinum-Tin Electrocatalysts", **Electrochimica Acta**, Vol. 49, pp. 3901-3908.
20. Colmati, F., Antolini, E. and Gonzalez, E.R., 2006, "Effect of Temperature on the Mechanism of Ethanol Oxidation on Carbon Supported Pt, PtRu and Pt_3Sn Electrocatalysts", **Journal of Power Sources**, Vol. 157, pp. 98-103.
21. Neto, A.O., Dias, R.R., Tusi, M.M., Linardi, M. and Spinacé, E.V., 2007, "Electro-Oxidation of Methanol and Ethanol Using PtRu/C, PtSn/C and PtSnRu/C Electrocatalysts Prepared by an Alcohol-Reduction Process", **Journal of Power Sources**, Vol. 166, pp. 87-91.
22. Jiang, L., Sun, G., Sun, S., Liu, J., Tang, S., Li, H., Zhou, B. and Xin, Q., 2005, "Structure and Chemical Composition of Supported Pt-Sn Electrocatalysts for Ethanol Oxidation", **Electrochimica Acta**, Vol. 50, pp. 5384-5389.
23. Prasanna, M., Ha, H.Y., Cho, E.A., Hong, S.A. and Oh, I.H., 2004, "Investigation of Oxygen Gain in Polymer Electrolyte Membrane Fuel Cells", **Journal of Power Sources**, Vol. 137, pp. 1-8.
24. Attard, G.S., Bartlett, P.N., Coleman, N.R.B., Elliott, J.M., Owen, J.R. and Wang, J.H., 1997, "Mesoporous Platinum Films from Lyotropic Liquid Crystalline Phases", **Science**, Vol. 278, pp. 838-840.
25. Attard, G.S., Corker, J.M., Göltner, C.G., Henke, S. and Templer, R.H., 1997, "Liquid-Crystal Templates for Nanostructured Metals", **Angewandte Chemie International Edition in English**, Vol. 36, pp. 1315-1317.
26. Whitehead, A.H., Elliott, J.M., Owen, J.R. and Attard, G.S., 1999, "Electrodeposition of Mesoporous Tin Films", **Chemical Communications**, pp. 331-332.
27. Nelson, P.A., Elliott, J.M., Attard, G.S. and Owen, J.R., 2002, "Mesoporous Nickel/Nickel Oxide a Nanoarchitectured Electrode", **Chemistry of Materials**, Vol. 14, pp. 524-529.
28. Kucernak, A. and Jiang, J., 2003, "Mesoporous Platinum as a Catalyst for Oxygen Electroreduction and Methanol Electrooxidation", **Chemical Engineering Journal**, Vol. 93, pp. 81-90.
29. Jiang, J. and Kucernak, A., 2004, "Mesoporous Microspheres Composed of PtRu Alloy", **Chemistry of Materials**, Vol. 16, pp. 1362-1367.
30. Jiang, J. and Kucernak, A., 2009, "Electrocatalytic Properties of Nanoporous PtRu Alloy towards the Electrooxidation of Formic Acid", **Journal of Electroanalytical Chemistry**, Vol. 630, pp. 10-18.

31. Jiang, J. and Kucernak, A., 2009, "Electrodeposition of Highly Alloyed Quaternary PtPdRuOs Catalyst with Highly Ordered Nanostructure", **Electrochemistry Communications**, Vol. 11, pp. 1005-1008.
32. Li, H., Sun, G., Cao, L., Jiang, L. and Xin, Q., 2007, "Comparison of Different Promotion Effect of PtRu/C and PtSn/C Electrocatalysts for Ethanol Electro-Oxidation", **Electrochimica Acta**, Vol. 52, pp. 6622-6629.
33. Gurau, B., Viswanathan, R., Liu, R., Lafrenz, T.J., Ley, K.L., Smotkin, E.S., Reddington, E., Sapienza, A., Chan, B.C., Mallouk, T.E. and Sarangapani, S., 1998, "Structural and Electrochemical Characterization of Binary, Ternary, and Quaternary Platinum Alloy Catalysts for Methanol Electro-Oxidation", **The Journal of Physical Chemistry B**, Vol. 102, pp. 9997-10003.
34. Ley, K.L., Liu, R., Pu, C., Fan, Q., Leyarovska, N., Segre, C. and Smotkin, E.S., 1997, "Methanol Oxidation on Single-Phase Pt-Ru-Os Ternary Alloys", **Journal of The Electrochemical Society**, Vol. 144, pp. 1543-1548.
35. Huang, J., Yang, H., Huang, Q., Tang, Y., Lu, T. and Akins, D.L., 2004, "Methanol Oxidation on Carbon-Supported Pt-Os Bimetallic Nanoparticle Electrocatalysts", **Journal of The Electrochemical Society**, Vol. 151, pp. A1810-A1815.
36. Jiang, J. and Kucernak, A., 2003, "Electrooxidation of Small Organic Molecules on Mesoporous Precious Metal Catalysts: II: CO and Methanol on Platinum-Ruthenium Alloy", **Journal of Electroanalytical Chemistry**, Vol. 543, pp. 187-199.
37. **Rules of Thumb** [Online], Available : http://www.brucelin.ca/scooters/thumb.html [2011, September 15].
38. **Gasoline** [Online], Available : http://en.wikipedia.org/wiki/Gasoline#Energy_content_.28high_and_low_heating_value.29 [2011, September 15].
39. de Souza, J.P.I., Queiroz, S.L., Bergamaski, K., Gonzalez, E.R. and Nart, F.C., 2002, "Electro-Oxidation of Ethanol on Pt, Rh, and PtRh Electrodes. A Study Using DEMS and in-Situ FTIR Techniques", **The Journal of Physical Chemistry B**, Vol. 106, pp. 9825-9830.
40. Vigier, F., Coutanceau, C., Hahn, F., Belgsir, E.M. and Lamy, C., 2004, "On the Mechanism of Ethanol Electro-Oxidation on Pt and PtSn Catalysts: Electrochemical and in situ IR Reflectance Spectroscopy Studies", **Journal of Electroanalytical Chemistry**, Vol. 563, pp. 81-89.
41. Léger, J.M., Rousseau, S., Coutanceau, C., Hahn, F. and Lamy, C., 2005, "How Bimetallic Electrocatalysts Does Work for Reactions Involved in Fuel Cells?: Example of Ethanol Oxidation and Comparison to Methanol", **Electrochimica Acta**, Vol. 50, pp. 5118-5125.
42. dos Anjos, D., Hahn, F., Léger, J.M., Kokoh, K.B. and Tremiliosi-Filho, G., 2007, "In Situ FTIRS Studies of the Electrocatalytic Oxidation of Ethanol on Pt Alloy Electrodes", **Journal of Solid State Electrochemistry**, Vol. 11, pp. 1567-1573.
43. Ribeiro, J., dos Anjos, D.M., Kokoh, K.B., Coutanceau, C., Léger, J.M., Olivi, P., de Andrade, A.R. and Tremiliosi-Filho, G., 2007, "Carbon-Supported Ternary PtSnIr Catalysts for Direct Ethanol Fuel Cell", **Electrochimica Acta**, Vol. 52, pp. 6997-7006.
44. Wang, Q., Sun, G.Q., Jiang, L.H., Xin, Q., Sun, S.G., Jiang, Y.X., Chen, S.P., Jusys, Z. and Behm, R.J., 2007, "Adsorption and Oxidation of Ethanol on Colloid-Based Pt/C, PtRu/C and Pt_3Sn/C Catalysts: In Situ FTIR Spectroscopy and On-

Line DEMS Studies", **Physical Chemistry Chemical Physics**, Vol. 9, pp. 2686-2696.

45. Vigier, F., Coutanceau, C., Perrard, A., Belgsir, E.M. and Lamy, C., 2004, "Development of Anode Catalysts for a Direct Ethanol Fuel Cell", **Journal of Applied Electrochemistry**, Vol. 34, pp. 439-446.
46. Song, S.Q., Zhou, W.J., Zhou, Z.H., Jiang, L.H., Sun, G.Q., Xin, Q., Leontidis, V., Kontou, S. and Tsiakaras, P., 2005, "Direct Ethanol PEM Fuel Cells: The Case of Platinum Based Anodes", **International Journal of Hydrogen Energy**, Vol. 30, pp. 995-1001.
47. Zhu, M., Sun, G. and Xin, Q., 2009, "Effect of Alloying Degree in PtSn Catalyst on the Catalytic Behavior for Ethanol Electro-Oxidation", **Electrochimica Acta**, Vol. 54, pp. 1511-1518.
48. Fujiwara, N., Friedrich, K.A. and Stimming, U., 1999, "Ethanol Oxidation on PtRu Electrodes Studied by Differential Electrochemical Mass Spectrometry", **Journal of Electroanalytical Chemistry**, Vol. 472, pp. 120-125.
49. Wang, H., Jusys, Z. and Behm, R.J., 2006, "Ethanol Electro-Oxidation on Carbon-Supported Pt, PtRu and Pt_3Sn Catalysts: A Quantitative DEMS Study", **Journal of Power Sources**, Vol. 154, pp. 351-359.
50. Iwasita, T. and Pastor, E., 1994, "A DEMS and FTir Spectroscopic Investigation of Adsorbed Ethanol on Polycrystalline Platinum", **Electrochimica Acta**, Vol. 39, pp. 531-537.
51. Colmenares, L., Wang, H., Jusys, Z., Jiang, L., Yan, S., Sun, G.Q. and Behm, R.J., 2006, "Ethanol Oxidation on Novel, Carbon Supported Pt Alloy Catalysts--Model Studies Under Defined Diffusion Conditions", **Electrochimica Acta**, Vol. 52, pp. 221-233.
52. Boehm, H.P., 1994, "Some Aspects of the Surface Chemistry of Carbon Blacks and Other Carbons", **Carbon**, Vol. 32, pp. 759-769.
53. Suh, D.J., Tae-Jin, P. and Son-Ki, I., 1993, "Effect of Surface Oxygen Groups of Carbon Supports on the Characteristics of Pd/C Catalysts", **Carbon**, Vol. 31, pp. 427-435.
54. Torres, G.C., Jablonski, E.L., Baronetti, G.T., Castro, A.A., de Miguel, S.R., Scelza, O.A., Blanco, M.D., Pena Jiménez, M.A. and Fierro, J.L.G., 1997, "Effect of the Carbon Pre-Treatment on the Properties and Performance for Nitrobenzene Hydrogenation of Pt/C Catalysts", **Applied Catalysis A: General**, Vol. 161, pp. 213-226.
55. Fraga, M.A., Jordão, E., Mendes, M.J., Freitas, M.M.A., Faria, J.L. and Figueiredo, J.L., 2002, "Properties of Carbon-Supported Platinum Catalysts: Role of Carbon Surface Sites", **Journal of Catalysis**, Vol. 209, pp. 355-364.
56. Kim, S. and Park, S.J., 2007, "Effect of Acid/Base Treatment to Carbon Blacks on Preparation of Carbon-Supported Platinum Nanoclusters", **Electrochimica Acta**, Vol. 52, pp. 3013-3021.
57. Coloma, F., Sepulvedaescribano, A. and Rodriguezreinoso, F., 1995, "Heat-Treated Carbon-Blacks as Supports for Platinum Catalysts", **Journal of Catalysis**, Vol. 154, pp. 299-305.
58. Figueiredo, J.L., Pereira, M.F.R., Freitas, M.M.A. and Órfão, J.J.M., 1999, "Modification of the Surface Chemistry of Activated Carbons", **Carbon**, Vol. 37, pp. 1379-1389.
59. Ermete, A., 2007, "Platinum-Based Ternary Catalysts for Low Temperature Fuel Cells: Part I. Preparation Methods and Structural Characteristics", **Applied Catalysis B: Environmental**, Vol. 74, pp. 324-336.

60. Liu, H., Song, C., Zhang, L., Zhang, J., Wang, H. and Wilkinson, D.P., 2006, "A Review of Anode Catalysis in the Direct Methanol Fuel Cell", **Journal of Power Sources**, Vol. 155, pp. 95-110.
61. Oliveira Neto, A., Franco, E.G., Aricó, E., Linardi, M. and Gonzalez, E.R., 2003, "Electro-Oxidation of Methanol and Ethanol on Pt-Ru/C and Pt-Ru-Mo/C Electrocatalysts Prepared by Bönnemann's Method", **Journal of the European Ceramic Society**, Vol. 23, pp. 2987-2992.
62. Bock, C., Paquet, C., Couillard, M., Botton, G.A. and MacDougall, B.R., 2004, "Size-Selected Synthesis of PtRu Nano-Catalysts: Reaction and Size Control Mechanism", **Journal of the American Chemical Society**, Vol. 126, pp. 8028-8037.
63. Laine, R.M. and Sellinger, A., 2000, "**Preparation of Supported Nano-Sized Catalyst Particles via a Polyol Process**", United States, 6,551,960.
64. Mao, S.S. and Mao, G., 2001, "**Supported Nanoparticle Catalyst**", United States, 6,686,308.
65. Oh, H.S., Oh, J.G., Hong, Y.G. and Kim, H., 2007, "Investigation of Carbon-Supported Pt Nanocatalyst Preparation by the Polyol Process for Fuel Cell Applications", **Electrochimica Acta**, Vol. 52, pp. 7278-7285.
66. Jiang, L., Sun, G., Zhou, Z., Sun, S., Wang, Q., Yan, S., Li, H., Tian, J., Guo, J., Zhou, B. and Xin, Q., 2005, "Size-Controllable Synthesis of Monodispersed SnO_2 Nanoparticles and Application in Electrocatalysts", **The Journal of Physical Chemistry B**, Vol. 109, pp. 8774-8778.
67. Jiang, L., Zang, H., Sun, G. and Xin, Q., 2006, "Influence of Preparation Method on the Performance of PtSn/C Anode Electrocatalyst for Direct Ethanol Fuel Cells", **Chinese Journal of Catalysis**, Vol. 27, pp. 15-19.
68. Zhou, W.J., Li, W.Z., Song, S.Q., Zhou, Z.H., Jiang, L.H., Sun, G.Q., Xin, Q., Poulianitis, K., Kontou, S. and Tsiakaras, P., 2004, "Bi- and Tri-Metallic Pt-Based Anode Catalysts for Direct Ethanol Fuel Cells", **Journal of Power Sources**, Vol. 131, pp. 217-223.
69. Spinacé, E.V., Linardi, M. and Neto, A.O., 2005, "Co-Catalytic Effect of Nickel in the Electro-Oxidation of Ethanol on Binary Pt-Sn Electrocatalysts", **Electrochemistry Communications**, Vol. 7, pp. 365-369.
70. Tayal, J., Rawat, B. and Basu, S., "Bi-Metallic and Tri-Metallic Pt-Sn/C, Pt-Ir/C, Pt-Ir-Sn/C Catalysts for Electro-Oxidation of Ethanol in Direct Ethanol Fuel Cell", **International Journal of Hydrogen Energy**, In Press.
71. Colmati, F., Antolini, E. and Gonzalez, E.R., 2007, "Ethanol Oxidation on a Carbon-Supported $Pt_{75}Sn_{25}$ Electrocatalyst Prepared by Reduction with Formic Acid: Effect of Thermal Treatment", **Applied Catalysis B: Environmental**, Vol. 73, pp. 106-115.
72. Antolini, E., Colmati, F. and Gonzalez, E.R., 2007, "Effect of Ru Addition on the Structural Characteristics and the Electrochemical Activity for Ethanol Oxidation of Carbon Supported Pt-Sn Alloy Catalysts", **Electrochemistry Communications**, Vol. 9, pp. 398-404.
73. Wang, Z.B., Yin, G.P. and Lin, Y.G., 2007, "Synthesis and Characterization of PtRuMo/C Nanoparticle Electrocatalyst for Direct Ethanol Fuel Cell", **Journal of Power Sources**, Vol. 170, pp. 242-250.
74. Perez, J., Paganin, V.A. and Antolini, E., "Particle Size Effect for Ethanol Electro-Oxidation on Pt/C Catalysts in Half-Cell and in a Single Direct Ethanol Fuel Cell", **Journal of Electroanalytical Chemistry**, Vol. 654, pp. 108-115.

75. Jiang, J. and Kucernak, A., 2002, "Electrooxidation of Small Organic Molecules on Mesoporous Precious Metal Catalysts I: CO and Methanol on Platinum", **Journal of Electroanalytical Chemistry**, Vol. 533, pp. 153-165.
76. Yamauchi, Y., Momma, T., Fuziwara, M., Nair, S.S., Ohsuna, T., Terasaki, O., Osaka, T. and Kuroda, K., 2005, "Unique Microstructure of Mesoporous Pt (H_I-Pt) Prepared via Direct Physical Casting in Lyotropic Liquid Crystalline Media", **Chemistry of Materials**, Vol. 17, pp. 6342-6348.
77. Yamauchi, Y., Sadasivan Nair, S., Momma, T., Ohsuna, T., Osaka, T. and Kuroda, K., 2006, "Synthesis and Characterization of Mesoporous Pt-Ni (H_I-Pt/Ni) Alloy Particles Prepared from Lyotropic Liquid Crystalline Media", **Journal of Materials Chemistry**, Vol. 16, pp. 2229-2234.
78. **Powder Diffraction** [Online], Available : http://en.wikipedia.org/wiki/Powder_diffraction [2011, December 13].
79. **X-ray Analysis of a Solid** [Online], Available : http://materials.binghamton.edu/labs/xray/xray.html [2011, December 13].
80. **Nanotechnology: A Brief Overview** [Online], Available : http://barrett-group.mcgill.ca/teaching/nanotechnology/nano02.htm [2011, December 13].
81. **Energy Dispersive X-ray Spectroscopy (EDS)** [Online], Available : http://www.eaglabs.com/techniques/analytical_techniques/eds.php [2011, December 14].
82. **Energy Dispersive X - ray Spectroscopy** [Online], Available : http://www.cranfield.ac.uk/cds/cfi/eds.html [2011, December 14].
83. **Energy Dispersive X - ray Spectroscopy** [Online], Available : http://www.ifw-dresden.de/institutes/ikm/organisation/dep-31/methods/energy-dispersive-x-ray-spectroscopy-eels [2011, December 13].
84. **Atomic Spectroscopy** [Online], Available : http://www.andor.com/chemistry/?app=91 [2011, December 13].
85. **Cyclic Voltammetry** [Online], Available : http://en.wikipedia.org/wiki/Cyclic_voltammetry [2011, December 13].
86. Southampton Electrochemistry Group, 2001, **Instrumental Methods in Electrochemistry**, 4th ed., Horwood Publishing Limited, England, pp. 50-51.
87. Reymond, J.P. and Kolenda, F., 1999, "Estimation of the Point of Zero Charge of Simple and Mixed Oxides by Mass Titration", **Powder Technology**, Vol. 103, pp. 30-36.
88. Thepkaew, J., Therdthianwong, A. and Therdthianwong, S., 2008, "Key Parameters of Active Layers Affecting Proton Exchange Membrane (PEM) Fuel Cell Performance", **Energy**, Vol. 33, pp. 1794-1800.
89. Wang, S. and Lu, G.Q., 1998, "Effects of Acidic Treatments on the Pore and Surface Properties of Ni Catalyst Supported on Activated Carbon", **Carbon**, Vol. 36, pp. 283-292.
90. Chen, J. P. and Wu, 2004, "Acid/Base-Treated Activated Carbons: Characterization of Functional Groups and Metal Adsorptive Properties", **Langmuir**, Vol. 20, pp. 2233-2242.
91. Scibioh, M.A., Oh, I.H., Lim, T.H., Hong, S.A. and Ha, H.Y., 2008, "Investigation of Various Ionomer-Coated Carbon Supports for Direct Methanol Fuel Cell Applications", **Applied Catalysis B: Environmental**, Vol. 77, pp. 373-385.

92. Song, H., Qiu, X., Li, F., Zhu, W. and Chen, L., 2007, "Ethanol Electro-Oxidation on Catalysts with TiO_2 Coated Carbon Nanotubes as Support", **Electrochemistry Communications**, Vol. 9, pp. 1416-1421.
93. Surampudi, S., Narayanan, S.R., Vamos, E., Frank, H.A., Halpert, G., Olah, G.A. and Prakash, G.K.S., 1993, "**Aqueous Liquid Feed Organic Fuel Cell Using Solid Polymer Electrolyte Membrane**", United States, 5,599,638.
94. Jiang, L., Zhou, Z., Li, W., Zhou, W., Song, S., Li, H., Sun, G. and Xin, Q., 2004, "Effects of Treatment in Different Atmosphere on Pt_3Sn/C Electrocatalysts for Ethanol Electro-Oxidation", **Energy & Fuels**, Vol. 18, pp. 866-871.
95. Zhu, M., Sun, G., Li, H., Cao, L. and Xin, Q., 2008, "Effect of the Sn(II)/Sn(IV) Redox Couple on the Activity of PtSn/C for Ethanol Electro-Oxidation", **Chinese Journal of Catalysis**, Vol. 29, pp. 765-770.
96. Radmilovic, V., Gasteiger, H.A. and Ross, P.N., 1995, "Structure and Chemical Composition of a Supported Pt-Ru Electrocatalyst for Methanol Oxidation", **Journal of Catalysis**, Vol. 154, pp. 98-106.
97. de Oliveira, M.B., Profeti, L.P.R. and Olivi, P., 2005, "Electrooxidation of Methanol on PtMyOx (M = Sn, Mo, Os or W) Electrodes", **Electrochemistry Communications**, Vol. 7, pp. 703-709.
98. Santiago, E.I. and Ticianelli, E.A., 2005, "The Performance of Carbon-Supported PtOs Electrocatalysts for the Hydrogen Oxidation in the Presence of CO", **International Journal of Hydrogen Energy**, Vol. 30, pp. 159-165.
99. Jusys, Z., Schmidt, T.J., Dubau, L., Lasch, K., Jьrissen, L., Garche, J. and Behm, R.J., 2002, "Activity of PtRuMeOx (Me = W, Mo or V) Catalysts Towards Methanol Oxidation and Their Characterization", **Journal of Power Sources**, Vol. 105, pp. 297-304.
100. Lee, E., Murthy, A. and Manthiram, A., "Comparison of the Stabilities and Activities of Pt-Ru/C and Pt_3-Sn/C Electrocatalysts Synthesized by the Polyol Method for Methanol Electro-Oxidation Reaction", **Journal of Electroanalytical Chemistry**, Vol. 659, pp. 168-175.
101. Wu, G., Swaidan, R. and Cui, G., 2007, "Electrooxidations of Ethanol, Acetaldehyde and Acetic Acid Using PtRuSn/C Catalysts Prepared by Modified Alcohol-Reduction Process", **Journal of Power Sources**, Vol. 172, pp. 180-188.
102. Lin, W.F., Iwasita, T. and Vielstich, W., 1999, "Catalysis of CO Electrooxidation at Pt, Ru, and PtRu Alloy. An in Situ FTIR Study", **The Journal of Physical Chemistry B**, Vol. 103, pp. 3250-3257.
103. Crabb, E.M., Marshall, R. and Thompsett, D., 2000, "Carbon Monoxide Electro-oxidation Properties of Carbon-Supported PtSn Catalysts Prepared Using Surface Organometallic Chemistry", **Journal of The Electrochemical Society**, Vol. 147, pp. 4440-4447.
104. Morimoto, Y. and Yeager, E.B., 1998, "CO Oxidation on Smooth and High Area Pt, Pt-Ru and Pt-Sn Electrodes", **Journal of Electroanalytical Chemistry**, Vol. 441, pp. 77-81.
105. Samjeské, G., Komatsu, K.I. and Osawa, M., 2009, "Dynamics of CO Oxidation on a Polycrystalline Platinum Electrode: A Time-Resolved Infrared Study", **The Journal of Physical Chemistry C**, Vol. 113, pp. 10222-10228.
106. Orozco, G. and Gutiérrez, C., 2000, "Adsorption and Electro-Oxidation of Carbon Monoxide, Methanol, Ethanol and Formic Acid on Osmium Electrodeposited on Glassy Carbon", **Journal of Electroanalytical Chemistry**, Vol. 484, pp. 64-72.

107. Shubina, T.E. and Koper, M.T.M., 2002, "Quantum-Chemical Calculations of CO and OH Interacting with Bimetallic Surfaces", **Electrochimica Acta**, Vol. 47, pp. 3621-3628.
108. Guo, J.W., Zhao, T.S., Prabhuram, J., Chen, R. and Wong, C.W., 2006, "Development of PtRu-CeO_2/C Anode Electrocatalyst for Direct Methanol Fuel Cells", **Journal of Power Sources**, Vol. 156, pp. 345-354.
109. Kawaguchi, T., Sugimoto, W., Murakami, Y. and Takasu, Y., 2004, "Temperature Dependence of the Oxidation of Carbon Monoxide on Carbon Supported Pt, Ru, and PtRu", **Electrochemistry Communications**, Vol. 6, pp. 480-483.
110. Marković, N.M., Grgur, B.N., Lucas, C.A. and Ross, P.N., 1999, "Electrooxidation of CO and H_2/CO Mixtures on Pt(111) in Acid Solutions", **The Journal of Physical Chemistry B**, Vol. 103, pp. 487-495.
111. Egerton, R.F., 2005, **Physical Principles of Electron Microscopy: An Introduction to TEM, SEM, and AEM**, Springer Science+Business Media, Inc., USA, pp. 107.

APPENDIX A

Example of Calculations

A.1 Calculations for Catalyst Preparation

A.1.1 Carbon-Supported Catalysts

- Prepare 2 mgSn/ml of SnO_2 colloid

In 50 ml of solution, the required amount of Sn is 100 mg.

It is noted that the molecular weight of Sn and $SnCl_2.2H_2O$ is 118.71 g.mole^{-1} and 225.65 g.mole^{-1}, respectively.

$$\text{So, the weight of } SnCl_2.2H_2O = \frac{100\,\text{mg} \times 225.65\,\text{g.mole}^{-1}}{118.71\,\text{g.mole}^{-1} \times 0.98}$$

$$= 194 \text{ mg}$$

- Prepare PtSn/C catalyst (Pt:Sn atomic ratio = 3)

In 6 ml of SnO_2 colloid, the amount of Sn is 12 mg or 0.1 mmole.

$$\text{So, the weight of } H_2PtCl_6.6H_2O = 0.3 \times 10^{-3}\,\text{mole} \times 517.9\,\text{g.mole}^{-1}$$

$$= 155 \text{ mg}$$

A.1.2 Unsupported Catalysts

- Prepare mesoporous PtSn catalyst (Pt:Sn atomic ratio = 1)

It is noted that the total amount of catalyst precursors is 1.51 g and the molecular weight of $SnCl_2$ is 189.62 g.mole^{-1}.

So, the required amount of $H_2PtCl_6.6H_2O$ is assumed to be x.

$$\text{Then, } \frac{x}{517.9} = \frac{(1.51 - x)}{189.62}$$

$$x = 1.1053 \text{ g}$$

And, the required amount of $SnCl_2$ is 0.4047 g.

For the other samples, the amount of all the relevant catalyst precursors is calculated in the similar way as above.

A.2 Calculations of Acid/Base Value on Support Surfaces

The acid/base surface value of the supports can be calculated by Eq. (A.1) and Eq. (A.2), respectively.

$$\text{Acid value} = \frac{C_{NaOH}V_{NaOH} - \left[(C_{HCl}V_{HCl}) \times \frac{V_{NaOH}}{V_s}\right]}{w} \quad \text{(A.1)}$$

$$\text{Base value} = \frac{C_{HCl}V_{HCl} - \left[(C_{NaOH}V_{NaOH}) \times \frac{V_{HCl}}{V_s}\right]}{w} \quad \text{(A.2)}$$

where C_{NaOH} = Concentration of NaOH (mol.L^{-1})

V_{NaOH} = Volume of NaOH solution (mL)

C_{HCl} = Concentration of HCl (mol.L^{-1})

V_{HCl} = Volume of HCl solution (mL)
V_s = Volume of filtrate (mL)
w = Weight of support (g)

For example, the acid value on F-C surface is as follows.

$$\text{Acid value} = \frac{0.097 \times 50 - \left[(0.102 \times 9.02) \times \frac{50}{10} \right]}{0.1070}$$
$$= 2.319 \text{ mol.g}^{-1}$$
$$= 2319 \text{ mmol.g}^{-1}$$

For monovalent ions, 1 mmol = 1 meq
So, the acid surface value of F-C is 2319 meq.g^{-1}.
According to Eq. (A.2), the base value on F-C surface is then determined as below.

$$\text{Base value} = \frac{0.102 \times 50 - \left[(0.097 \times 10.25) \times \frac{50}{10} \right]}{0.1067}$$
$$= 1.222 \text{ mol.g}^{-1}$$
$$= 1222 \text{ mmol.g}^{-1}$$
$$= 1222 \text{ meq.g}^{-1}$$

A.3 Calculations of Average Particle Sizes of Metal

A.3.1 XRD Diffractogram

The average Pt particle sizes were calculated according to the Debye-Scherrer formula.

$$d = \frac{0.9\lambda_{K\alpha_1}}{B_{(2\theta)}\cos\theta_{max}} \quad \text{(A.3)}$$

where $\lambda_{K\alpha_1}$ = The wavelength of Cu Kα radiation source (1.5406 Å)
$B_{(2\theta)}$ = Full width at half-maximum peak (rad)
θ_{max} = The angular position of the peak maxima (^{o})

The lattice parameter of Pt can also be determined from the Bragg's law as follows.

$$n\lambda = 2d\sin\theta \quad \text{(A.4)}$$

And, the d-spacing formula for face-centered cubic is shown in Eq. (A.5).

$$\frac{1}{d^2} = \frac{\left(h^2 + k^2 + l^2\right)}{a^2} \quad \text{(A.5)}$$

Then, we get

$$a_{fcc} = \frac{\sqrt{2}\lambda_{K\alpha_1}}{\sin\theta_{max}} \quad (A.6)$$

where a_{fcc} = Lattice parameter of Pt in (220) plane

For example, Figure A.1 displays the Pt (220) reflection peak of mesoporous Pt, which is then fitted a Gaussian as shown by the red line.

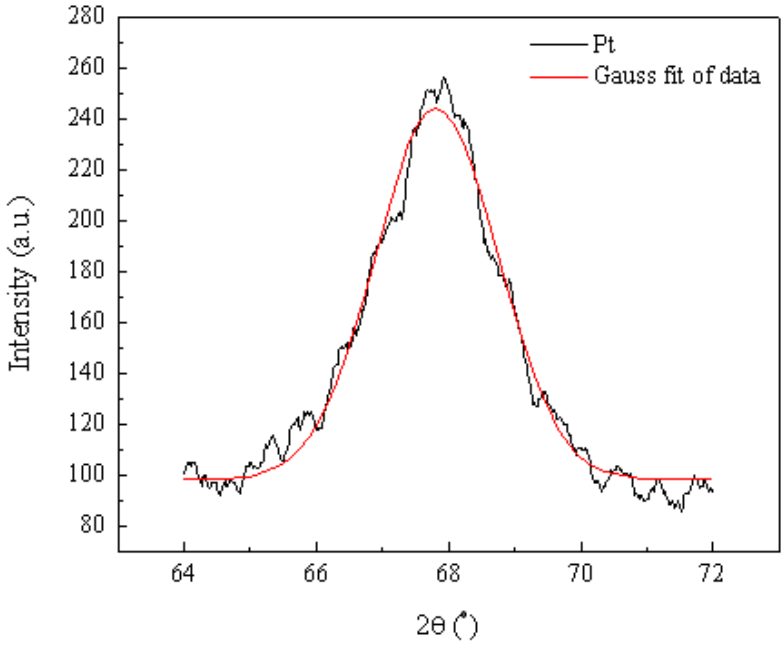

Figure A.1 The Pt (220) reflection peak of mesoporous Pt

From fitting a Gaussian, the full width at half-maximum peak and angle at the maximum of the peak are 0.0381 rad and 33.91°, respectively.

So,
$$d = \frac{0.9 \times 0.15406\,nm}{0.0381 \times \cos(33.91)}$$
$$d = 4.4 \text{ nm}$$

And,
$$a_{fcc} = \frac{\sqrt{2} \times 0.15406\,nm}{\sin(33.91)}$$
$$a_{fcc} = 0.3905 \text{ nm}$$

A.3.2 TEM Image

More than 300 particles were measured and counted to calculate the average Pt particle size by using Eq. (A.7). The standard deviation (SD) was also calculated to show how the Pt particle size deviates from the average particle size through Eq. (A.8).

$$\mu = \sum xP(x) \quad (A.7)$$

$$\sigma = \sqrt{\Sigma (x-\mu)^2 P(x)} \quad \text{(A.8)}$$

where μ = Population mean
σ = Standard deviation
x = Particle size
$P(x)$ = Probability

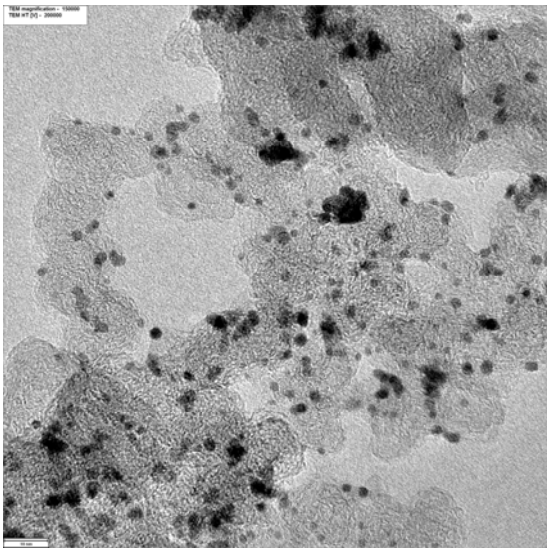

Figure A.2 TEM image of PtSn/HT-C at the magnification of 150,000

From Figure A.2, the sizes of metal as revealed by the black spot were measured and then tabulated in Table A.1. According to Eq. (A.7) and Eq. (A.8), the mean particle sizes of metal and the standard deviation were also calculated. It can be seen from Table A.1 that PtSn/HT-C has the average particle sizes of 2.2±0.5 nm.

Table A.1 Raw data and the corresponding results from PtSn/HT-C images

Particle size, x (nm)	Counts	P(x)	xP(x)	$(x-\mu)^2P(x)$
1.38	26	0.07	0.10	0.04
1.72	99	0.27	0.46	0.05
2.07	107	0.29	0.60	0.00
2.41	60	0.16	0.39	0.01
2.76	56	0.15	0.42	0.05
3.10	16	0.04	0.13	0.04
3.45	5	0.01	0.05	0.02
3.79	3	0.01	0.03	0.02
Sum	372	1.00	2.16	0.5

A.4 Calculations of d-spacing in Electron Diffraction Patterns

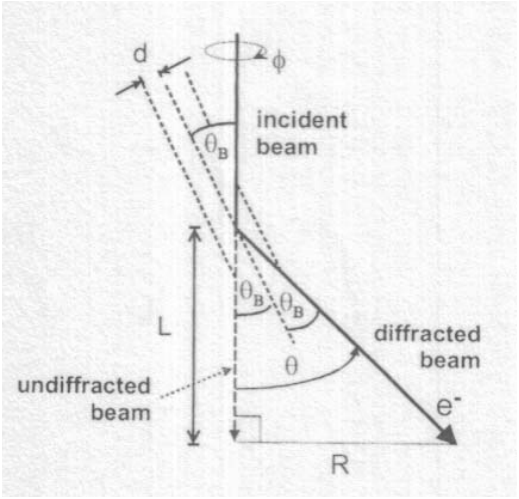

Figure A.3 Geometry of X-ray or fast-electron diffraction from atomic planes [111]

From Figure A.3,

Bragg's law; $n\lambda = 2d\sin\theta_B$

And, $\frac{R}{L} = \tan 2\theta_B$

Using the small-angle approximation,

$$\tan 2\theta = 2\sin\theta$$

Then,

$$\frac{\lambda}{d} = \frac{R}{L}$$

$$\lambda L = Rd \qquad \text{(A.9)}$$

where λ = X-ray wavelength (0.0251 Å for 200 kV TEM)
L = Camera length (100 cm)
R = Ring radius
d = Spacing between atomic planes, measured in a direction perpendicular to the planes

After obtaining the d-spacing of each ring, Miller indices (*h, k, and l*) can be then known by using Eq. (A.5) as follows.

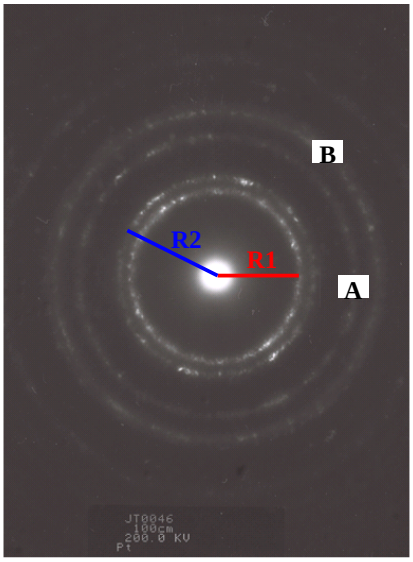

Figure A.4 Electron diffraction pattern of mesoporous Pt

From Figure A.4, R1 = 1.1 cm and R2 = 1.275 cm
So, d-spacing of R1 = 2.282 Å → (h, k, l) = (111)
d-spacing of R2 = 1.969 Å → (h, k, l) = (200)
Similarly, R3 at the point A → (h, k, l) = (220)
R4 at the point B → (h, k, l) = (311)

APPENDIX B

Graphs Between pH of the Suspensions and Carbon Contents

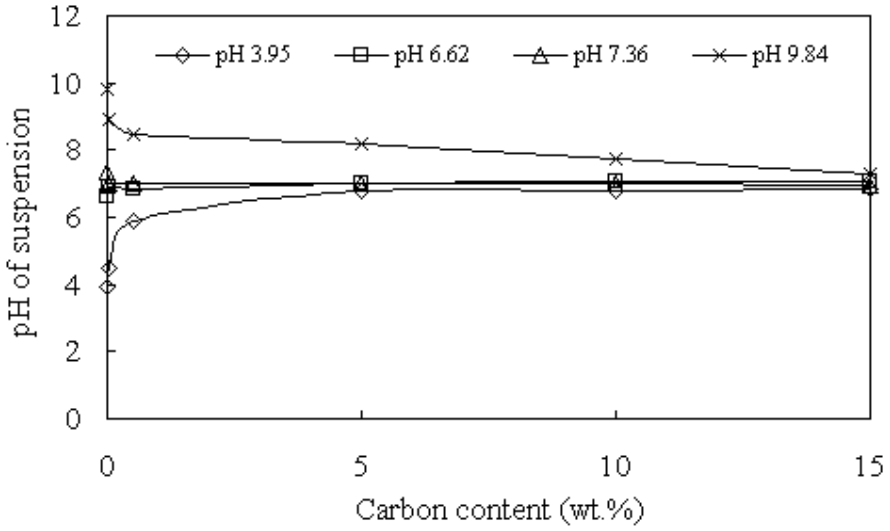
pH 3.95
pH 6.62
pH 7.36
pH 9.84
pH of suspension
Carbon content (wt.%)
0
2
4
6
8
10
12
0
5
10
15

(a)

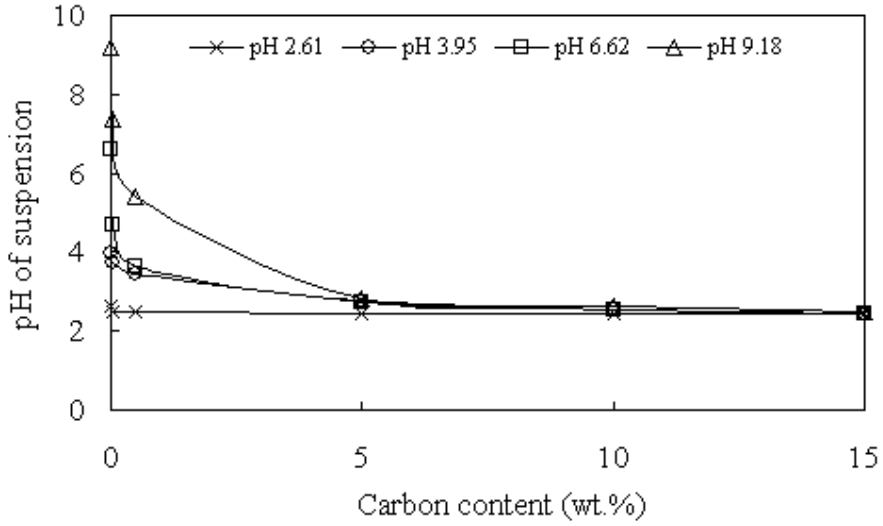
pH 2.61
pH 3.95
pH 6.62
pH 9.18
pH of suspension
Carbon content (wt.%)
0
2
4
6
8
10
0
5
10
15

(b)

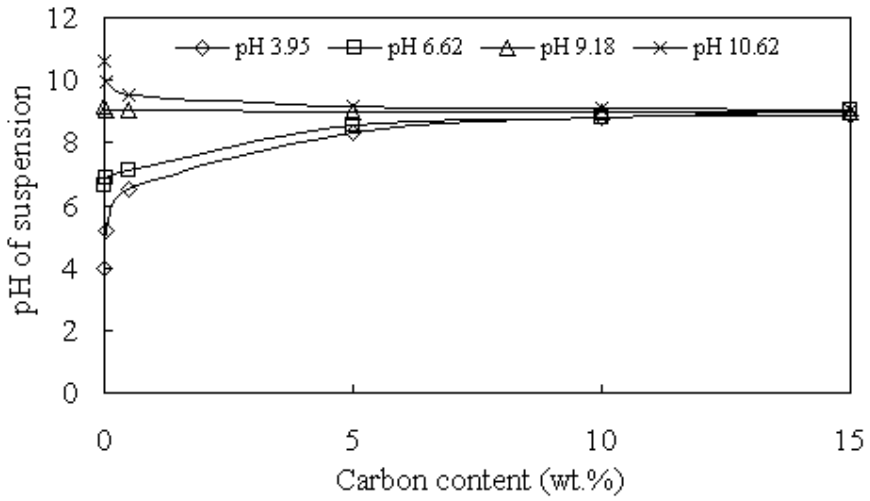

(c)

Figure A.5 pH of the suspensions with different carbon contents: a F-C, b NA-C, c HT-C

CURRICULUM VITAE

NAME Ms. Jarupuk Thepkaew

DATE OF BIRTH 19 January 1982

EDUCATIONAL RECORD

HIGH SCHOOL	High School Graduation Bunyawat Witthayalai School, 1999
BACHELOR DEGREE	Bachelor of Science (Industrial Chemistry) Chiang Mai University, 2003
MASTER DEGREE	Master of Engineering (Chemical Engineering) King Mongkut's University of Technology Thonburi, 2005
DOCTORAL DEGREE	Doctor of Engineering (Chemical Engineering) King Mongkut's University of Technology Thonburi, 2011

RESEARCH GRANTS

2006-2011	Thailand Research Fund (TRF) through the Royal Golden Jubilee Ph.D. Program (Grant No. PHD/0198/2548)
2004-2005	The Chemical Engineering Practice School (ChEPS) Scholarships

PUBLICATIONS

1. Thepkaew, J., Therdthianwong, S. and Therdthianwong, A., 2011, "Effect of Pre-Treatment Approach of a Carbon Support on Activity of PtSn/C Electrocatalysts for Direct Ethanol Fuel Cells", **Journal of Applied Electrochemistry**, Vol. 41, pp. 435-444.
2. Thepkaew, J., Therdthianwong, A. and Therdthianwong, S., 2008, "Key Parameters of Active Layers Affecting Proton Exchange Membrane (PEM) Fuel Cell Performance", **Energy**, Vol. 33, pp. 1794-1800.
3. Thepkaew, J., Therdthianwong, S., Kucernak, A. and Therdthianwong, A., 2011, "Promotion Role of Ru and Sn in Mesoporous PtRu and PtRuSn Alloys towards Ethanol Oxidation Reaction", **The 3rd International Conference on Fuel Cell & Hydrogen Technology**, 22-23 November 2011, Kuala Lumpur, Malaysia.
4. Thepkaew, J., Therdthianwong, S., and Therdthianwong, A., 2011, "Performance of Platinum Electrodes in Direct Ethanol Fuel Cells", **The 1st EnvironmentAsia International**

Conference on "Environmental Supporting in Food and Energy Security: Crisis and Opportunity", 22-25 March 2011, Bangkok, Thailand, pp. 431-436.
5. Thepkaew, J., Therdthianwong, S., and Therdthianwong, A., 2006, "Investigation of Active Layer Compositions for Proton Exchange Membrane Fuel Cell", **The 2nd Joint International Conference on "Sustainable Energy and Environment (SEE 2006)"**, 21-23 November 2006, Bangkok, Thailand, pp. 19-23.